TOPICAL REVIEW

The progress and perspectives of terahertz technology for diagnosis of neoplasms: a review

To cite this article: K I Zaytsev *et al* 2020 *J. Opt.* **22** 013001

View the article online for updates and enhancements.

IOP ebooks™

Bringing you innovative digital publishing with leading voices to create your essential collection of books in STEM research.

Start exploring the collection - download the first chapter of every title for free.

Topical Review

The progress and perspectives of terahertz technology for diagnosis of neoplasms: a review

K I Zaytsev[1,2,3,13] ⓘ, I N Dolganova[2,3,4], N V Chernomyrdin[1,2,3],
G M Katyba[2,4], A A Gavdush[1,2], O P Cherkasova[1,5,6], G A Komandin[1],
M A Shchedrina[3] ⓘ, A N Khodan[7], D S Ponomarev[1,8], I V Reshetov[3,9],
V E Karasik[2], M Skorobogatiy[10], V N Kurlov[3,4] and V V Tuchin[6,11,12]

[1] Prokhorov General Physics Institute of the Russian Academy of Sciences, Moscow 119991, Russia
[2] Bauman Moscow State Technical University, Moscow 105005, Russia
[3] Institute for Regenerative Medicine, Sechenov First Moscow State Medical University (Sechenov University), Moscow 119991, Russia
[4] Institute of Solid State Physics of the Russian Academy of Sciences, Chernogolovka 142432, Russia
[5] Institute of Laser Physics of the Siberian Branch of the Russian Academy of Sciences, Novosibirsk 630090, Russia
[6] Tomsk State University, Tomsk 634050, Russia
[7] Frumkin Institute of Physical Chemistry and Electrochemistry of the Russian Academy of Sciences, Moscow 119071, Russia
[8] Institute of Ultra High Frequency Semiconductor Electronics of the Russian Academy of Sciences, Moscow 117105, Russia
[9] Academy of Postgraduate Education Under FSBU FSCC of FMBA of Russia, Moscow 125371, Russia
[10] Department of Engineering Physics, Polytechnique Montreal, Montreal, Quebec H3T 1J4, Canada
[11] Saratov State University, Saratov 410012, Russia
[12] Institute of Precision Mechanics and Control of the Russian Academy of Sciences, Saratov 410028, Russia

E-mail: kirzay@gmail.com, in.dolganova@gmail.com and tuchinvv@mail.ru

CrossMark

Abstract

Over the past few decades, significant attention has been paid to the biomedical applications of terahertz (THz) technology. Nowadays, THz spectroscopy and imaging have allowed numerous demanding problems in the biological, medical, food, plant and pharmaceutical sciences to be solved. Among the biomedical applications, the label-free diagnosis of malignant and benign neoplasms represents one of the most attractive branches of THz technology. Despite this attractiveness, THz diagnosis methods are still far from being ready for use in medical practice. In this review, we consider modern research results in the THz diagnosis of malignant and benign neoplasms, along with the topical research and engineering problems which restrain the translation of THz technology to clinics. We start by analyzing the common models of THz-wave–tissue interactions and the effects of tissue exposure to THz waves. Then, we discuss the existing modalities of THz spectroscopic and imaging systems, which have either already been applied in medical imaging, or hold strong potential. We summarize the earlier-reported and original results of the THz measurements of neoplasms with different nosology and localization. We pay attention to the origin of contrast between healthy and pathological tissues in the THz spectra and images, and discuss the prospects of THz technology in

[13] Author to whom any correspondence should be addressed.

non-invasive, minimally invasive and intraoperative diagnosis, as well as in aiding histology. Finally, we review the challenging problems of THz diagnosis, as well as attempts to solve them, which should bring THz technology much closer to medical practice. This review allows one to objectively uncover the benefits and weaknesses of THz technology in the diagnosis of malignant and benign neoplasms.

(Some figures may appear in colour only in the online journal)

The development of novel methods for the early non-invasive, minimally invasive and intraoperative diagnosis of malignant and benign neoplasms with different localization and nosology remains a challenging problem of modern medicine, applied physics and engineering sciences, which is confirmed by the statistics on morbidity and mortality of the population [1–5]. The non-invasive and minimally invasive diagnosis of malignancies at early stages is a key factor for efficient treatment. As an example, we consider the problem of the early non-invasive diagnosis of skin cancers (which are by far the most common form of all cancers) [2, 6], and, in particular, of melanoma (which totals only about 1% of all skin cancers, but is reportedly the most dangerous) [7]. The lifetime risk of getting a melanoma is in the range of about 0.1%–2.5%. The diagnosis of melanoma at the stage of dysplastic nevi or at early stages, accompanied by the appropriate treatment, provides a much better prognosis of patient survival, as compared to its detection at late stages [8]. Furthermore, we should stress the importance of the intraoperative diagnosis of malignant and benign neoplasms, where rapid and accurate delineation of their margins is required in order to ensure total removal. For example, a gross-total resection is among the most important prognostic factors in the treatment of human brain gliomas [9], i.e. the most common type of primary tumor of the brain, representing about 26% of all primary tumors and about 81% of malignant primary tumors of the brain [3]. However, because of the unclear margins of gliomas due to their infiltrative character, gross-total resection is almost impossible, even for a highly experienced surgeon. This has stimulated the further development of novel intraoperative brain imaging modalities [10].

In order to mitigate the challenging problems posed by the diagnosis of malignant and benign neoplasms, the different modalities of tissue spectroscopy and imaging have rapidly developed recently, with their unique sets of advantages and drawbacks [11–13]. Among the modern instruments of diagnosis, we would like to particularly mention: magnetic resonance imaging (MRI) [14, 15]; white-light and multi-spectral imaging and microscopy [16–18]; polarization-sensitive imaging [19–22]; fluorescence spectroscopy and imaging, relying on either endogenous or exogenous fluorophores [23–26]; optical coherence tomography (OCT) [27–30], diffuse-light-scattering and photon migration spectroscopy [31–33]; confocal laser-scanning microscopy [34]; infrared (IR) imaging and thermography [35–37]; Raman scattering spectroscopy and imaging [38–40]; ultrasonography [41] and photoacoustic measurements [42–44]; and Brillouin-light-scattering microscopy [45]. Despite such a wide variability of novel tissue imaging modalities, the majority of them are still considered as laboratory research tools; thus, it would take a certain amount of time to transfer them to clinical practice. Most of these techniques rely on the exogenous labels of pathological tissues and cells, which makes the diagnosis process invasive and expensive. Furthermore, each of them provides high accuracy, sensitivity and specificity of diagnosis for a set of neoplasms of particular nosologies and localizations. This justifies the importance of further developing novel instruments for the diagnosis of malignant and benign neoplasms.

Novel prospective methods of malignancy diagnosis can be based on the label-free spectroscopy and imaging of tissues in the THz range [46], which spans frequencies between 0.1 and 3.0 THz, or wavelengths between 3 mm and 100 μm, correspondingly; see figure 1. Since the pilot observations of THz waves by Rubens and Nichols, who were the first to measure the THz radiation of black bodies at the end of the 19th century [47], THz technology has attracted considerable attention in fundamental and applied physics [46]. The research by Auston [48] on photoswitching/photoconductivity in semiconductors, excited by ultrashort laser pulses in the visible or near-infrared (NIR) ranges, has stimulated rapid progress in the generation and detection of THz pulses, as well as in THz pulsed spectroscopy (TPS) and THz pulsed imaging (TPI), observed at the end of the 20th and the beginning of the 21st centuries [46]. During the past few decades, TPS and TPI have been extensively developed and applications found in biology and medicine, thanks to their well-developed component base, the flexibility of their design, as well as the ability to fabricate portable and ergonomic systems [49, 50].

One of the most attractive and socially important branches of THz biophotonics is the label-free diagnosis of malignant and benign neoplasms, which is justified by the annually increasing number of research items in this area, according to Scopus and the Web of Science databases; see figure 2. THz radiation is non-ionizing in nature; therefore, low-power THz beams are harmless to humans. THz waves are strongly absorbed by water molecules, which limits their penetration into tissues by hundreds or even tens of microns, depending on the tissue type and the electromagnetic wave frequency. On the one hand, strong THz wave absorption by water limits the capabilities of THz diagnosis by probing only
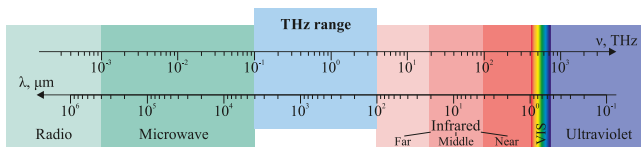
Figure 1. The THz range of the electromagnetic spectrum, where ν and λ stand for the electromagnetic wave frequency and wavelength, respectively. Courtesy of K I Zaytsev.
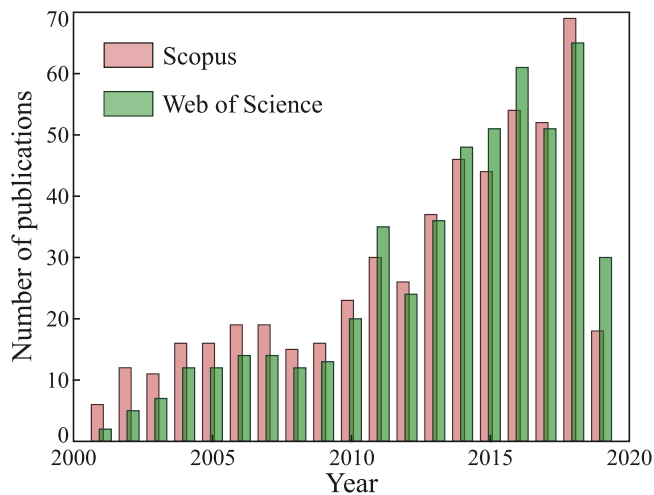

Figure 2. The annual number of publications (from 2000 to 2019) related to the terahertz diagnosis of malignancies, retrieved from the query ('terahertz' or 'THz') and ('malignancy' or 'cancer' or 'tumor') from the Scopus and Web of Science databases; search request dated May 6, 2019. Courtesy of A A Gavdush and K I Zaytsev.

the superficial layers of biological liquids and tissues *in vivo*. On the other hand, the high sensitivity of THz waves to water content in tissues makes THz technology attractive for label-free differentiation between healthy tissues and malignancies using water as an endogenous marker (malignant tissues usually feature increased water content owing to abnormal microvascularity and edema) [50]. Despite the attractiveness of THz technology, it is still a rather novel research direction, far from clinical application due to the restrictions of many scientific and technical problems.

In this review, we summarize the modern results in the area of the THz diagnosis of malignant and benign neoplasms as well as the related research and engineering branches. We discuss the existing models describing the THz-wave–tissue interactions, as well as the biological effects of tissue exposure to THz waves. We consider the common THz instruments and the related methods of signal processing and inverse problem solutions, which have either already been applied in THz bio-photonics and medical imaging, or still hold strong potential. We summarize the earlier-reported results of the THz measurements of malignant and benign neoplasms with different nosology and localization, paying attention to the origin of the observed contrasts. We discuss the prospects of THz technology in non-invasive, minimally invasive and intraoperative diagnosis, as well as in aiding histology. We review the challenging problems of THz diagnosis and their possible

solutions, which should bring THz technology much closer to use in clinical practice. This review allows one to objectively uncover the strengths and weaknesses of THz technology for the diagnosis of neoplasms.

The paper is organized as follows. In section 1, we describe the modern research results in the area of THz-wave–tissue interactions in the context of tissue diagnosis and exposure. We consider the effective medium theory, which is widely applied for describing THz-wave propagation in homogeneous isotropic tissues, the problem of accounting for the THz-wave scattering in tissues, which remains unaddressed, and the effects of tissue exposure to THz waves, which are of crucial importance for defining the safe limits in THz diagnosis and therapy. In section 2, we describe the modern instruments and methods of THz technology with strong emphasis on TPS and TPI, which are widely applied in THz biophotonics. In section 3, we discuss the recent advantages of THz diagnosis in malignant and benign neoplasms with different nosology and localization by classifying the existing methods into four distinct types: non-invasive, minimally invasive and intraoperative THz diagnosis, as well as THz aiding histology. Furthermore, we briefly consider the origin of the label-free contrast observed between intact (healthy) and pathological tissues in THz spectra and images. In section 4, we consider the challenging problems of THz technologies, restraining their transfer to clinical practice: the demand for novel THz optical materials; the absence of waveguides for THz-wave delivery to difficult-to-access tissue; the importance of boosting the performance of modern THz emitters and detectors; the diffraction-limited spatial resolution of conventional THz optical systems; and the limited depth of THz-wave penetration in biological tissues and liquids. Additionally, we consider the modern approaches to mitigating these challenges. In section 5, we summarize the discussed results highlighting the prospects of THz in medical diagnosis.

1. Terahertz-radiation–tissue interactions

In this section, we start with a description of THz-wave–tissue interactions, relying on the effective medium theory and an assumption of the homogeneous and isotropic character of tissues at the scale posed by THz wavelengths. Due to the relative simplicity, this approach is conventional for THz biophotonics. Next, we consider the problem of accounting for the THz-wave scattering effects in tissues, which has not received enough attention previously, and which might be inherent for a large number of tissues. Finally, we briefly discuss the effects of tissue exposure to THz waves, which is important for defining the safe limits in THz diagnosis.

1.1. Assumption of a homogeneous medium with relaxation dynamics of terahertz dielectric response

In figure 3, the dimensions of the typical structural elements of tissues (such as microfibrils, separate cells, cell organels [51]) are compared with an electromagnetic wavelength of 300 μm, which corresponds to 1.0 THz. With a vertical red solid line, we show the Abbe diffraction limit for the spatial
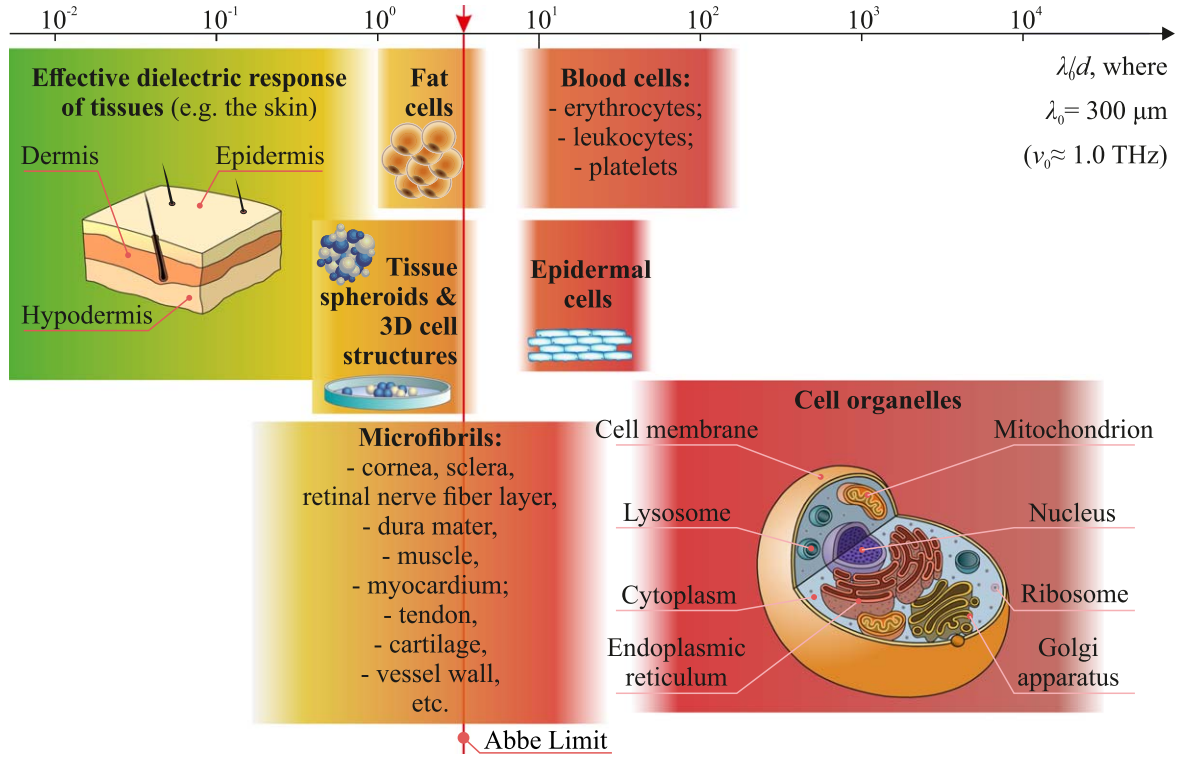
Figure 3. Structural elements of biological tissues at the scale posed by THz wavelengths; here, for simplicity the typical dimension of the structural components of the tissue δ are normalized by the wavelength of $\lambda_0 = 300\ \mu m$ corresponding to $\nu_0 = 1.0$ THz; the vertical solid red line stands for the $\lambda/2$-Abbe diffraction limit. Courtesy of I N Dolganova and K I Zaytsev.

resolution of lens- and mirror-based THz optical systems. From figure 3, we notice that the structural components of tissues are much smaller as compared to the defined THz wavelength. This leads to the Rayleigh scattering of THz waves in such tissues [12] and to a conventional assumption of homogeneous and isotropic medium [50].

THz waves strongly interact with polar molecules; thus, they are absorbed by liquid water (either free or bound) and tissue with a high water content [50, 52]. In order to justify the high impact of water on THz-radiation–tissue interaction, one should pay attention to the significantly higher THz refractive index and absorption coefficient of fibrous connective tissue (which features a volume water content of about 60%–75%), as compared to that of fat tissue of the breast (which normally contains less than 10% water [53]); the THz optical properties for these types of breast tissue were studied in [54]. We were also able to compare the THz response of hydrated tissues *in vivo* or *ex vivo* with that of completely dehydrated ones (for example, tissues embedded in paraffin), with the latter featuring a much smaller THz refractive index and absorption coefficient [55].

The majority of biological systems feature strong THz-wave absorption caused by a high water content; this limits the depth of THz-wave penetration into tissues by hundreds or even tens of microns, depending on the tissue type and the frequency [50]. Therefore, THz technology is only reliable for probing the superficial properties of tissues, while only the reflection-mode measurement schemes are reliable for the THz measurements of hydrated tissues *in vivo* or *ex vivo* [56, 57].

The above-mentioned assumption of the homogeneous and isotropic character of tissues allows the THz-wave–tissue interaction to be described in the framework of effective medium theory. Thus, similarly to the THz dielectric response of liquid water, water solutions and biological liquids [50], the THz response of the tissues features no resonant absorption peaks and can be defined by the relaxation models of the complex dielectric permittivity $\tilde{\varepsilon}$, such as the double-Debye model [58–65]

$$\tilde{\varepsilon} = \varepsilon_\infty + \frac{\Delta\varepsilon_1}{1 + i\omega\tau_1} + \frac{\Delta\varepsilon_2}{1 + i\omega\tau_2}, \tag{1}$$

where ε_∞ is a constant dielectric permittivity at a high-frequency limit; τ_1 and τ_2 stand for the times of the 'slow' and 'fast' relaxations; $\Delta\varepsilon_1$ and $\Delta\varepsilon_2$ represent the contributions of the slow and fast relaxation processes in the dielectric permittivity; and $\omega = 2\pi\nu$ is a circular electromagnetic wave frequency. For example, in table 1, we summarize the literature data on the double-Debye model parameters for water and several types of biological tissues, including healthy and pathological ones. The complex dielectric permittivity

$$\tilde{\varepsilon} = \varepsilon' - i\varepsilon'', \tag{2}$$

with its real ε' and imaginary ε'' parts, is related to the complex refractive index $\tilde{n}$ as

$$\tilde{n} = n' - in'' \equiv n - i\frac{c}{2\pi\nu}\alpha \equiv \sqrt{\tilde{\varepsilon}}, \tag{3}$$

where $n' \equiv n$ and n'' stand for the real and imaginary parts of $\tilde{n}$, $c \simeq 3 \times 10^8$ m s^{-1} is the speed of light in a free space, and α is the amplitude absorption coefficient in [cm^{-1}].

Table 1. The parameters of the double-Debye model for water and tissues.

#	Object	ε_∞	$\Delta\varepsilon_1$	$\Delta\varepsilon_2$	τ_1, ps	τ_2, ps	Source
1	Water	3.3	75	1.9	8.5	0.17	[66]
2	Water	3.5	73.5	1.4	8.2	0.18	[67]
3	Water	4.1	72.2	2.5	10.6	0.18	[58]
4	Water	3.2	73.6	1.6	8.0	0.18	[63]
5	Water	3.42	74.16	1.38	7.87	0.18	[68]
6	Segregated water	2.20 ± 0.10	1.17 ± 0.10	0.44 ± 0.10	7.20 ± 0.05	0.12 ± 0.05	[69]
7	Healthy skin *in vitro*	2.89 ± 0.14	20.34 ± 2.54	1.74 ± 0.16	3.82 ± 0.49	0.11 ± 0.01	[64]
8	Healthy skin *in vivo*	3.0	56.4	0.6	10.0	0.20	[58]
9	Healthy skin *ex vivo*	2.58	10.54	1.58	1.45	0.061 1	[59]
10	Healthy skin *in vitro*	2.859 3	25.696	1.76	4.803 7	0.103	[70]
11	Epidermis *in vivo*	3	54.4	0.6	9.4	0.18	[61]
12	BCC *in vitro*	2.90 ± 0.15	28.53 ± 5.48	1.9 ± 0.20	4.35 ± 0.67	0.11 ± 0.01	[64]
13	BCC *ex vivo*	2.58	13.37	1.58	1.55	0.061 4	[59]
14	BCC *in vitro*	3.021 7	72.246	1.95	11.019 5	0.127 7	[70]
15	Fibrous breast tissue *ex vivo*	2.1	72.6	1.8	10.3	0.07	[63]
16	Breast tumor *ex vivo*	2.5	73.6	2.8	9.1	0.08	[63]

In figure 4, we show (a) real ε' and (b) imaginary ε'' parts of the complex dielectric permittivity for water and epidermis of the skin, which rely on the double-Debye model parameters from [58]: for water, $\varepsilon_\infty^{\text{water}} = 4.1$, $\Delta\varepsilon_1^{\text{water}} = 72.2$, $\Delta\varepsilon_2^{\text{water}} = 2.5$, $\tau_1^{\text{water}} = 10.6$ ps, $\tau_2^{\text{water}} = 0.18$ ps, and for the epidermis of the skin *ex vivo*, $\varepsilon_\infty^{\text{epidermis}} = 3.0$, $\Delta\varepsilon_1^{\text{epidermis}} = 56.4$, $\Delta\varepsilon_2^{\text{epidermis}} = 0.6$, $\tau_1^{\text{epidermis}} = 10.0$ ps, $\tau_2^{\text{epidermis}} = 0.2$ ps. From figure 4, we noticed that the imaginary part of the double-Debye model is comprised of two broad absorption bands, one of which corresponds to the slow Debye relaxation term and is centered far below the THz range at the inverse relaxation time τ_1^{-1}, while another is attributed to the fast Debye relaxation, being centered at the high frequency edge of the THz range at τ_2^{-1}. In turn, the real part of the double-Debye complex dielectric permittivity decays with frequency.

When considering equation (1) for free bulk water, slow Debye relaxation with $\tau_1 \sim 10$ ps describes the cooperative reorganization of water molecules connected by hydrogen bonds, while fast Debye relaxation with $\tau_2 \sim 0.1$ ps describes the vibrational motion of water molecules, free from hydrogen bonds [71]. The hydration of biological molecules in aqueous solutions and tissue might lead to the more complex relaxation dynamics of their dielectric response [72, 73]. The electric charges of biological molecules create an electric field that orients the dipole water molecules and forms layers (shells) of hydrated water. For example, in 1906, Morozov proposed the existence of three hydrated shells in such complexes in addition to free water [74]. The first shell is comprised of a monolayer of water molecules, which is attached to the hydrophilic parts of biomolecules via hydrogen bonds, and features a relaxation time of $\tau \sim 10^{-7}$ s. The second shell (the intermediate one) is called the melting zone, in which water molecules are slightly disturbed by the dipoles of the water molecules from the first shell, and feature a relaxation time of $\tau \sim 10^{-9}-10^{-10}$ s. In the third shell, the
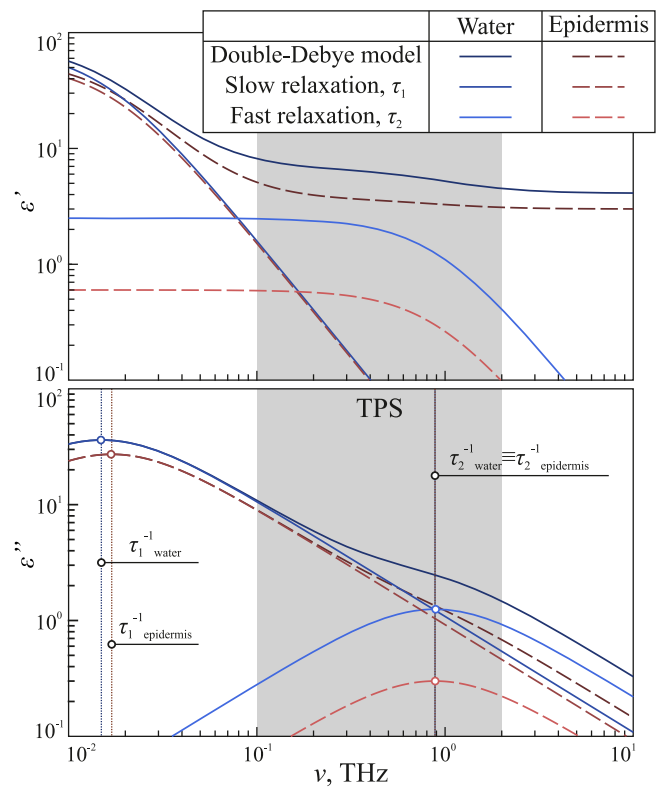

Figure 4. A comparison of the double-Debye models of complex dielectric permittivity for water and the epidermis of the skin *ex vivo* reported in [58]. Here, the gray colored area represents the spectral range of TPS sensitivity, used in [58]. Courtesy of A A Gavdush and K I Zaytsev.

tetrahedral structure of pure bulk water is maintained, where the formation and disruption of hydrogen bonds occur with a relaxation time of $\tau \sim 10^{-12}$ s [75]. Water in the third layer around the molecule represents bulk water, which is not influenced by the solute molecules and has the same physical

properties as pure bulk water. The methods of THz dielectric spectroscopy are sensitive to the picosecond relaxation dynamics in the media [76] and thus allow one to probe the state of water in the third hydrated shell, weakly connected to the biomolecules and associated with fast Debye relaxation [77]. Therefore, both the content and the state of water in a solution of biological molecules and tissue play an important role in the formation of their electodipole response at THz frequencies [78].

For example, THz spectroscopy allows the hydration state of sugar solutions to be characterized. It was demonstrated that the hydration state is closely related to the number of hydrophilic groups and the steric configuration of hydroxyl groups in sugar molecules [79]. The complex dielectric permittivity at the THz frequencies yields information about the presence of unassociated water molecules with picosecond relaxation times in a biological medium and about the amount of water replaced by the hydrated one with slower relaxation times [76]. In [80], about a 10% reduction in the amplitude of the first Debye relaxation term $\Delta\varepsilon_1$, as compared to that of pure bulk water, was reported for the water solution of a mixture containing bovine serum albumin (BSA) and fructose. Incubation of BSA with fructose is accompanied by the formation of covalent bonds between the sugar carbonyl groups and protein amino groups [81], which decreases the portion of fructose molecules with the associated water molecules. As a result, the imaginary part of the permittivity increases, and the THz-wave transmission through the mixture decreases after 96 hours of incubation [80]. Nevertheless, a detailed review of the modern research status in the area of understanding the THz dielectric response of pure bulk water, water solutions of biomolecules, segregated water and tissues is far beyond the scope of the present review. The reader can find an in-depth analysis of this problem in [50, 78].

Despite the double-Debye model forming a conventional approach for describing the picosecond relaxation dynamics in biological systems, we should notice that using this model is not physically rigorous, since it implies a fit of the experimental data with the two broad absorption peaks, centered either beyond or at the edge of the THz range. Thus, the extraction of the double-Debye model parameters is an extrapolation of the experimental data. However, in the case of taking appropriate initial conditions during the fitting procedure, the double-Debye model can provide a very convenient parametrization of the data using only five independent coefficients: ε_∞, $\Delta\varepsilon_1$, $\Delta\varepsilon_2$, τ_1 and τ_2, which makes it quite attractive in THz biophotonics.

Along with the Debye model, other numerous semi-empirical relaxation models of complex dielectric permittivity exist and could be applied to fit the THz spectroscopy data. Among them are the Cole–Cole [82, 83], Davison–Cole [84] and Havriliak–Negami [85] models, which imply more parameters in order to take into account the possible asymmetry of the discussed broad absorption bands.

The knowledge of a complex dielectric permittivity or a complex refractive index allows us to describe completely the THz-wave–tissue interaction in the framework of classical electrodynamics. In particular, it provides us the ability to:

- Model the THz-wave interaction with layered media using a plane-wave approximation along with the Fresnel equations (for describing the THz-wave transmission and reflection at interfaces between media), and the modified Bouguer–Lambert–Beer law (for describing the THz-wave phase shifts and absorption in a bulk medium) [58];
- Simulate numerically the THz-wave interaction with biological objects of a complex shape using methods of computational electrodynamics or statistical Monte-Carlo approaches [12];
- Use the double-Debye model parameters as physical principal components for discriminating between different types of tissue [64].

Finally, we should stress that there is an increasing number of works dedicated to the theoretical and experimental studies of a resonant (or quasi-resonant) dielectric response of biological media at THz frequencies, such as biological molecules in a crystal state and in different conformations [86, 87, 87–104], as well as biological tissues [105–108]. In particular, the sharp spectral fingerprints of cancer cells were reported in [106, 107], where the authors introduced a high-resolution THz resonance spectroscopy of biological tissues, combined with numerical analysis of the experimental data based on molecular dynamics, and studied a few samples of epithelial ovarian cancer, which allows us to highlight the potential of the proposed technique in early cancer diagnosis. Despite taking a significant amount of time to demonstrate the reproducibility of these results, involving an increase in the amount of samples, and examining the applicability of these techniques for cancers with different nosology and localization, novel opportunities may be opened up for the THz molecular diagnosis. A detailed analysis of the resonant features in the THz dielectric response of biological systems is out of the scope of this paper; in our opinion, this topic deserves a separate full-blown review paper.

1.2. The problem of accounting for terahertz-wave scattering in tissues

The simplicity of the aforementioned approach, which is based on the assumption of the homogeneous and isotropic character of tissues and the straightforward effective medium theory, makes it widely applied in THz biophotonics. However, a lot of biological objects and tissues possess structural inhomogeneities with dimensions comparable to the THz wavelengths; some of them are presented in figure 3.

As a representative example of such tissues, in figure 5, we show (a) the THz image and (b) the histological data for fat cells and their agglomerates embedded into the connective fibrous tissues of the breast. This THz image of a human breast specimen *ex vivo* was collected at $\lambda = 500$ μm using 0.15 λ-resolution THz solid immersion microscopy [109]. This technique, described below in section 4.3.2, allows fat cells and their agglomerates with dimensions of about 50–150 μm to be imaged. For such types of tissue, where inhomogeneities are no longer negligibly small particles compared to the wavelength (average size/wavelength ratio $d/\lambda > 0.1$), the Mie scattering
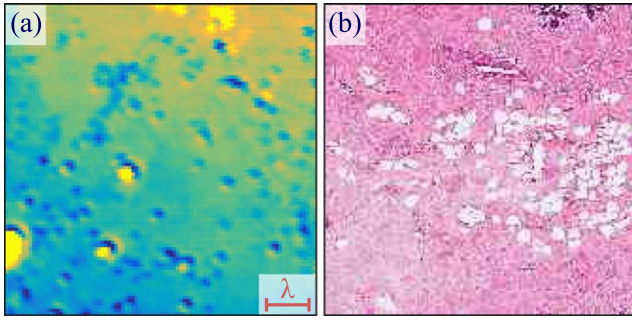
Figure 5. A THz image of the connective fibrous tissues of the breast *ex vivo* (a), compared to the histological optical image (b). The THz image was collected using 0.15 λ-resolution THz solid immersion microscopy at the wavelength of $\lambda = 500$ μm. Here, the THz image reveals sub-wavelength single fat cells and their agglomerates embedded into the connective fibrous tissues of the breast *ex vivo*. Reprinted from [109], with the permission of AIP Publishing.

Table 2. The THz optical properties of fat and connective fibrous tissues of the breast from [54], which were used in the calculation of the data from figure 6. Reprinted with permission from [54]. © The Optical Society of America.

ν, THz	Fat tissue		Fibrous tissue	
	n	α, cm^{-1}	n	α, cm^{-1}
0.5	1.58	36	2.05	129
1.0	1.57	60	1.95	200
2.0	1.56	81	1.89	260

effects would take place. This would push further research into the realm of the development of novel approaches for describing the THz-wave–tissue interactions, which takes into account both the dispersion and absorption properties of tissue components, as well as the structural properties of tissues. This approach would rely on radiation transfer theory, which is widely used for describing the electromagnetic response of tissues in the visible and IR spectral ranges [12]. The basis of radiation transfer theory is a radiation transfer equation, which defines the radiance $I(\mathbf{r}, \hat{s})$ at a point (radius vector) $\mathbf{r}$ in the direction $\hat{s}$

$$\frac{\partial I(\mathbf{r}, \hat{s})}{\partial s} = -\mu_t I(\mathbf{r}, \hat{s}) + \mu_s \int_{4\pi} I(\mathbf{r}, \hat{s}')p(\hat{s}, \hat{s}')d\Omega' + I_0(\mathbf{r}, \hat{s}),$$

(4)

where μ_s and μ_t are the scattering and total (absorption and scattering) coefficients, $p(\hat{s}, \hat{s}')$ is the scattering phase function, Ω' is the unit solid angle around $\hat{s}'$ and $I_0(\mathbf{r}, \hat{s})$ is the radiance of internal sources. The scattering phase function describes the anisotropy of the scattering properties of tissues and accounts for the characteristic angular distribution of the Mie scattering.

If we consider the above-mentioned example of breast tissues from figure 5 and apply the Mie theory in the THz range for the single fat cell of various diameters d surrounded by the fibrous connective tissues, we can observe the changing behavior of the scattering parameters, i.e. the differential scattering cross-section $\sigma(\theta)$, the total scattering cross-sections
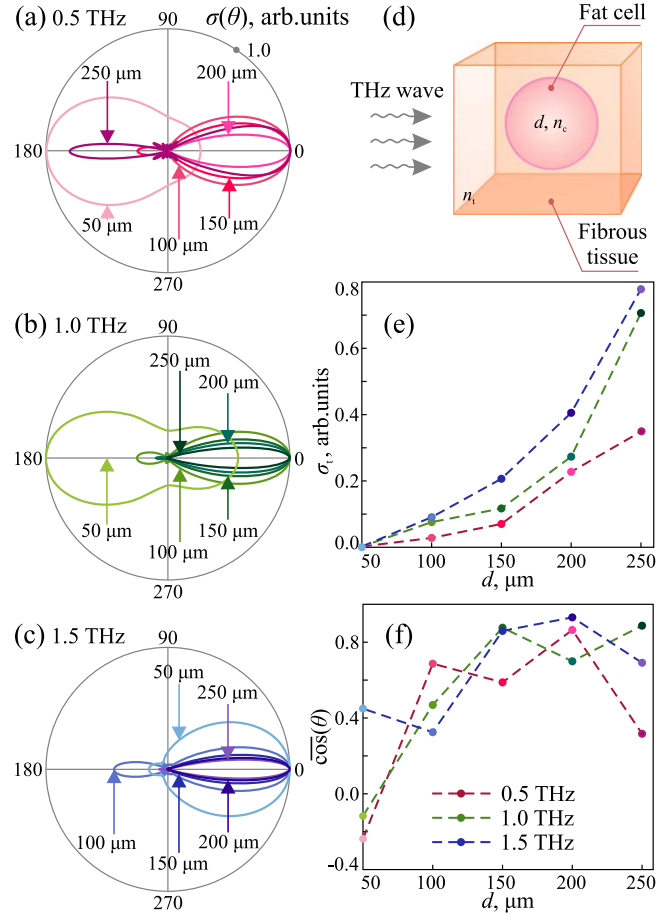

Figure 6. The Mie scattering properties of the single spherical fat cell surrounded by the homogeneous fibrous tissues of the breast with optical properties from table 2: (a)–(c) a normalized differential scattering cross-section $\sigma(\theta)$ for various diameters of fat cells ($d = 50, 100, 150, 200$ and 250 μm) and frequencies of the electromagnetic wave ($\nu = 0.5, 1.0$ and 1.5 THz); (d) a model of the spherical fat cell embedded into the connective fibrous tissues of the breast; (e) a total scattering cross-section σ_t as a function of d and ν; (e) a mean cosine (i.e. a scattering anisotropy factor) $\overline{\cos}(\theta)$ as a function of d and ν. Here, θ is the scattering angle between the directions $\hat{s}$ and $\hat{s}'$. Unpolarized incident THz radiation is considered. Courtesy of I N Dolganova.

σ_t and the scattering anisotropy factor $\overline{\cos}(\theta)$—as shown in figure 6 for depolarized light. Here, θ is the scattering angle between directions $\hat{s}$ and $\hat{s}'$. The dielectric parameters of the connective and fat tissues of the breast for three radiation frequencies 0.5, 1.0 and 1.5 THz are used in the calculations in accordance with the data from [54]; see table 2. Depending on the ratio between the particle diameter d and the wavelength λ, one can expect strong forward or backward scattering, as well as the diffuse scattering of incident radiation. Respectively, such results can impact the THz imaging and spectroscopic measurements of tissues, and possibly lead to a wrong interpretation of enhanced absorption/reflection, reducing the efficiency of THz diagnosis. Note that these calculations do not account for the possible increased water content in adipose cells.

Furthermore, to justify THz radiation scattering in tissue, we can also consider the results of polarization-sensitive THz

imaging [110–112], which were reported to provide useful information for the differentiation between healthy tissue and cancers of the skin *ex vivo*. Such changes in the THz-wave polarization could not, in principle, be predicted using the above-mentioned approach based on the effective medium theory, justifying the necessity of using radiation transfer theory in THz biophotonics. Nevertheless, this problem remains unaddressed.

1.3. Biological effects of tissue exposure to terahertz waves

The appearance of contemporary THz sources and detectors has stimulated the rapid development of medical applications and caused the exposure of the human population to THz waves to increase, arousing anxiety concerning the possible risks. At the same time, the biological effects of THz radiation remain insufficiently investigated. This raises the question on the response of biological systems to THz exposure with different physical parameters, as well as on the evaluation of the adverse health effect threshold. The International Commission on Non-Ionizing Radiation Protection (ICNIRP) sets safe limits of the power density of $2 \, \text{mW cm}^{-2}$ for the exposure of the population in the range of 2 to 300 GHz for the duration of 6 min [113]. Under an exposure of 30 min, this limit is equal to $1 \, \text{mW cm}^{-2}$. The safety limits are based on the estimated changes of body temperature during irradiation; thus, they rely on the thermal mechanisms of the THz-wave–biological-object interaction. No limits have been established for the exposure of a human to electromagnetic waves with frequencies above 300 GHz. Furthermore, the data extrapolation from the neighboring spectral ranges cannot be used to adopt scientifically substantiated standards [114].

Determination of the adverse health effect threshold is impossible without knowledge of the mechanisms of interaction between THz radiation and biological objects. Nowadays, these are the two most widespread hypotheses:

- The first hypothesis considers THz radiation to cause the heating of an object due to the strong THz-wave absorption by water, which is predominantly observed in work with continuous-wave THz radiation [115–118].
- The second hypothesis considers the non-thermal mechanisms of the interaction. Frohlich [119] reported (on the theoretical basis) that the excitation of quantum modes of vibration in contact with a thermal reservoir may lead to the steady states, 'Frohlich condensate', where under a rather high rate of energy supply, only specific low-frequency modes of vibration are strongly excited. This non-linear phenomenon was predicted to occur in biomolecular systems, which are known to exhibit complex vibrational spectral properties, especially in the THz range [120].

In addition, it was demonstrated that either linear or non-linear resonant interaction between THz radiation and deoxyribonucleic acid (DNA) is possible. Under certain conditions, this causes substantial changes in molecular dynamics and might lead to the local rupture of hydrogen bonds in double-stranded DNA chains, as well as to changes in gene expression [121, 122]. This statement is especially applicable to the use of THz pulsed radiation [123], whose average power is usually rather low (μW or mW), though the peak power can reach 1 MW and even higher [124–126], being sufficient for THz radiation to pass through cytoplasm and nuclear membranes [127, 128].

It was suggested that the coiled portion of a sweat duct in the upper skin layer could be regarded as a helical antenna in the sub-THz band [129–132]. Experimentally, it was shown that the reflectance of the human skin in the sub-THz region depends on the intensity of perspiration. One must consider the implications of human immersion in electromagnetic noise, caused by devices working at the very same frequencies as those to which the sweat duct (as a helical antenna) is most attuned. The authors warn that it is necessary to study the possible consequences for human health before unlimited use of sub-THz technologies for communications [133].

Some reviews have demonstrated the effect of THz radiation on conformations of biopolymer (proteins and DNA) [49, 115, 134, 135], genes and cells [115, 136] and the entire organism [115, 134, 137]. For instance, the exposure of mice to THz radiation with the frequency of 3.68 THz and the irradiance of $40 \, \text{mW cm}^{-2}$ for 30 min was reported to cause unfavorable effects on the behavior of animals: the escape response, the shift of motion activity and the anxiety state, which does not disappear within 24 hours after the exposure [138]. For the exposure of drosophila to pulsed broadband THz radiation featuring the spectral range of 0.1–2.2 THz, the pulse duration of 1 ps, the peak power of 8.5 mW, the repetition rate of 76 MHz and the exposure time of 30 min, it was established that THz radiation affects the lifetime of adults and the first-generation progeny, the duration of the period within which adulthood is achieved by individuals of the first generation, and the ratio of female to male individuals. These facts provide evidence of changes in the system signs, and this process may involve epigenetic gene regulation and various intercellular signaling pathways [139].

In [140], it was shown that the exposure of rats with a grafted Guerin carcinoma (a fast-growing malignant tumor) to THz radiation with the frequency of 0.89 THz and the irradiance of $1.6 \, \text{mW cm}^{-2}$ (two exposures of $1 \, \text{cm}^2$ area in 3 days, with the energy dose of $1.44 \, \text{J cm}^{-2}$) leads to a decrease in the tumor size, reliably almost to the same extent provided by x-ray irradiation. After the second exposure, a decrease in tumor growth by 26.5% and 36.2% was observed after 20 days for THz and x-ray exposures, respectively [141]. There is a significant difference between the two mechanisms: the x-rays destroy both tumor cells and normal cells that get into the irradiation zone, while the THz radiation stimulates the immune system, and thus causes selective damage of the tumor cells only. In turn, the everyday 7-day-duration regime of tumor exposure to THz waves (0.89 THz, $400 \, \mu\text{W cm}^{-2}$) accelerates its growth [141], highlighting the importance of accurately selecting the THz exposure regimes.
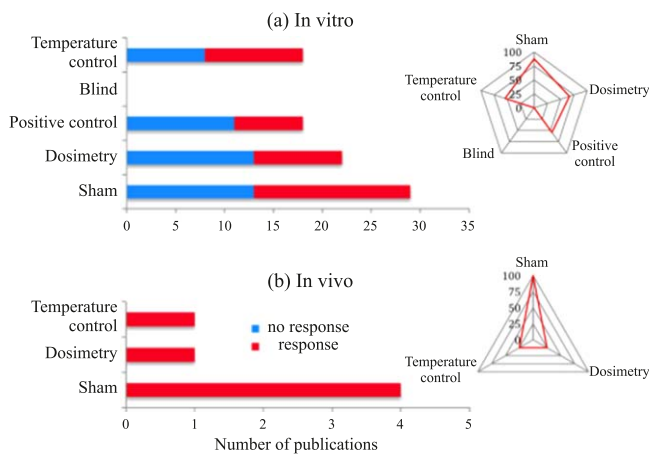
Figure 7. The quality of the THz-related data read out from 33 investigations: (a) *in vitro* experiments; (b) *in vivo* experiments. Here, the blue bars stand for no response while the red bars stand for a response employing the listed quality characteristics (*y*-axis). The spider net diagrams on the right present the percentage of investigations as a function of the quality characteristics. Reprinted from Springer Nature: Journal of Infrared, Millimeter and Terahertz Waves [143], 2018. With permission of Springer.

However, some studies did not reveal any THz radiation effects. According to the data described in the review embracing the works of 37 research groups all over the world, starting from the 1970s [142], it was demonstrated that:

- 43% of works did not detect any effects;
- 29% of works detected negative effects;
- 14% of works detected positive effects,
- 14% of works resulted in multidirectional effects in the studies of the same biological object.

This diversity of experimental data is explained by differences in the applied radiation sources (pulsed or continuous wave (CW)), the exposure time, the organism arrangement level, and the initial functional state of the biological object under investigation. Correspondingly, a thorough evaluation of the specificity of the biological effect caused by THz radiation requires an account of each of the above-mentioned aspects. Indeed, experimental studies aimed at investigating the THz radiation effects need adequate dosimetry, object temperature control, the use of sham exposure, positive control and blinded analysis in order to obtain reproducible results [143]. In figure 7, we show the analysis of the data reported in 33 published works from [143]. This summarizes the results of numerous *in vitro* and *in vivo* studies of various biological systems exposed to THz waves, demonstrating that not all of these studies provide the necessary controls; therefore, these results are not completely credible [143].

The study of THz exposure effects implies several aspects:

- Safety within diagnostic procedures. For this purpose, it is necessary to develop standardized conditions for determining the limitations of THz source applicability in medical diagnostics systems during sufficient time intervals, such as 10–20 min. When working in this direction, it is convenient to deal with cells and cell cultures.

- The capabilities of THz waves to participate in programming cell growth and development, its effect on the functional state, proliferation, and intercellular interactions, which may be urgent for tissue engineering. In this case, it is necessary to exclude the damage of the genetic apparatus of cells.
- Investigation of the long-term consequences (delayed effects) on the functions of complicated multicellular organisms. It is critically important to determine the threshold values of the THz radiation energy parameters, within which the action turns out to be reversible and safe for further vital activity of the biological objects.

One should keep in mind the impact of the applied analysis approaches on the obtained results when studying the biological response, since they can affect the revealed specific structural or functional changes at one level of biological system organization or another. This circumstance also strongly hinders the correct comparison of the data obtained by different authors [142, 143]. There is great significance in the studies of THz radiation effects belonging to new genome technologies, which allow us to determine the DNA damage in cells, as well as to analyze the expression of certain genes and the synthesis of specific proteins [136, 144]. The most simple and rapid method, which allows one to detect the damage and changes in the structure of DNA in cells, is the molecular gene toxicology comet test, i.e. the DNA comet method or the electrophoresis of individual cells in agarose gel. This method was successfully used in a number of studies [115, 116, 134, 136, 137, 142]. The authors of [145] carried out an investigation in order to determine the safe thresholds of THz radiation energies using a set of THz pulsed systems and the DNA comet method, considering THz-wave-induced damages of blood leukocyte DNA. Calculations of the temperature change within the chosen irradiation modes were carried out. They demonstrate that the action of THz-pulsed radiation, spanning the frequency range of 0.1 to 6.5 THz, on blood leukocytes does not induce DNA damage after irradiation for 20 min, even in cases where the maximal irradiance reaches 200 μW cm^{-2}; the electromagnetic-wave-induced heating of the sample does not exceed 1 °C. For comparison, it was demonstrated in [146] that exposure of blood samples from healthy donors to THz-pulsed radiation, which spans the frequency range of 0.12 and 0.13 THz, does not cause genetic changes in blood leukocytes and does not affect the kinetics of the cell cycle for THz-wave irradiance in the range of 30–250 μWcm^{-2} and for the exposure duration of 20 min. An increase in the intensity of THz-pulsed radiation to 2 mW cm^{-2} is able to induce DNA damage [147]. In turn, irradiation of 30 min duration with a CW source of THz radiation, featuring the output frequency of 3.68 THz and the irradiance of about 40 mW cm^{-2}, causes a decrease in the number of vital cells, while irradiation for 90 min leads to a further decrease of twice as much in the number of living cells [140].

At the same time, the exposure of human blood leukocytes to 0.1 THz CW radiation with the irradiance of 31 μW cm^{-2} and the duration of 2 and 24 hours causes an

Table 3. Effects of cell exposure to THz radiation; here, CW and P stand for the continuous-wave and pulsed emitters.

#	Emitter type	Frequency, THz	Cell type	Irradiance, mW cm^{-2}	Exposure time, min	Effects	Source
1	CW	0.12–0.18	Rat glioma cells, lone C6	3.2	1–5	Dose-dependent cytotoxic effect	[148]
2	CW	2.52	Jurkat cells	636	30–50	Up-regulation of the expression of genes of chaperones, transcriptional activators, cellular growth regulators and inflammatory cytokines	[149, 150]
3	CW	2.52	Jurkat cells	227	5–40	Decrease in cell viability	[137]
4	CW	3.68	Human blood lymphocytes	40	30, 90	Decrease in cell viability	[140]
5	CW	0.1	Human blood lymphocytes	0.031	120, 1440	Genomic instability (increase in asynchronous replication)	[151]
6	P	0.1–0.15	Human blood lymphocytes	2, 5	20	DNA damage	[147]
7	P	0.002–0.3	Human blood lymphocytes	2	6	None	[113]
8	P	0.002–0.3	Human blood lymphocytes	1	30	None	[113]
9	P	0.5–6.5	Human blood leukocytes	0.008	20	None	[145]
10	P	0.1–2.0	Human blood leukocytes	0.125	20	None	[145]
11	P	0.1–1.0	Human blood leukocytes	0.2	20	None	[145]
12	P	0.1–0.15	Human blood lymphocytes	0.03–0.25	20	None	[146]
13	CW	0.1	Human blood lymphocytes	0.031	60	None	[151]
14	P	0.2–3.0	Primary human keratinocytes	0.001	10–30	None	[137]
15	CW	0.106	Human dermal fibroblasts	0.04–2.0	120, 480	None	[152]
16	CW	0.07–0.3	Human dermal fibroblasts	<0.001	180, 4200, 5760	None	[153]

increase in the aneuploidy of chromosomes 11 and 17 during cell division, which causes genome instability and could lead to the development of cancer [151]. Exposure of a culture of human T-lymphocytes to 2.52 THz CW radiation with the irradiance of 636 μWcm^{-2} and the duration of 30–50 min was accompanied by sample heating by 3 °C [154]. The effects of THz radiation and of heating to the equal temperature were compared; it was shown that THz irradiation causes the activation of 75% of genes, encoding (among others) the proteins of the plasmatic membrane and the proteins of the intracellular signaling pathways, as compared with 55%-activation as a result of heating. The same authors also demonstrated that after irradiation (4 hours later), increased expression is exhibited by the genes of heat shock proteins, transcriptional regulators, cell growth factors and anti-inflammatory cytokines [149]. The authors concluded that THz radiation may affect gene expression, and this effect is not connected with an increase in cell temperature [150].

Human epidermal keratinocytes and dermal fibroblasts within artificial multilayer human skin tissue were exposed to broadband THz radiation, with the frequency range of 0.1–2.5 THz, the irradiance of 5.7 and 57.0 mW cm^{-2} and the duration of 10 min; for comparison, the cells were also irradiated by pulsed violet radiation with the wavelength of 400 nm for the exposure time of 2 min [155, 156]. The results of this investigation showed that THz radiation causes a selective decrease in the expression of genes associated with the development of skin diseases, such as psoriasis, atopic dermatitis and other inflammatory diseases, as well as the genes of proteins participating in apoptosis [155]. As far as the genes of carcinogenesis are concerned, it was demonstrated that THz radiation suppresses the activity of the genes of proteins enhancing the proliferation of tumor cells, tumor growth and metastasis, and stimulating the expression of proteins suppressing tumor growth [155, 156]. Relying on these results, the authors propose using THz radiation for therapeutic purposes in order to normalize the functions of genes associated with the development of skin diseases.

In [157], murine keratinocytes within the dorsal skin were exposed *in vivo* to broadband THz radiation with the spectral range of 0.1–2.6 THz, the irradiance of 0.32 mW cm^{-2} for the duration of 1 hour. After exposure (24 hours later), the activation of 149 genes was demonstrated. These genes are responsible for such biological functions as healing, tissue growth, organogenesis and cell migration. The pattern of gene expression of the cells exposed to THz waves was different from the pattern characteristic of those exposed to ultraviolet or neutron radiation [157]. The authors assume that THz radiation causes a decrease in skin hydration, and this leads to changes in the activity of the intracellular signaling pathways.

In [158], the cultures of human keratinocytes were exposed for 20 min to THz CW radiation with three frequencies of 1.4, 2.52 and 3.11 THz, while the irradiance was 44.2 mW cm^{-2}. Analysis of mRNA, carried out 4 hours later, showed that the expressed genes turned out to be almost unique for irradiation at one or another frequency. The authors concluded that the irradiation of cell cultures with

different THz frequencies may lead to unique biochemical and cell reactions. Thus, it is necessary to choose the frequency carefully when THz radiation is used as a potential tool to stimulate specific cell properties [158]. A brief overview of the data is given in table 3.

From table 3, we notice that radiation doses below the established safe limits of about 1–2 mW cm^{-2} do not lead to morphological or genotoxic disturbances in cells. Genomic instability, which can lead to the development of cancer, is observed with a low intensity of radiation, but with a long-term duration [151, 159]. A number of cells, such as fibroblasts, do not show changes in the genes at intensities that exceed the threshold values. Perhaps there is a certain amount of cellular and tissue selectivity in the THz radiation. It should be noted that the effects on healthy and diseased cells may differ.

Summarizing all the above-mentioned results, there are still many questions regarding the effects of THz radiation on biological objects to be addressed before applying THz technologies in a clinical practice for diagnosis and therapeutic purposes.

2. Modern instruments of terahertz biophotonics

Since the 1980s, the development of laser-based THz technologies has entailed the appearance of various imaging and spectroscopic techniques in the THz range. Among them are systems employing pulsed and CW radiation, featuring a rather large variety of output parameters, dimensions, capabilities and cost. All of them have been applied to biophotonic tasks to a greater or lesser extent, studying the properties of biological tissues and processes, and developing novel diagnostic tools of different diseases. In this section, we outline the present problems of applying THz radiation to spectroscopy and imaging of tissues. Then, we briefly describe the most common techniques and instruments, with a strong emphasis on the methods that use pulsed THz radiation.

2.1. The problem of tissue measurements at terahertz frequencies

When measuring the physical properties of tissue at THz frequencies, one must deal with the severe problem of the small penetration depth in freshly excised specimens *ex vivo* or tissues *in vivo* caused by strong THz-wave absorption by free and bound water, whose concentration in biological tissues is rather high [160]. Thus, in transmission mode measurements, one should use sliced thin samples with parallel sides and a thickness of <100 μm [161]. The exact sample thickness has to be known with high precision since the thickness parameter is explicitly included in the equations used for determining both the refractive index and the absorption coefficient of a sample. Unfortunately, the preparation of thin sample specimens with parallel sides and exact thicknesses is rarely possible, thus, reflection mode is more common for the THz measurements of tissues. However, the
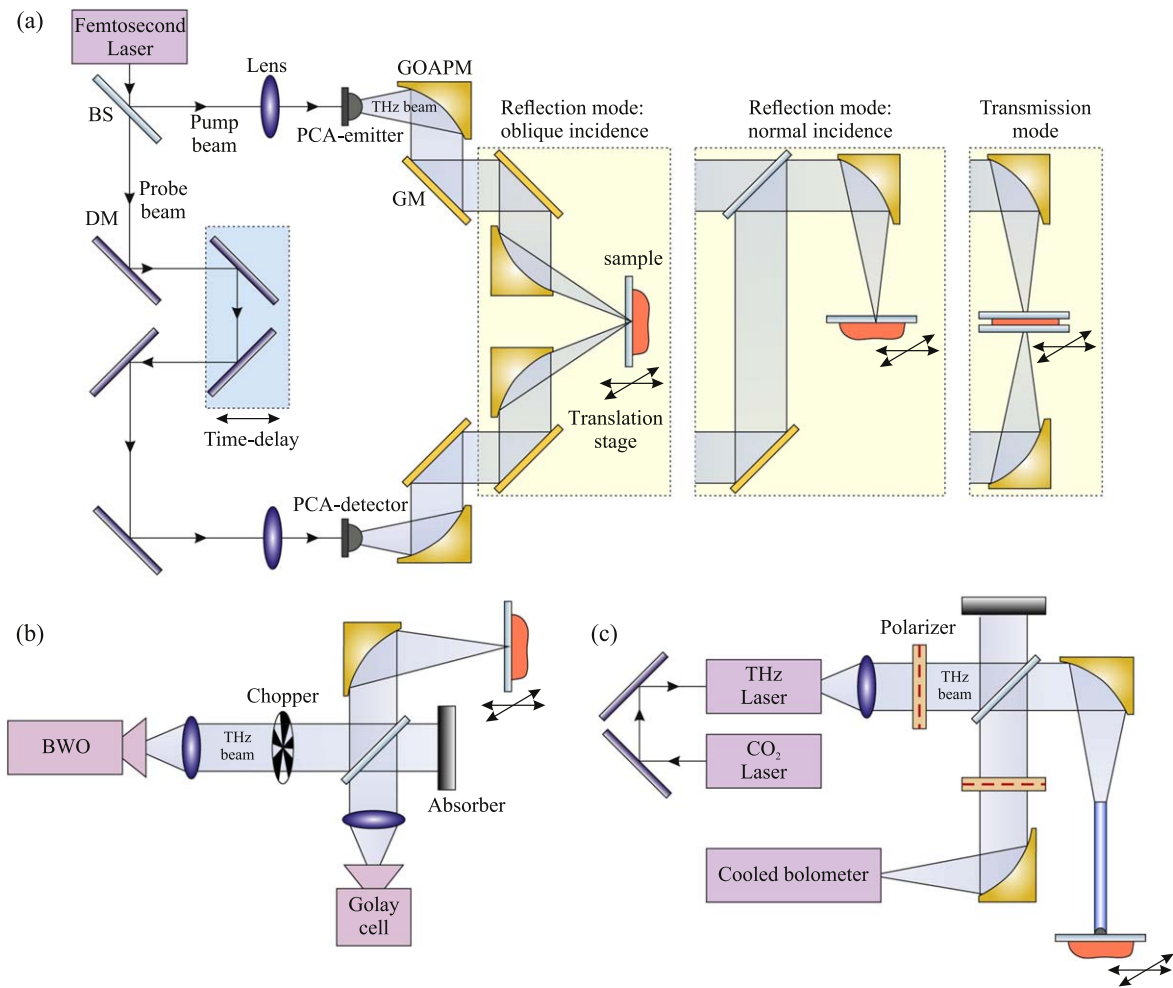
Figure 8. Common tissue measurement schemes in the THz range: (a) imaging and spectroscopy using TPS in reflection and transmission modes, (b) CW imaging and spectroscopy using BWO and the Golay cell, (c) a promising scheme of THz imaging system equipped by the waveguide, a CO_2 pumped THz gas laser and a cooled bolometer; (b), (c) are both in reflection mode and admit transmission mode as well. Here, BS stands for beam-splitter, GOAPM is the THz gold off-axis parabolic mirror, DM is the NIR dielectric mirror and GM is the THz gold mirror. Courtesy of I N Dolganova.

reflection mode involves stronger requirements for aligning the optical components and the sample position, as well as their maintenance during the experiment [57].

Meanwhile, the problem of strong THz-wave absorption by water can be solved by dehydration of a tissue sample (see section 3.4), which allows the morphological properties of tissues to be measured. However, in such measurements a huge amount of information about tissue properties related to water content is lost within the dehydrated layers. Both the reflection and transmission modes are applied to the dehydrated sample. Nevertheless, the choice of measurement modality and the appropriate setup depend on the particular tasks and conditions.

Today the range of THz measurement approaches is rather wide [50]. Besides the transmission and reflection arrangements, it comprises schemes for pulsed and CW spectroscopy as well as schemes for the measurement of optical properties at a single THz frequency. Both can be applied to single-point measurements or imaging, and the latter is implemented via raster-scanning of a sample. Several examples of imaging arrangements are shown in figure 8.

For *in vivo* measurements, the next urgent problem is the delivery of THz radiation to the site of interest, particularly to the difficult-to-access tissues and internal organs, since unlike the visible and NIR ranges, there are no commercially-available low-cost and effective THz waveguides. However, recent developments will allow one to have a solution in the near future, as we mention below in section 4.2. Therefore, the location of the target tissue in the measurement schemes plays an important role and often restricts the experimental arrangement.

2.2. Instruments of terahertz spectroscopy and imaging for tissue diagnosis

The whole set of THz sources, detectors and various measurement schemes available today cover a wide spectral range from far-IR up to sub-millimeter and millimeter waves [46]. In this paragraph, we will give a short description of the most common instruments of THz spectroscopy and imaging, already applied in THz biophotonics.

Fourier transform infrared (FTIR) spectrometers are widely used in the IR range, but some of the modifications can operate at far-IR and even THz frequencies, capturing the short-wave part of the THz range. They are mostly based on the Michelson interferometer scheme, where the inverse Fourier transform of the recorded interferogram represents the spectral flux of interest. In these instruments, the radiation of a broadband CW thermal source (often mercury lamps and globars) with a blackbody-like spectrum is detected by means of either cryogenic bolometer or pyroelectric detectors, such as deuterated triglycine sulfate (DTGS) or lithium tantalate [162–164]. The latter features low sensitivity and dynamic range at low frequencies. Due to the high complexity of cryogenic detectors, only a few FTIR spectrometers operate below 1.0 THz [165].

It is rather common to perform ultra-broadband spectroscopic measurements combining FTIR with TPS, which typically covers a range from 0.1 to 4.5 THz [166–168]. However, TPS is often applied without FTIR, since it provides important broadband spectral information. TPS employs THz pulsed radiation converted from the ultrashort laser pulses of sub-picosecond duration to probe a sample of interest. The most common technique for the generation and detection of THz pulses is the application of photoconductive antennas (PCAs) [48, 169–171]. However, other options are also available, for example, the generation and detection of THz pulses via optical rectification and electro-optical sampling, respectively [46, 172]. In typical TPS, the laser beam is divided by the beamsplitter in the pump and probe beams, which proceed to the PCA-emitter and PCA-detector, respectively, with the difference in the optical path obtained by adding a time delay to the probing path. THz detection is implemented by mixing the THz and laser pulses in the PCA-detector. The photocurrent in the PCA-detector is proportional to the THz electric field and provides the detected THz signal. By changing the temporal delay one can register the THz waveform, after its transmission through a sample or reflection from it. The TPS signal is a sequence of pulses with the possible appearance of Fabry–Perot resonances in the frequency domain, when the corresponding pulses of multiple reflections are not excluded from the analyzed time-domain interval. Thus, specific post-processing procedures should be carefully applied for the reconstruction of the pulse response or optical properties of the sample [173].

Today, TPS systems have overcome the limitation of being cumbersome laboratory equipment, and they are extensively applied in THz biphotonics. In our opinion, the widespread use of TPS and related imaging modalities has been caused by:

- The ability for the simultaneous detection of both frequency-dependent amplitude and the phase of the THz wave in a broad spectral range, as a result of a single measurement. Such comprehensive information about the THz wave yields an analysis of the dielectric response of a sample without applying the Kramers–Kronig relations [174–177], thus, providing complete characterization of tissues in the framework of the effective medium theory (see section 1.1).

- The ability to analyze tissue response either in the time or in the frequency domains, which opens up wide opportunities in processing the TPS data.
- The well-developed component base of TPS and TPI and the opportunity to produce portable handheld and ergonomic THz systems for clinical applications [178, 179].
- The existence of numerous methods for processing the data and for solving the inverse ill-posed problems of TPS for accurate tissue characterization [180–187].

Along with FTIR and TPS, the methods of CW THz spectroscopy based on backward-wave oscillators (BWOs) have been extensively applied in fundamental research [188]. BWO came from the millimeter and sub-millimeter ranges [189], being a sort of electro-vacuum tube that emits coherent quasi-monochromatic radiation with a linewidth of 10^{-5} ν and admitting frequency tuning in the typical band of 10 cm^{-1} by changing the cathode voltage. BWO provides a rather high radiation power, up to several tens of milliwatts. A combination of several BWOs allows high-resolution spectroscopy [190, 191] and imaging [109, 192] to be performed in the wide frequency range of 30 GHz to 1.5 THz. Such devices need a magnetic field to focus the electron beam and power-supply unit. The detection in BWO spectrometers is usually implemented by pyroelectric and opto-acoustic (Golay cell) detectors, or even by cooled bolometers; the choice depends on the desired sensitivity and performance.

Another arrangement, which uses CW THz radiation, is based on the application of solid-state oscillators and amplifiers. Among them are Gunn diodes, impact ionization avalanche transit time (IMPATT) diodes, and tunnel injection transit time (TUNNETT) diodes [193]. These devices are used as sources of sub-millimeter frequencies with a narrow band, but could be included in heterodyne detection schemes as local oscillators; moreover, another arrangement for detection is based on zero-biased Schottky diodes. Operating at room temperature, they demonstrate a significant decrease of output power of $\sim 1/\nu^3$ from approximately 100 mW at 100 GHz to less than 100 μW at 1.0 THz [46, 194]. In our opinion, due to the small frequency band, the spectroscopic measurements of relaxation dynamics in condensed matter are almost impossible; nevertheless, such sources are fine for resonance spectroscopy [106, 107], or for imaging at particular wavelengths: for example, for monitoring water content in sclera and cornea *ex vivo* [195] and *in vivo* [196, 197].

PCAs enable not only THz pulsed generation but CW as well. For this aim, two CW laser sources with slightly shifted frequencies are applied for the excitation of PCA, while the latter serves as a photomixer and generates radiation at a difference frequency [46, 194]. The application of a tunable optical source allows one to build a spectroscopic system [198], which enables a high spectral resolution, required for molecular spectroscopy, gas analysis, etc [199]. Photomixing enables spectroscopy within the range of about 0.5 to 2.0 THz, while another spectroscopic scheme based on the parametric conversion of a laser pump in non-linear optical

crystal (typically, LiNbO$_3$ or MgO:LiNbO$_3$) expands this range up to 3.0 THz [200].

One more THz CW source is the quantum cascade laser (QCL). QCLs have developed rapidly in the past two decades, since they provide coherent and rather powerful CW radiation (up to 100 mW) at frequencies above 1.0 THz with high stability and polarization control [201, 202]. Such devices are based on intersubband transitions in a modular semiconductor heterostructure. Despite being compact, they operate at temperatures below 200 K and mostly need helium cooling. However, attempts to develop THz QCLs, operating close to room temperature, have been successfully made very recently [203]. Moreover, the holographic imaging of tissues with signal amplitude and phase reconstruction is possible using QCL [204].

2.3. Data processing in terahertz pulsed spectroscopy

It is clear from a brief overview of measurement instruments that there are various schemes for the analysis and imaging of biological samples in the THz range. However, one should pay strong attention to implementing the data processing, especially while using TPS principles. The basic sequence of data processing assumes preprocessing techniques for raw signals, data deconvolution, reconstruction of the sample dielectric properties, fitting of the reconstructed dielectric response to the theoretical models, statistical analysis and dimensionality reduction of the observed data. The applied TPS scheme and the method of further data processing mainly determines the choice of the preprocessing technique. The most common ones are signal apodization (windowing) and wavelet-domain denoising, which aim to distinguish between the useful part of the signal and random or systematic noises [205, 206].

Originating from FTIR spectroscopy, [207] apodization of the time-domain signal can be expressed in a general form

$$E_{\text{filtered}}(t) = E_{\text{raw}}(t)H(t - t'), \tag{5}$$

where E_{raw} and E_{filtered} represent TPS waveforms before and after the apodization, correspondingly, while $H(t - t')$ stands for a time-domain window (apodization) filter centered at t'. This procedure allows random noise to be suppressed in the considered time-domain data regions, reducing the Gibbs effect/noise in the frequency-domain data and filtering out the contribution of unaccounted satellite THz pulses that can form unnecessary modulations in the Fourier domain. However, one has to choose the apodization window, which depends on the type of TPS measurements and the object under study [208–210], since optimal apodization improves the effective frequency range and increases the dynamic range of the measurements, which is important for the correct reconstruction of the dielectric response of a sample. The most common windows are Norton–Beer [211], Hamming or the different term Blackman–Harris [207] and Tukey [212].

Wavelet-domain denoising is based on the decomposition of the waveform using the particular wavelet basis and suppression of the decomposition coefficients that are below the defined threshold [213–218]. Selection of the optimal

wavelet basis and threshold is rather challenging. For this purpose, one can use different criteria such as the wavelet basis efficiency index (WBEI), pulse spectral relative entropy (PSRE) and pulse spectral cumulative error (PSCE) [213, 216]. Alternatively, denoising can be implemented with the algorithms based on the Hilbert–Huang transform [219], such as the mean estimation empirical mode decomposition method (ME-EMD) [220], with no need to choose the decomposition basis. Denoising techniques accompany the analysis of raw THz pulses in the algorithms of malignancy diagnosis as well [221].

Signal deconvolution is often aimed at differentiating between various object classes, for instance, malignant, benign and healthy tissues [61, 222]. It usually operates with two TPS waveforms—the reference $E_{\text{r}}(t)$ and sample $E_{\text{s}}(t)$—and implies the calculation of the pulse response function $R(t)$ [214, 223]

$$R(t) = \mathcal{F}_{\nu}^{-1}\left[\frac{\mathcal{F}_{\nu}[E_{\text{s}}(t)]}{\mathcal{F}_{\nu}[E_{\text{r}}(t)]}\right], \tag{6}$$

where $\mathcal{F}_{\nu}[\ldots]$ and $\mathcal{F}_{\nu}^{-1}[\ldots]$ stand for the direct and inverse Fourier transform operators, respectively. Deconvolution, in general, includes additional denoising techniques, commonly implemented for the analyzed transfer function in the frequency-domain. For example, one can apply a double Gaussian filter to the suppression of high- and low-frequency noises [214], or Wiener filtering [224], which can be supplemented with the additional wavelet-domain filtering of a pulse response function [214]. This method is quite simple and with adequate filtering, provides a good contrast between tissues in combination with a high processing rate [214, 221, 225–227]. It is rather common for the study of neoplasms; see for example [228].

However, the results of the TPS data analysis relying on the pulse response function $R(t)$ strongly depend on the TPS spectral operation range and on the parameters of the data processing routine. From this point of view, $R(t)$ seems to be a sub-optimal characteristic for differentiating between normal and pathological tissues. This problem can be solved by reconstructing the THz dielectric response of a tissue—i.e. the frequency-dependent complex dielectric permittivity $\tilde{\varepsilon}$ or complex refractive index $\tilde{n}$ [54, 182, 229, 230]. Reconstructing $\tilde{\varepsilon}$ or $\tilde{n}$ relying on the TPS waveforms implies solving an ill-posed inverse spectroscopy problem, based on the minimization of a discrepancy between the experimental data and the theoretical model. Numerous approaches for solving inverse problems with THz pulsed spectroscopy have been introduced recently, considering either transmission- [69, 231, 232] or reflection-mode [233] measurement geometry, the normal angle of THz beam incidence on a sample surface [57] or off-axial measurements with a pair of parabolic mirrors [173], and even highly sensitive measurements using the total internal reflection configuration [234, 235], which has been attracting increasing interest in THz biophotonics, thanks to its ability to be used in the study of the dielectric permittivity of very thin biological objects, such as the monolayer of cells [236]. One should notice that reflection-mode TPS measurements are often less sensitive
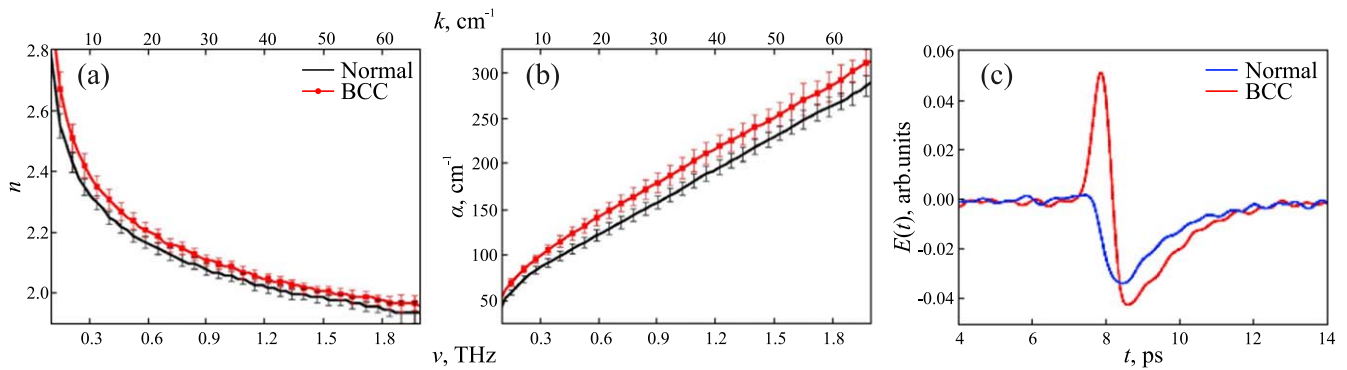
Figure 9. A comparison of the TPS data representation (a), (b) in the frequency domain, as a frequency-dependent refractive index n and absorption coefficient α, and (c) in the time domain, as a TPS waveform $E(t)$, for healthy skin and BCC *ex vivo*. Reproduced from [59]. CC BY 4.0.

and require some specific preprocessing, especially when accounting for the phase changes in received signals [57, 182].

In contrast to the aforementioned pulse response function $R(t)$, the complex dielectric permittivity $\tilde{\varepsilon}$ and the complex refractive index $\tilde{n}$ are almost independent from the TPS setup properties and the parameters of the data-processing procedures. Only the apodization filter smooths the frequency-domain data, suppresses Gibbs noise and limits the spectral resolution to $\Delta\nu = T^{-1}$, where T is the width of the apodization filter. Therefore, $\tilde{\varepsilon}$ or $\tilde{n}$, obtained by different TPS systems, measurement geometries, or even other THz spectroscopic techniques, can be directly compared. These physical characteristics provide a complete description of tissues in the framework of classical electrodynamics, obviously, when the effective medium theory is applicable, and with the assumption that the homogeneous and isotropic character of the tissues is valid; see section 1.1. In our opinion, a frequency-dependent representation of the TPS data via the $\tilde{\varepsilon}$ or $\tilde{n}$ functions seems to present much more unified characteristics when analyzing the physical response and discriminating between various classes of tissues.

In figure 9, we illustrate the ability to use both the frequency domain information (represented by the refractive index n and the absorption coefficient α; see figures 9(a) and (b), respectively) and the time domain data (represented by the TPS waveform $E(t)$; see figure 9(c)), for differentiating between healthy skin and basal cell carcinomas (BCCs) *ex vivo*; this data is adapted from [59]. Despite both frequency-domain and time-domain data revealing statistical differences between healthy and abnormal tissues, one should mention that while the time-domain data provide better differentiation between these two particular tissue classes, the optical properties can be directly compared, even when different modalities of THz spectroscopy are applied, as well as allowing one to model THz-wave–tissue interactions and predict the performance of tissue spectroscopy, reflectometry and imaging using pulsed or CW THz waves.

Finally, we should stress that processing the TPS and TPI data often includes statistical analysis of either the pulse or dielectric responses accompanied by a reduction in the dimensionality of the experimental data [50, 237, 238]. Such a significant variety of TPS and TPI data processing methods opens wide possibilities in their application for the diagnosis of malignant and benign neoplasms. Nevertheless, one should accurately choose the appropriate approach depending on the final intended aim. A further in-depth review of the existing methods of TPS data analysis and the inverse ill-posed problem solution seems to be an important topic for a separate comprehensive review paper.

3. Terahertz spectroscopy and imaging in diagnosis of malignant and benign neoplasms

During the past few decades, THz technology has attracted considerable attention in the diagnosis of malignant and benign neoplasms thanks to the high social importance of this problem [49, 50, 239, 240]. Statistically distinguishable label-free differences in the THz optical constants of healthy and pathological tissues have been reported for neoplasms with different nosology and localization in both *in vivo* and *ex vivo* experiments, revealing the prospect of their non-invasive, minimally invasive and intraoperative diagnosis using modern modalities of THz spectroscopy and imaging [50]. Reasonably, much more attention has been paid to malignant neoplasms. The small depth of THz-wave penetration into tissue (see section 1.1) restricts the capabilities of THz systems to probing only the superficial tissue properties, while only the reflection-mode THz measurements are reliable for *in vivo* applications [56, 57] (see section 2.1).

A contrast between healthy and pathological tissues in the THz range reportedly originates from the differences in content and state (free or bound) of tissue water, as well as from structural variations in tissues [50]. As a result of abundant vascularity and edema, neoplasms can contain more water, and thus possess a higher refractive index and absorption coefficient at THz frequencies [173, 241, 242]. In turn, microscopic and large-scale variations of tissue structure and optical properties, caused by variational tissue microenvironments, deteriorative cellular morphology, variation of cell density, presence of mutative biomolecules, changes in the protein or ion concentration, and (in certain cases) the presence of necrotic debris [55, 243–248], can also contribute to the contrast between healthy tissues and neoplasms in

their THz spectra and images; however the impact of these factors is smaller than that of water [55]. We should mention that all these factors can also alter the quality and decrease the reproducibility of the measured THz data, especially when operating at high frequencies—above $\sim$1.0 THz [233]—where the Mie scattering effects become sufficient; see section 1.2. At the same time, in [110, 249–251], changes in THz beam polarization owing to Mie scattering on tissue inhomogeneities were reported as a source of useful information for the delineation of cancer margins.

The majority of THz systems for biomedical research rely on the principles of TPS and TPI (see section 2); the latter implies point-by-point scanning of the sample surface with a focused beam of TPS with further processing of the collected three-dimensional data set [178]. A typical configuration of TPS and TPI systems relies on diffraction-limited lens- or mirror-based optical systems; see section 2. This optical system does not allow the structural components of tissues to be resolved and yields the determination of the effective physical response of tissues, averaged within the area of the THz beam spot, i.e. the effective values of the pulsed response, dielectric properties, or reflectivity of tissue, either in single-point-measurement or raster-scan imaging modalities [50]. Therefore, in this section, we will address the results of diffraction-limited THz spectroscopy and the imaging of tissues.

Let us review the modern research status in the area of the THz diagnosis of neoplasms, with an emphasis on malignant ones, by classifying them into four distinct classes, depending on the type of medical diagnosis:

- Non-invasive diagnosis;
- Minimally invasive diagnosis;
- Intraoperative diagnosis;
- Accompanying histopathology.

3.1. Non-invasive diagnosis

Here, we consider a medical procedure to be non-invasive when it does not imply a break in tissues, such as the skin and the mucosa, and it does not involve the use of artificial body cavities, which are beyond natural orifices. From this viewpoint, malignant and benign neoplasms of the skin represent prospective objects of THz diagnosis, and can be non-invasively studied using reflection-mode THz measurements. In most research works in the area of non-invasive THz diagnosis of the skin, the latter is assumed to be homogeneous and isotropic. This allows the THz-radiation–skin interactions to be modeled and experimentally studied, defining the skin as a multilayer object (see figure 3) comprised of several layers:

- Stratum corneum (the outermost layer of the epidermis, consisting of dead cells),
- Epidermis,
- Dermis,
- Hypodermis (adipose tissue).

The THz dielectric response of the skin varies significantly in the human body due to both fluctuations of the
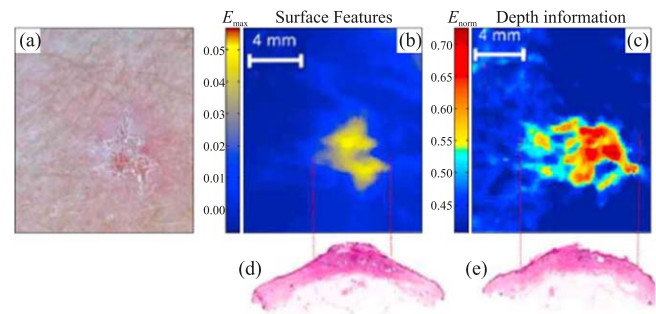

Figure 10. The reflection-mode TPI of the BCC *in vivo*: (a) a clinical photo; (b) a THz parametric image, in which the pixels represent the minimal amplitude of the THz pulse $\min_t[E(t)]$, reflected from the sample; this representation of the TPI image shows the surface features of the tissues; (c) a THz parametric image, in which the pixels represent the normalized amplitude of the THz pulse corresponding to a time-delay of $t = 2.8$ ps; the latter reveals the depth features of the tissues. [222] John Wiley & Sons. Copyright © 2004 WILEY-VCH Verlag GmbH & Co. KGaA, Weinheim.

dielectric properties of tissues (caused by changes in water content and pigmentation), changes in the thickness of the skin layers and the presence of THz-wave scatterers (such as hair follicles and sweat glands) [57, 252–259]. The depth of THz wave penetration into the skin *in vivo* is limited within a few hundred microns. Such a small penetration depth allows THz waves to probe only the superficial layer of the skin, i.e. the stratum corneum and epidermis. In turn, the thickness of the stratum corneum is usually small, as compared to the THz wavelengths; thus, the stratum corneum normally does not affect the THz characterization of the skin, and thus is neglected during data processing. Therefore, one usually deals with characterization of the epidermis during the THz measurements of the skin.

During the past few decades, statistical differences between intact (healthy) and malignant tissues in the THz spectra and images have been demonstrated for non-melanoma cancers of the skin, such as BCCs and squamous cell carcinomas (SCCs) [110, 222, 250, 251, 260–263]. Non-melanoma skin cancers *in vivo* and *in vitro* feature a higher refractive index, absorption coefficient and dispersion than those of healthy skin tissues [59, 222, 261], thus leading to the higher THz reflectivity of cancerous tissues. In figure 9, we have already reprinted the time-domain pulse response and the frequency-domain THz optical properties of healthy tissues and BCCs of the skin *ex vivo*, which were detected in [59] using TPS. Notice that both the time and frequency domains of the THz data representation reveal statistical differences between the THz responses of healthy and malignant tissues. In turn, in figure 10 we show representative examples of the TPI of non-melanoma skin cancer *in vivo*, which were reprinted from [222] and collected using the TPI. The authors of [222] proposed two distinct approaches for processing the three-dimensional data of TPI, which allow THz images to be obtained revealing either the surface or depth features of tissues. Finally, in figure 11, we illustrate another THz imaging modality applied to non-melanoma skin cancer diagnosis: CW reflection-mode polarization-sensitive THz
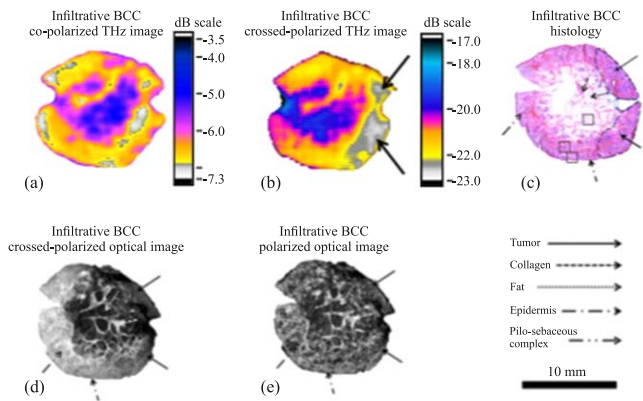
Figure 11. Reflection-mode polarization-sensitive THz imaging of tissue specimen *ex vivo* with infiltrative BCC: (a) a co-polarized THz image; (b) a cross-polarized THz image; (c) a H&E-stained histology of the 5-mm thick frozen tissue section; (d) a cross-polarized optical image; (e) a co-polarized optical image. [110] John Wiley & Sons. Copyright © 2014 WILEY-VCH Verlag GmbH & Co. KGaA, Weinheim.

imaging, i.e. we reprinted the data of the THz imaging of an infiltrative BCC *ex vivo* from [110], where the differences between the scattering properties of the tissues were reported as an alternative source of physical information for tissue diagnosis.

Figures 10 and 11 illustrate that either the time- and frequency-domain data of TPS and TPI (which are sensitive to the effective dielectric response of tissues) or the data of CW polarization THz imaging (which is sensitive to the scattering properties of tissues) can provide useful information for differentiating between intact tissues and non-melanoma cancers of the skin in order to detect margins and ensure the total resection of a cancer. The THz detection of non-melanoma skin cancer margins can be applied either to planning the surgery (i.e. measurements *in vivo*), or during Moh's micrographic surgery, accompanying the complete removal of malignant tissues with maximal preservation of the surrounding healthy ones [264, 265].

Along with the diagnosis of non-melanoma cancers of the skin, THz spectroscopy and imaging are reported to be promising instruments for non-invasively differentiating between ordinary and displastic nevi (moles) of the skin [233, 257, 266]. The problem of rapid discrimination between ordinary and dysplastic nevi is of crucial social importance, since the dysplastic nevus is considered to be a precursor or an initial stage of the development of a melanoma [267]; in turn, the latter is reportedly the most dangerous cancer of the skin [7]. Despite THz technology being able to yield the early non-invasive diagnosis of dysplastic skin nevi and melanomas *in situ*, a comprehensive full-blown study involving a large amount of tissue samples is still to be performed in order to objectively uncover the strengths and weaknesses of THz technology, as compared to other rapidly developing techniques of the dysplastic skin nevi screening [17, 268–270].

Although many works have been dedicated to the THz diagnosis of skin cancers, applications of THz technology can
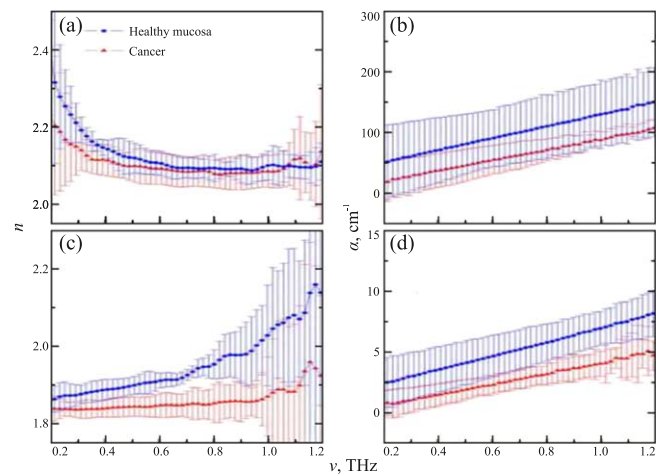

Figure 12. The THz refractive index *n* and absorption coefficient α of normal mucosa and oral cancer *ex vivo* (mucoepidermoid carcinoma and squamous cell carcinoma (SCC)), averaged for six oral samples and measured at the temperatures of 20 °C (a), (b) and −20 °C (c), (d). Here, the dots represent the average values, while the error bars stand for the 95% confidential interval. Reprinted with permission from [271]. © The Optical Society of America.

also be found in the diagnosis of malignancies of the mucosa. For example, the authors of [271] demonstrate the differences between the THz response of a freshly excised healthy and cancerous tissues (two samples of mucoepidermoid carcinoma and five samples of SCC) of the oral mucosa at the ambient temperature of 20 °C. Moreover, they proposed the ability to improve this contrast by freezing tissue down to −20 °C; see figure 12, adapted from [271]. Nevertheless, in our opinion, the potential of using THz technology in the diagnosis of malignancies of the mucosa has not been studied appropriately yet, since it requires further collection and statistical analysis of the THz response of healthy and pathological tissues, either *ex vivo* or *in vivo*.

3.2. Minimally invasive diagnosis

Applications of THz technologies can be found in the minimally invasive diagnosis of malignancies. Here, as for a minimally invasive medical procedure, we consider those that encompass minimally invasive surgical techniques, such as endoscopic or laparoscopic surgery (commonly called keyhole surgery). The latter surgical technique uses natural orifices or limits the size of incisions and thus reduces the time of wound healing, pain and risk of infection [272].

In particular, a contrast in the THz response of healthy and pathological tissues *ex vivo* has been reported for cancers of the colon [249, 273–275], gastric [276, 277] and liver [278–280]. For example, in figure 13, we reprint from [273] the TPI images of a freshly excised colon specimen, containing regions of healthy, dysplastic and cancerous tissues. In turn, in figure 14 we show the results of the polarization-sensitive CW THz imaging of healthy tissues and cancers of the colon. The observed results demonstrate that both TPI and polarization-sensitive CW THz imaging have the potential to
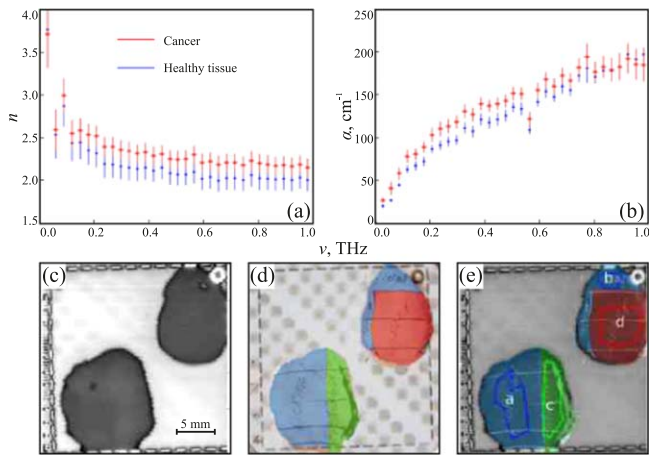
Figure 13. The reflection-mode TPS and TPI of colon cancers *ex vivo*: (a) the mean refractive index *n* and (b) absorption coefficient α of healthy tissues and cancers (carcinoma) of the colon; (c) a TPI image of the colon cancer, each pixel of which shows a minimal amplitude of the THz waveform $\min_t[E(t)]$ reflected by tissues; (d) results of the tissue histology overlapping the visible image; (e) results of the tissue histology overlapping the THz image. (e) Regions A and B correspond to the normal tissues, while C and D stand for the dysplastic and cancerous tissues, respectively. The authors studied different types of cancers by averaging their THz response. Reproduced from [273]. © IOP Publishing Ltd. All rights reserved.
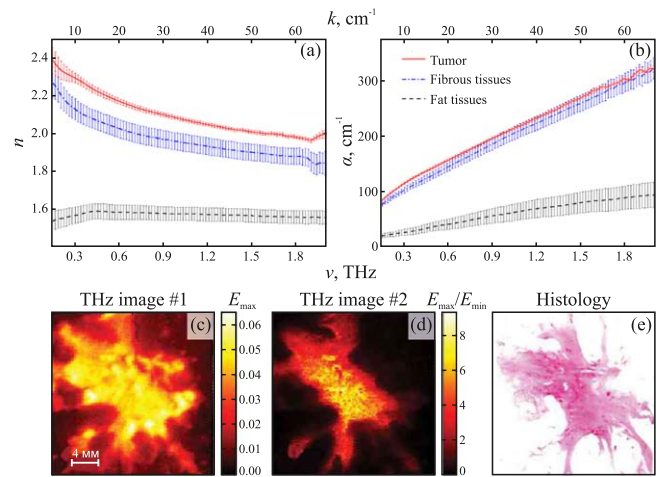

Figure 14. The reflection-mode cross-polarized THz imaging of a colorectal cancer *ex vivo*: (a), (b) and (c), (d) are the two data sets corresponding to different tissue samples. The type of cancer was not specified by the authors. Reproduced from [249]. CC BY 3.0.

aid oncosurgery of the colon or other internal organs of the body.

Nevertheless, the considered results of the THz imaging of a colon cancer allow us to highlight the prospect of using THz technology in the diagnosis of internal organs. These measurements were performed using predominantly *ex vivo* tissue specimens, while such measurements *in vivo* remain impossible due to the problem of THz-wave delivery to/from the objects of interest, associated with the absence of commercially available hard THz waveguides, flexible fibers and endoscopic systems [281, 282]. Possible solutions to this problem and recent developments in the area of THz waveguiding are considered below, in section 4.2. At this stage

Figure 15. The reflection-mode TPS and TPI of human breast tumors *ex vivo*: (a), (b) the mean refractive index *n* and absorption coefficient α of the tumor, fibrous and fat tissues, averaged within several specimens of the breast tissues, where the error bars represent a 95% confidential interval of measurements; (c)–(e) TPI images based on the maximal amplitude of the THz pulse $\max_t[E(t)]$ and the normalized amplitude $\max_t[E(t)]/\min_t[E(t)]$, as well as results of histology. The ductal and lobular carcinomas of the breast were studied by the authors. Reprinted with permission from [54]. © The Optical Society of America.
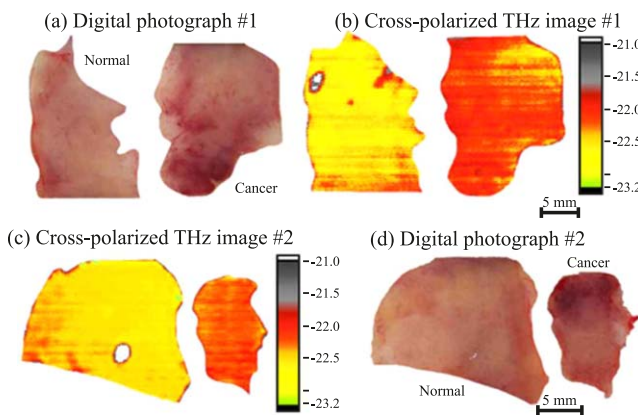
of THz technology development, the analysis of its potential in minimally invasive diagnosis, and an objective comparison of THz technology with the existing instruments of minimally invasive diagnosis seem to be quite a daunting task.

3.3. Intraoperative diagnosis

Besides the non-invasive and minimally invasive diagnosis of malignancies, THz technologies are reliable for intraoperative studies of tissues, particularly when the rapid and accurate delineation of malignancy margins is required. Here, for the intraoperative procedure, we consider one which is performed during surgery, requiring open access to the internal tissues and organs of the body, and thus implying imminent tissue damage.

In [54, 283–287], the ability to use THz waves in the diagnosis of breast tumors (mainly ductal and lobular carcinomas) has been considered. From figures 15(a) and (b), we notice that significant contrast is observed between the THz optical properties of three tissue types—tumor, fibrous and fat tissues [54]. This contrast shows the difference between healthy tissues and tumors of the breast. In figures 15(c)–(e), we show the results of the TPI of freshly excised breast tumor reprinted from [54]: (c) and (d) represent the THz parametric images calculated via two different approaches of THz waveform processing, while (e) shows the results of H&E-stained histology. The origin of the contrast in the THz images is primarily associated with the higher water content in the abnormal tissues [286]. Good agreement between the data of THz imaging and H&E-stained histology indicates that THz instruments can be applied to the intraoperative mapping of breast tumors in order to maximally preserve
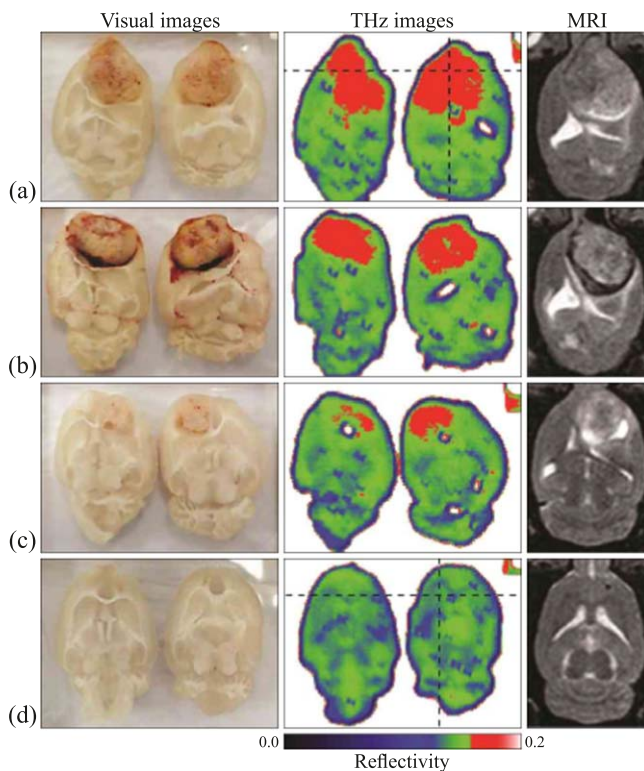
Figure 16. A comparison of visual, THz and MR images of freshly excised whole rat brain tissues with (a)–(c) and without (d) tumors. The dimensions of the THz images are 4×3 cm^2, while the scanning resolution is 250 μm. An orthotopic glioma model from rats with clear tumor margins is used. Reprinted with permission from [55]. © The Optical Society of America.

healthy tissue from resection, and thus to reduce the cosmetic harm caused during the surgical treatment of a breast tumor.

Most recently, the potential of THz technology in intraoperative neurodiagosis, including the diagnosis of brain tumors, has been highlighted by several research papers [55, 173, 288–292]. Among them, we would particularly like to mention [55], where a pilot study of both freshly excised and paraffin-embedded orthotopic glioma models in a whole rat brain was performed using the reflection-mode TPI. As shown in figure 16, the observed results reveal a contrast between the normal tissues and tumors, showing good correlation between the visual images, THz images and MRI data. By comparing the results of the THz imaging of freshly excised and paraffin-embedded tissues, the difference between the normal and tumorous tissues of the rat brain are attributed to the increased water content in a tumor (which is caused both by the newly generated blood vessels and by the body fluids of necrotic debris [293]), as well as to changes in the density of cells in a tumor. It is essential to note that the impact of water content in tissues is reportedly several times higher than that of other factors. Furthermore, in [55], the difference between the THz responses of the gray matter and the white matter of the brain was observed, originating from the higher content of myelin in the white matter; however, this difference does not obstruct the THz differentiation between intact tissues and tumors. Next, in [289] a

comprehensive analysis of the THz optical properties of paraffin-embedded brain glioma models from mice was performed by means of the TPS, revealing the optimal spectral bands and features for the differentiation between paraffin-embedded healthy tissues and tumors of the brain. A few years later, in [290, 291] the potential of THz reflectometry and imaging in intraoperative neurodiagnosis was highlighted, involving both glioma models from mice and rats, *ex vivo* and *in vivo*, and a few pilot samples of human brain gliomas *ex vivo*.

Finally, in [173, 292] TPS was applied to the study of the THz optical properties of gelatin-embedded human brain gliomas *ex vivo*, featuring different World Health Organization (WHO) grades. In this study, the gelatin embedding of tissues [294] was applied in order to fix the tissues for THz measurements after their surgical resection. This tissue fixation procedure prevents tissues from hydration/dehydration, and thus keeps the THz response of tissues unaltered for several hours after surgery, as compared to that of freshly excised tissues. Statistical analysis of the experimental data, shown in figure 17, reveals the ability to discriminate between intact tissues and gliomas of different WHO grades, including low-grade (I, II) and high-grade (III, IV), while the THz response of edematous tissues in the perifocal region was close to that of a tumor, which might lead to false positive diagnosis results. Thus, the prospects of using THz technology in the intraoperative diagnosis of human brain gliomas has been demonstrated. It is noticeable that the recent results of the THz imaging of traumatic brain injuries in a mouse model, reported in [295, 296], also reveal the contrast between healthy brain tissues and different degrees of brain injury. This can make THz diagnosis difficult in the presence of injured brain areas, also leading to false positive diagnosis results.

The discussed papers show the bright prospects of THz technology in the intraoperative diagnosis of brain tumors, where they can yield the label-free rapid detection of unclear tumor margins [297] in order to ensure the gross-total resection of a tumor. The latter is one of the most important prognostic factors of tumor treatment [298]. The intraoperative serodiagnosis of tumors could become a very socially important application of THz technology, since nowadays it is difficult to clearly delineate tumor borders during surgery using conventional instruments of intraoperative diagnosis [10], such as pre- and intraoperative MRI [14, 15] and exogenous fluorescence spectroscopy and imaging [24, 25, 299]. THz technology could compete with modern rapidly developing instruments of neurodiagnosis, such as Raman spectroscopy and imaging [39, 40], photoacoustic imaging [43], optical coherence tomography [28, 217, 300], etc.

Despite the attractiveness of THz technology in the intraoperative label-free diagnosis of malignancies of different nosology and localization, it is still far from being ready to use in clinical practice due to the high cost and low ergonomics of THz spectroscopy and imaging systems. For
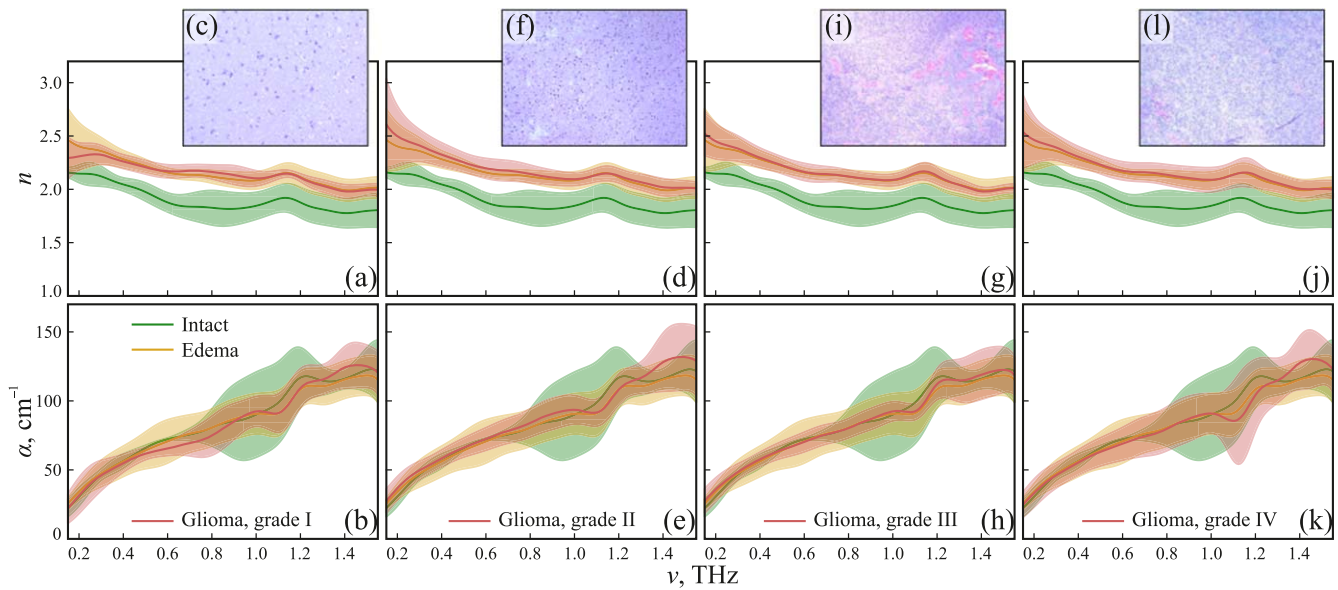
Figure 17. The THz refractive index n and absorption coefficient α, as well as representative examples of the H&E-stained histology of gelatin-embedded human brain gliomas *ex vivo* of different WHO grades: (a)–(c) grade I; (d)–(f) grade II; (g)–(i) grade III; (j)–(l) grade IV. The THz optical properties of gliomas are compared with those of intact and edematous tissues. The error bars represent a 95% confidential interval of measurements. Reproduced from [173]. CC BY 4.0.
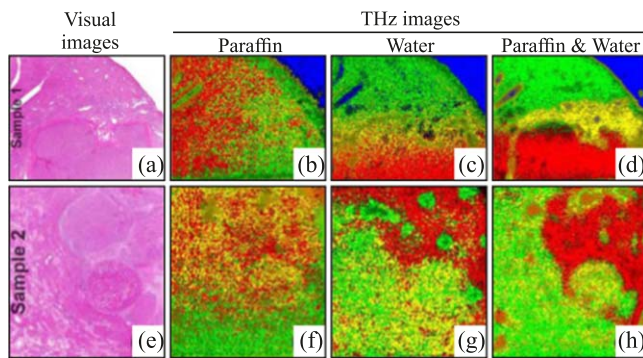

Figure 18. A comparison of the visible microscopic images and the reflection-mode TPI images of the histopathologic tissue sections (a hepatocellular carcinoma of the liver *ex vivo*) fixed in paraffin, water and paraffin emulsion, respectively, where (a)–(d) correspond to sample 1 and (e)–(h) correspond to sample 2. Reprinted with permission from [278]. © The Optical Society of America.

3.4. Accompanying histopathology

Along with the discussed approaches for non-invasive, minimally invasive and intraoperative THz diagnosis, which involve *in vivo* measurements, THz spectroscopy and imaging has the potential to aid the histopathological examination of excised tissues *ex vivo* [278, 303]. Such THz measurements of histological samples could be useful both for:

- The delineation of margins of the skin [222], breast [54] and brain [173] malignancies during the intraoperative express-histology of tissues;
- The rapid automatic distinguishing of various types of tissues in a sample in order to minimize the amount of tissues to be manually examined by a histopathologist using conventional visual microscopy [278].

The development of THz methods for aiding histology requires the optimization of the tissue fixation procedures. As shown in figure 18, the reflection-mode TPI of a hepatocellular carcinoma of the liver *ex vivo*, coming from two distinct patients, provides significantly different contrast when the samples are immersed in paraffin, water or paraffin emulsion in water [278], i.e. the contrast between the normal and malignant tissues in the THz images is higher for the tissue immersed in the emulsion of water and paraffin.

Recently, numerous approaches to the fixation of tissues have been considered for use in the THz spectral range; among them are the following:

- Formalin fixing [304];
- Gelatin embedding, which sustains the water content in tissues and preserves them from hydration/dehydration [294];
- The dehydration of tissues involving various immersion agents in order to increase the depth of THz-wave penetration into tissues and highlight the non-water-related differences between normal and pathological tissues [305–310];
- Fixation in paraffin emulsion and paraffin embedding, which reveal the non-water-related differences between normal and pathological tissues [278, 289];

example, the integration of THz reflectometry or spectroscopy into conventional neurosurgical workflow and neuroprobes [301, 302] seems to be very challenging at the moment, considering modern materials and the components of THz optics.

- Tissue freezing, which can increase the tissue probing depth and reveal the non-water-related features of tissues, including the quasi-resonant response of DNA methylation in cancer DNA [105, 271, 311].

THz spectroscopy and imaging thereby have numerous prospective applications in the diagnosis of malignant and benign neoplasms, including non-invasive, minimally invasive and intraoperative diagnosis, as well as accompanying the histological examination of tissues. Despite considerable progress in the area of THz science and technology, numerous problems still restrain the transfer of THz technology to medical clinics and hospitals. Among them are the complexity, cumbersomeness and high cost of THz instruments. These problems are to be briefly considered in the next section of this review. Nevertheless, the unique ability of THz spectroscopy and imaging to discriminate healthy and malignant tissues quickly, accurately and label-free in a number of localizations leaves no doubt that applications will be found in clinical practice in the next few decades, accompanied by rapid progress in materials, components and instrumentation.

4. Challenging problems in terahertz diagnosis of neoplasms

We mention the following problems that restrict the transfer of THz technology to medical practice:

- As compared to the visible and IR ranges, in which the study and analysis of the optical properties of tissue have been extensively performed since the middle of the 20th century [312], THz biophotonics remains a novel research direction, in which much fewer data on THz-wave–tissue interactions have accumulated [50]. Further study of the optical properties of tissue at THz frequencies, and analysis of the physical effects underlying its THz response are required in order to analyze the advantages of THz technology over other medical spectroscopy and imaging instruments.
- THz instruments remain rare, cumbersome and expensive. It would take significant research and engineering effort to develop low-cost, portable and effective THz components and instruments, required for applications in a clinical environment. In particular, we should emphasize the need for novel THz materials for the fabrication of optical elements, hard and flexible waveguides for THz-wave delivery to difficult-to-access tissues and internal organs, as well as THz emitters and detectors with improved performance.
- Most THz instruments possess diffraction-limited spatial resolution, a moderate signal-to-noise ratio and poor performance. Enhancement of the spatial resolution (beyond the diffraction limit) and the performance (up to the real-time operation) of THz spectroscopy and

imaging is of crucial importance for THz technology to compete with the existing modalities of tissue imaging.
- Improving the depth of THz-wave penetration into tissues could broaden the range of THz technology applications in malignant and benign neoplasm diagnosis. For this aim, modern methods of immersion and compression optical clearing of tissues could be adapted from the visible and IR ranges [312]; however, the capabilities of these methods at THz frequencies have not been studied enough [50].
- Finally, similarly to other label-free malignancy diagnosis techniques, significant variability is inherent to the data of the THz measurements of tissues. In order to improve the sensitivity and specificity of diagnosis, THz spectroscopy and imaging could be combined with other label-free imaging modalities [110].

Below, we briefly discuss existing attempts and prospects for solving the listed problems.

4.1. Development of novel materials for terahertz optics

Nowadays, significant attention is being paid to the development of novel materials for THz optics [46], driven in particular by the demands of THz biophotonics [50].

A number of polymers (e.g. high-density polyethylene (HDPE), polytetrauoroethylene, TPX polymethylpentene (PMP), Mylar, cyclo olefin copolymer (COC), etc), and crystals (e.g. sapphire, high-resistivity float-zone silicon (HRFZ-Si), crystalline quartz, MgO, polycrystalline diamond, etc), are already being applied to the fabrication of THz optical elements [313, 314]. However, the following list of disadvantages is inherent to the existing THz materials:

- Despite a favorable ability to produce complex-shaped polymer THz optical elements, such as lenses and waveguides, the majority of modern polymers are characterized by the significant dispersion of optical properties and a low refractive index at THz frequencies, as well as poor heat resistance.
- High-purity crystalline materials feature low THz-wave absorption, but they are difficult to manufacture and process due to their high strength, and in many cases, the anisotropy of their physical properties [301]; thus, optical elements based on crystalline media remain rather expensive.
- The limited list of THz materials (as compared to the visible and IR ranges) reduces optical system optimization capability, i.e. researchers and engineers have a limited discrete set of materials with unique fixed refractive indices for the aim of optical system synthesis and optimization [315].
- Very few types of THz material can be employed for measurements in aggressive environments, i.e. in the presence of aggressive chemical compounds, in high irradiance conditions and at high temperatures and pressures (especially concerning polymer materials) [316].

Therefore, searching for novel THz optics materials and developing novel technologies for their fabrication and processing seem to be very important topical research problems.

In our opinion, a prospective approach for the development of advanced materials for THz optics is associated with the use of composite nanostructured media, the optical properties of which could be tuned in relatively wide limits by changing their chemical/phase composition, porosity and 3D structure in order to accommodate the specific needs of THz applications. In particular, monolithic blocks of porous alumina form a representative example of this concept. In the past 15 years, the original laboratory technology for growing highly porous monolithic nanomaterials at the surface of Me–Al liquid metal alloys (Me = Hg, Ga, In, Bi, Pb) has been progressively developing [317, 318]. Currently, highly porous monolithic blocks, comprised of aluminum oxyhydroxide nanofibrils with a diameter of 4–7 nm and an average length of 120–250 nm, can be grown with a given cross section geometry, the cross-section dimension of 1–100 cm^2, and the height of about 20 cm [319, 320]. Annealing these blocks at the temperatures of 400 °C–1700 °C yields materials with a density in the range of 0.02 to $\leqslant$3 g cm^{-3} and an open porosity in the range of 99.3%–25%. The dimensions of the block decrease isotropically during annealing, while its integrity and open porosity remain unaltered [317–319]. A quantitative model of the evolution of a 3D structure in porous alumina during the annealing process is proposed in [318]. Rather low THz-wave absorption in α-Al$_2$O$_3$ (sapphire) [314], along with a wide tunability of material density, porosity, and, as a consequence, THz optical properties, make porous alumina the ideal candidate for applications in THz optics.

Furthermore, the open porosity of 3D materials consisting of alumina nanofibrils makes it possible to apply various chemical modification methods in order to create new nanocomposites and hybrid structures to manage their THz optical properties. The simplest chemical modification method is to fill the pores of 3D alumina with liquid solutions of salts, polymers, colloids or suspensions. After impregnation, the solvent is removed by evaporation and the nanoparticles precipitate inside. In this way, Al$_2$O$_3$–TiO$_2$ (titania nanoparticles in a porous alumina) [321, 322], or alumina-nickel Al$_2$O$_3$–Ni (obtained by a reduction of NiO nanoparticles during annealing in hydrogen) [323] nanocomposites were prepared and studied.

Thus, porous alumina and related nanocomposites have the ability to vary their THz optical properties in a wide range, which might make porous Al$_2$O$_3$ the ideal material platform for expanding the capabilities of THz optical system development and fabrication. Nevertheless, the problem of systematically studying the electrodynamic response of porous Al$_2$O$_3$ nanostructures at THz frequency remains unaddressed. Such a study should be performed in order to reveal the strengths and weaknesses of this material in THz optics.

4.2. Terahertz-wave delivery to difficult-to-access tissue and internal organs

Despite considerable progress in THz medical diagnosis (see section 3), the problem of THz-wave delivery to difficult-to-access tissues and internal organs of the body remains challenging due to the absence of commercially available THz waveguides and endoscopes [316]. This significantly limits the utility of THz technology for minimally invasive and intraoperative diagnosis.

The biomedical applications of THz technology pose a set of unique demands to THz waveguides. In particular, THz biophotonics require waveguides that:

- Provide high optical performance, including a single- or few-mode operation regime, low THz-wave propagation loss and small dispersion over a broad range of frequencies;
- Minimize the variations and instabilities of THz measurements caused by dynamic bending and mechanical loads, in order to make possible analysis of the absolute values of the tissue physical properties;
- Are made of biofriendly materials, featuring high chemical resistance and inertness to the *in vivo* chemical composition of biological tissues and liquids;
- Possess small outer cross-section dimensions, in order to make possible their use in minimally invasive diagnosis, endoscopy and laparoscopy.

Furthermore, modern tissue diagnosis and exposure tendencies, which increasingly combine the electromagnetic waves of different spectral ranges and the various physical principles of radiation–tissue interactions in a single instrument [265], require waveguides capable for multimodal and multispectral operation. Therefore, in this part of our review, we discuss the latest developments of THz waveguides, with an emphasis on their applicability in THz biomedical spectroscopy and imaging.

Various THz waveguiding modalities have been vigorously explored during the past few decades. Here, we briefly review the existing types of THz waveguides, fabricated using various materials featuring different cross-section geometries, and exploiting diverse physical principles of operation. In table 4, we summarize ten types of practically important THz waveguides.

The first type is a cylindrical metal tube waveguide [333] (see table 4, line 1). Electromagnetic modes are confined in a hollow core due to reflection at the 'free space–metal' interface. The finite conductivity of metals that are in direct contact with the guided wave lead to high propagation loss and the significant dispersion of metal tube waveguides, which can be partially suppressed using inner dielectric coatings [334]. In order to overcome the disadvantages of simple metal tubes, waveguides based on hollow-core dielectric tubes [330, 335, 336] (see table 4, line 2) or glass tubes with an inner metal-polystyrene (PS) coating [331] (see table 4, line 3) were developed. They are technologically reliable, use the antiresonant waveguiding (ARROW) principle, and yield a

Table 4. Examples of modern THz waveguides, exploiting different materials and guiding principles. (Lines 1–4) Courtesy of G M Katyba. (Line 5) [324] John Wiley & Sons. © 2014 WILEY-VCH Verlag GmbH & Co. KGaA, Weinheim. (Line 6) Reprinted from [326], with the permission of AIP Publishing. (Line 7) Reprinted with permission from [327]. © The Optical Society of America. (Line 8) Reprinted with permission from [328]. © The Optical Society of America. (Line 9) [325] John Wiley & Sons. © 2016 WILEY-VCH Verlag GmbH & Co. KGaA, Weinheim. (Line 10) [316] John Wiley & Sons. © 2018 WILEY-VCH Verlag GmbH & Co. KGaA, Weinheim.
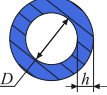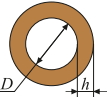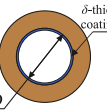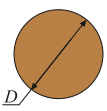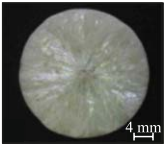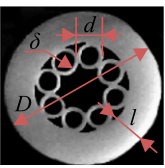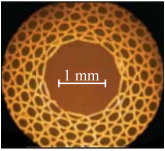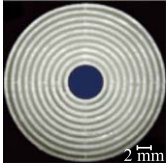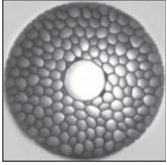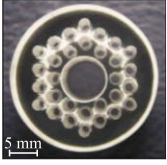
#	Waveguide	Cross-section	Dimensions	Material	Loss α, cm^{-1}	Comments	Reference
1	Metal tube waveguide		$D = 240\ \mu m \sim \lambda$	Stainless steel	<1.0 cm^{-1} at 0.65 −3.5 THz	Guiding mechanism: reflection from metal; high dispersion	[329]
2	Dielectric tube waveguide		$D = 4$ mm$\sim$5–10 · λ; $h = 2.95$ mm	Polymethyl-methacrylate (PMMA)	0.5 cm^{-1} at 0.3 −1.0 THz	Guiding mechanism: ARROW; small dispersion <10 ps THz^{-1} cm^{-1}; high absorbing cladding	[330]
3	Dielectric tube waveguide with inner coating		$D = 2.2$ mm$\sim$10 · λ; $\delta = 1.0\ \mu m$	Tube material—glass; coating material—polystyrene (PS) + Ag	0.0011 cm^{-1} at 2.5 THz	Guiding mechanism: ARROW	[331]
4	Dielectric step-index waveguide		$D = 300\ \mu m \sim \lambda/3$	Polyethylene (PE)	0.01 cm^{-1} at 0.36 THz; 0.001 cm^{-1} at 0.31 THz	Guiding mechanism: TIR	[332]
5	Foam-based step-index waveguide		$D = 5$ mm$\sim$5–10 · λ	Silk foam	$\alpha = 0.035 + 3.1\nu^2$ [THz^2]; one order less than that of a bulk material	Guiding mechanism: TIR; low dispersion 0.2 ps THz^{-1} cm^{-1}; near-unity effective refractive index	[324]
6	Revolver micro-structured waveguide		$\delta = 0.06$ mm; $d = 0.8$ mm; $D = 4.45$ mm$\sim$10 · λ; $l = 0.79$ mm	Polypropylene (PP)	0.0087 cm^{-1} at 1.9 −2.2 THz	Guiding mechanism: ARROW; low dispersion <1.0 ps THz^{-1} cm^{-1}	[326]
7	Kagome micro-structured waveguide		$D_{core} = 2.2$ mm$\sim$7 · λ; $D_{outer} = 6.8$ mm$\sim$20 · λ	PMMA	0.2 cm^{-1} at 1.0 THz; approximately 20 times lower than that of bulk PMMA	Guiding mechanism: ARROW	[327]

Table 4. (Continued.)

#	Waveguide	Cross-section	Dimensions	Material	Loss α, cm^{-1}	Comments	Reference
8	Polymer micro-structured Bragg fiber		$D_{core} = 4.5$ mm$\sim 3 \cdot \lambda$; $D_{outer} \sim 10$–$20 \cdot \lambda$; $l_{resin} = 512\ \mu$m; $l_{air} = 512\ \mu$m	3D-printed resin (PlasClear, Asiga)	0.12 cm^{-1} at 0.18 THz (i.e. at the center of bandgap)	Guiding mechanism: Bragg scattering/PBG	[328]
9	Hyperuniform microstructured waveguide		$D_{core} = 5$ mm$\sim 3 \cdot \lambda$; $D_{outer} = 22$ mm~ 10–$20 \cdot \lambda$; 250 μm thick resin bridges	3D-printed resin (VisyJet Crystal)	0.06 cm^{-1} at 0.21 THz	Guiding mechanism: Bragg scattering/PBG; the largest photonic bandgap	[325]
10	Sapphire micro-structured waveguide		$D_{core} = 7.15$ mm$\sim 20 \cdot \lambda$; $D_{outer} = 24.0$ mm$\sim 100 \cdot \lambda$	Sapphire shaped crystal	0.003 cm^{-1} at 1.2 THz	Guiding mechanism: Bragg scattering/PBG or ARROW; low dispersion 0.06$-$1.0 ps THz^{-1} cm^{-1} in the range 0.65–1.2 THz	[316]

significant reduction in propagation loss, especially for large core diameters. However, for the smaller core, tube-based ARROW waveguides possess significant material and radiation losses. For a larger core, they feature multi-mode guidance and intermodal dispersion [329], while extreme dispersion is difficult to avoid near the modal cut-off frequencies. These factors limit the reliability of data collected with tube-based waveguides in broadband THz sensing (i.e. TPS, TPI and THz time-of-flight tomography), on which the biomedical applications of THz technology often rely.

When high spatial resolution is needed in spectroscopy and imaging, plasmonic waveguides might be preferable. This type of waveguide is based on plasmonic modes, propagating along the surface of single [337, 338] or dual [339] metal wires, metal ribbons, or arrays of metal wires suspended in a free space [340]. Thanks to guidance in air, these waveguides provide low dispersion and propagation loss in a wide spectral range. In particular, the first single plasmonic waveguides [338] featured a propagation loss of $\sim$0.03 cm^{-1}, while the later dual-wire ones [339] had losses below 0.01 cm^{-1}, and were also resistant to bending. At the same time, the majority of plasmonic waveguides suffer from relatively low coupling efficiency and difficulties in handling due to weak modal confinement by the wires [341, 342]. Attempts to mitigate these difficulties by surrounding the plasmonic waveguide with a highly porous dielectric support were proposed in [343]. However, the resultant waveguides have somewhat lost their attractive optical performance due to an increase in THz-wave absorption and dispersion owing to coupling of modes to dielectric cladding. Problems of efficient plasmonic waveguide excitation and of their handling still exist, making them sub-optimal for THz biophotonics.

Another class of THz waveguide is based on a simple step-index geometry and uses various dielectric materials in the core, such as crystals (quartz, sapphire, silicon, etc) or polymers (polystyrene (PS), polyethylene (PE), polytetrafluoroethylene (PTFE), COC, etc). Such waveguides have recently been fabricated using PS, [344] PE [332] (see table 4, line 4), porous polymers [345, 346], bulk crystalline media, [347, 348] and even silk foam [324] (see table 4, line 5). Waveguidance in such structures is due to the total internal reflection (TIR) at the interface between the high refractive index core and the low refractive index cladding (in many cases, the latter is air/free space). Sub-wavelength step-index flexible THz fibers can feature very small propagation losses. For example, a fiber described in [332] has losses of 0.01 cm^{-1} around 0.3 THz. This is possible because its diameter 200 μm is much smaller than the operation wavelengths 830–970 μm, thus forcing modal fields into low-loss cladding [349]. In addition, such fibers are promising for THz biophotonics due to the biocompatibility of many crystalline and polymer media. Meanwhile, the simple cylindrical geometry of the fiber cross-section does not leave any room for further optimization, reduction of propagation loss or dispersion, restricting the utility of step-index waveguides in broadband THz measurements.

This motivated the development of THz microstructured dielectric waveguides, which allow further optimization of the dispersion and minimization of the propagation loss via judicious design of the waveguide cross-section. Among the microstructured waveguides, we single out polymer ARROW waveguides, such as:

- The revolver waveguide [326, 350, 351] (see table 4, line 6), the cross-section of which is formed by a hollow-core polymer tube containing one layer of inner capillary channels, which serve as Fabry–Perot reflectors [352];
- The Kagome waveguide [327] (see table 4, line 7), containing a hollow core and cladding formed by several layers of aperiodic cylindrical channels.

The main advantage of ARROW waveguides is associated with a wide spectral operation range, which results in both low dispersion and small propagation losses.

Another group of microstructured waveguides relies on the photonic bandgap guiding (PBG) principle, which provides modal confinement in the hollow core thanks to the Bragg scattering of electromagnetic waves in a cladding with periodic changes of the refractive index. A representative example of a PBG waveguide with complete rotational symmetry is a polymer Bragg fiber (see table 4, line 8) [328, 353, 354]. The photonic crystal cladding is formed by a periodic sequence of two media possessing different refractive indexes ('air + polymer' or 'polymer + doped polymer'). Such a periodic layered structure forms a one-dimensional (1D) photonic crystal in the radial direction, and the electromagnetic modes are confined in the waveguide core thanks to the appearance of PBG for the transverse component of the wave vector of a guided wave. For example, the Bragg fiber described in [328] provides low losses and almost zero dispersion for the fundamental mode in the narrow frequency range within PBG and seems to be a good candidate for applications in resonant surface biosensing. A favorable combination of modern polymer technologies (including the additive manufacturing of polymer microstructures) with the principles of photonic crystal waveguidance provides an opportunity to design waveguide performance via optimization of the photonic crystal geometry [355]. Thus, single- or multi-mode hollow-core THz waveguides have been proposed based on regular hexagonal, [356, 357] triangular [358] and honeycomb [359] photonic crystal lattices. In [325], a 3D-printed THz photonic crystal waveguide with a disordered photonic crystal lattice was reported (see table 4, line 9). Thanks to the disordered lattice, it has a very broad PBG, which allows the spectral range of waveguide operation to be extended. However, such waveguides also require thicker photonic crystal cladding.

Finally, we mention THz microstructured waveguides, which have recently been fabricated based on sapphire-shaped crystals using edge-defined film-fed growth (EFG)/ Stepanov technology [301]. These waveguides exploit either ARROW or PBG guidance modalities [316, 360, 361]. For example, the sapphire PBG waveguide with a hollow core and two layers of hexagonal photonic crystal lattice in cladding

[316] (see table 4, line 10) effectively supports two-mode electromagnetic-wave propagation in a wide spectral range with small dispersion (<0.1 ps THz^{-1} cm^{-1}) and propagation losses (<0.003 cm^{-1}). Microstructured sapphire waveguides combine:

- High optical performance;
- The unique physical properties of sapphire, including a high refractive index and relatively low absorption at THz frequencies; high hardness and mechanical strength; an impressive melting point and chemical resistance, even when operating at high temperatures and pressures;
- The advantages of EFG technology, i.e. the ability to produce sapphire crystal with a complex shape directly from the melt without mechanical processing (cutting, drilling, grinding and polishing).

As demonstrated in [316], a favorable combination of physical properties allows microstructured sapphire waveguides to be used for THz sensing in aggressive environments, at high temperatures and pressures. Furthermore, such waveguides are transparent in both the visible and THz ranges, which makes them attractive for applications in multispectral sensing and exposure.

We should stress that, in general, PBG waveguides tend to have larger transverse sizes than ARROW waveguides, which make the latter more attractive for THz diagnosis. In fact, ARROW waveguides resemble PBG waveguides, but contain a significantly smaller number of resonant elements in their cladding. As a result ARROW waveguides also tend to be much lossier, but feature a broader operation range compared to PBG. Unfortunately, the cladding region and core size in ARROW and PBG waveguides are usually rather large ($\sim$10–20 λ) for applications in the THz minimally invasive diagnosis of difficult-to-access tissues and internal organs.

After considering the recent developments in THz waveguides from the viewpoint of their applications in THz biophotonics, we conclude that many waveguide types are promising for biomedical applications of THz technology. Unfortunately, it is still not possible to combine all the required functionalities into a single THz waveguide, as there is always a compromise between the waveguide transversal dimensions, dispersion and propagation losses, flexibility and bandwidth. Novel THz materials and fabrication technologies, as well as significant research and engineering efforts are required to solve the demanding problems of THz-wave delivery to difficult-to-access tissues and internal organs for the aim of THz medical diagnosis.

4.3. Boosting performance of the terahertz spectroscopy and imaging of tissues

4.3.1. Improving efficiency of the terahertz emitters and detectors. Improving the efficiency of THz emitters and detectors is of crucial importance for contemporary instruments of THz spectroscopy, imaging and microscopy [46]. State-of-the-art THz emitters and detectors are based on PCAs [170, 171], parametric optical-to-THz-wave converters [362], optical rectifiers and electro-optical detectors [172],

quantum-well-, dot-, wire-, and ring-structures [363, 364], superconductor- and semiconductor-based hot-electron bolometers [163, 164], plasmonic high-electron-mobility field-effect transistors, known as TeraFETs [365], collapsing-field-domain sources [366, 367] avalanche THz emitters and picosecond switchers [368], etc, demonstrating superior performance in a wide range of operation temperatures. Here, we highlight some novel trends in the development of THz emitters and detectors, which, in our opinion, could lead to the appearance of more efficient portable, ergonomic, and even low-cost devices for THz biophotonics in the near future.

Undoubtedly, PCAs are the prevalent THz emitters and detectors, widely applied in THz spectroscopy and imaging— either pulsed or CW— thanks to their reliability, cost effectiveness, relative ease of fabrication, and flexibility in design [169]. Recently, an approach for boosting PCA performance using plasmonic or dielectric nanoantennas incorporated into a photoconductive gap has been proposed, where strong confinement of the optical pump field at the interface between nanoantennas and the semiconductor leads to enhanced light–matter interactions and to the improved thermal stability of PCA [369]. PCA-emitters and PCA-detectors with different geometries consisting of metal and dielectric nanoantennas, such as Ag nano-islands or arrays of nanoscale apertures [370], fractal antennas [371], two- and three-dimensional plasmonic gratings [372, 373], plasmonic nanocavities based on Bragg reflectors [374], metal colloidal particles deposited onto the photoconductive substrate [375], or even all-dielectric gratings [376], demonstrate impressive performance enhancement. For example, in figure 19, we show a plasmonic THz PCA with a high-aspect-ratio dielectric-embedded metal grating and compare it with an ordinary one with equal electrode topology and without a plasmonic grating [372]. One should notice that the considered plasmonic PCA provides about a three-order enhancement of the THz beam power; furthermore, it is capable of operating with low-power optical pumps.

In contrast to PCAs, the ability to radiate THz pulses without an applied bias has also been shown by focusing the laser beam onto the boundary between a metal mask and semiconductor due to the lateral photo-Dember effect (LPD) [377]. Since partially masked optical excitation produces an asymmetric carrier concentration in a semiconductor, LPD-emitters exhibit enhanced THz emission compared with conventional PD-emitters [171], but concede to modern PCAs. In order to overcome this issue, various types of multiple LPD-emitters, which could compete with modern commercially available PCAs, have been proposed [378]. Obviously, the absence of electrical bias and the rather high efficiency of LPD-emitters make them attractive for use in novel THz systems, which are extensively applied in THz medical diagnosis.

Finally, we should mention rapidly emerging novel materials, which could be used either for THz emitters or detectors in the foreseeable future. For instance, the lateral *p*–*n* junctions in FET structures with graphene layer channels and the plasmonic device structures based on carbon
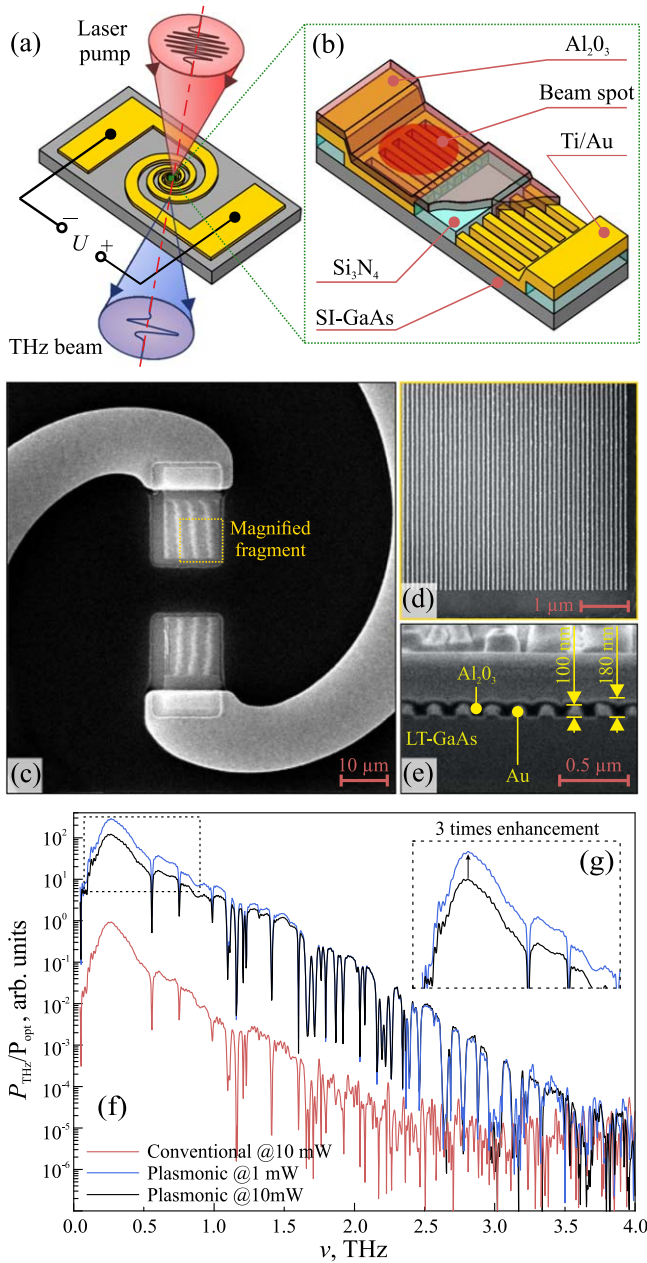
Figure 19. Plasmonic THz PCA with high-aspect-ratio dielectric-embedded metal gratings: (a), (b) a scheme of the PCA; (c) a microscopic image of the passivated photoconductive gap with log-spiral Au-electrodes and two plasmonic gratings; (d) a magnified microscopic image of the plasmonic grating; (e) a microscopic image of the plasmonic grating cross-section, which shows an Al_2O_3-coating/protection layer; (f) normalized THz power spectra P_{THz}/P_{opt} for optical pump powers of $P_{opt} = 1$ to 10 mW for both the plasmonic PCA and the ordinary one with equal topology; (g) normalized THz power spectra P_{THz}/P_{opt} for the plasmonic PCA at various optical pump powers (g). Reproduced from [372]. CC BY 4.0.

nanotubes [379], as well as gated graphene-phosphorene hybrid structures, which possess substantially non-linear current–voltage characteristics exhibiting negative differential conductivity [380, 381], represent promising candidates for THz detectors. Recently, it was shown that gated GaAs-structures with self-assembled Sn-nanothreads embedded into

a GaAs volume could potentially become efficient room-temperature THz detectors [382]. Due to the polarization sensitivity (selectivity) of its response to in-plane polarized THz radiation, such a detector might be useful for various biomedical applications [383].

4.3.2. Terahertz spectroscopy and imaging with resolution beyond the Abbe limit. Common THz spectrometers and imaging systems rely on lens- and mirror-based optics, which demonstrate limited spatial resolution, resulting from the diffraction phenomenon [384]. Ernst Abbe has shown that the spatial resolution of a diffraction-limited focusing system is determined by the following expression for the Airy disc radius [385, 386]

$$r = \frac{\lambda}{2\text{NA}} \equiv \frac{\lambda}{2n \sin \sigma_A}, \tag{7}$$

where λ is the electromagnetic wavelength, NA is the numerical aperture of an optical system, n is the refractive index of a medium, in which the electromagnetic wave is focused, and σ_A is the aperture angle. Notice that for simplicity, in equation (7), we consider the Abbe limit for a cylindrical wave. When the electromagnetic wave is focused in a free space ($n = 1.0$) by a cylindrical optical system with the widest possible aperture ($\sigma_A = \pi/2$), the Abbe limit can be reduced to $r = \lambda/2$. Since the THz diagnosis of malignancies is usually performed in the low-frequency part of the THz range (i.e. at frequencies below 1.0 THz or at wavelengths above 300 μm) due to the the higher sensitivity, lower THz-wave scattering, and lower impact of water vapor on THz measurements, the diffraction phenomenon poses a significant limitation on

- The minimal dimensions of lesions, which can be studied by THz spectroscopy and imaging;
- The accuracy of the THz delineation of tumor margins.

As shown above in section 1 and figure 3 the dimensions of the structural elements of tissues (microfibrils, separate cells, cell organelles) are usually negligibly small as compared to the THz wavelengths. This does not allow THz waves to be used for studying pathological processes in tissues at the scale of their structural elements. Therefore, only the effective THz response of tissue averaged within the radiation beam spot can be measured.

Recently, in order to mitigate the challenging problem posed by the diffraction-limited spatial resolution of THz measurements, several approaches have been proposed. Among them, first, we consider wide-aperture polymer aspherical singlets (single lenses), which provide slightly sub-wavelength resolution thanks to the good aberration correction of aspherical refractive surfaces. Such systems can achieve a spatial resolution of about 0.7–0.9 λ [384, 387], but they still obey the Abbe diffraction limit and are difficult to fabricate.

Next, we consider approaches for enhancing the resolution relying on the effects of electromagnetic field localization at a small distance ($\leqslant \lambda$) behind mesoscale dielectric or metal (plasmonic) particles—i.e. the so-called photonic or plasmonic jets [388], and photonic or plasmonic hooks [348, 389].
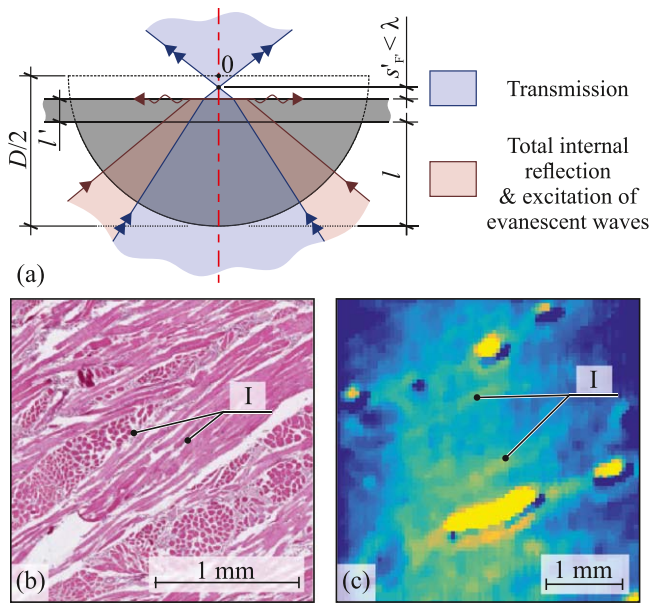
Figure 20. THz solid immersion microscopy of soft biological tissues with the spatial resolution of 0.15 λ: (a) a scheme of the caustic formation of the THz beam using a solid immersion lens; (b), (c) a H&E-stained histology and a THz image of the muscle tissue *ex vivo*, where marker I shows muscle fiber. (a) Reprinted from [109], with the permission of AIP Publishing. (b), (c) Reprinted from Springer Nature: Optics and Spectroscopy [394], 2019. With permission of Springer.

The term 'photonic nanojet' was introduced in [390], describing electromagnetic caustics generated at the shadow side of a symmetric mesoscale dielectric particle in the visible range. Later, this effect was observed experimentally and applied to THz imaging purposes [391]. Furthermore, the ability to generate a 'photonic hook' (i.e. a curved photonic jet, featuring the smallest radius of curvature ever recorded for any electromagnetic beam) behind a dielectric particle with broken symmetry was theoretically predicted [392] and experimentally observed in the THz domain [348]. The phenomena of photonic jets and hooks yield a simple approach to boosting the performance of almost any focusing system by simply placing the mesoscale dielectric particle in front of the focal point. Such optical systems can provide a spatial resolution of about 0.3–0.5 λ, which is slightly beyond the Abbe diffraction limit. Nevertheless, difficulties in sample handling at the focal plane, in close proximity behind a dielectric particle, remain unaddressed, thus restraining the application of the described imaging modality in THz biophotonics.

Another sub-wavelength-resolution THz imaging method relies on the so-called solid immersion effect [393], i.e. a reduction in the dimensions of the electromagnetic beam caustic when it is formed in an evanescent field volume (in a free space at a small distance, $\leqslant \lambda$, behind a medium with a high refractive index). THz solid immersion microscopy was introduced in [393] and then adapted to the imaging of soft biological tissues *ex vivo* in [109], providing an advanced spatial resolution of 0.15 λ and high energy throughout. THz solid immersion microscopy requires a small working

distance ($\sim \lambda/2$) between the high-refractive index material and the object of interest. In [109], the problem of tissue handling at the focal plane was solved by applying a configuration of the solid immersion lens shown in figure 20(a); here, the solid immersion resolution enhancer is comprised of two parts—a hypohemisphere and a plane window both made of HRFZ-Si with $n_{\text{HRFZ}-\text{Si}} = 3.41$. On the one hand, these two components serve as separate mechanical elements, one of which (the hypohemisphere) is rigidly fixed, while the other (the window) serves as a sample holder being mounted onto an *xy* motorized translation stage; on the other hand, they form a unitary optical element—a HRFZ-Si hemisphere. The described THz solid immersion lens was applied to the reflection-mode imaging of different biological objects, among them a leaf, cell-spheroids, connective fibrous tissues of the breast *ex vivo* (see figure 5) [109], and muscle tissues of the tongue *ex vivo* (see figures 20(b) and (c)) [394]. The observed images reveal the sub-wavelength structural elements of tissues, promising new applications of the THz solid immersion microscopy in biology and medicine.

The spatial resolution of digital holography [395] and synthetic aperture imaging [396, 397] is determined by a scheme of interferometric pattern detection and by a data processing routine applied to the inverse problem solution [398–400]. This technique allows one to obtain close-to-wavelength or slightly sub-wavelength resolution THz images; for example, the ability to achieve 1.0–1.2 λ-resolution THz synthetic aperture imaging was demonstrated in [401, 402]. Furthermore, they are capable of achieving real-time operation regimes [400]. THz digital holography methods were applied for imaging the whole insect [401] and structure of insect wings [402, 403], breast tissue cancer [404] and human hepatocellular carcinoma [405], as well as for controlling the dehydration dynamics in tissues [406]. Slightly sub-wavelength resolution and a high acquisition rate are the advantages of holographic THz imaging. Nevertheless, in many cases, image reconstruction in holography requires the solution of a complicated inverse ill-posed problem, which is usually rather time-consuming.

Finally, we consider THz scanning-probe near-field microscopy, which provides an impressive spatial resolution thanks to the strongly sub-wavelength confinement of electromagnetic waves on a scanning probe [407, 408]. The resolution of scanning-probe microscopy depends on the diameter of a sub-wavelength aperture (see figures 21(a) and (b)), or the curvature of a sub-wavelength metal or dielectric cantilever (see figures 21(c) and (d)), placed in front of the object of interest. In [409], the advanced 10^{-3} λ-resolution of THz scanning-probe near-field microscopy was reported. In spite of the above-mentioned advantages, THz scanning-probe near-field microscopy suffers from very low energy efficiency due to the effects of THz-wave scattering on a sub-wavelength probe. In [410, 411], the problem of low energy was partially mitigated using bull's-eye or bow-tie apertures, correspondingly. As near-field microscopy implies a very small working distance between the probe/aperture and the object, its application for studying biological objects appears to be rather challenging. Nevertheless, in [412], THz scanning-probe
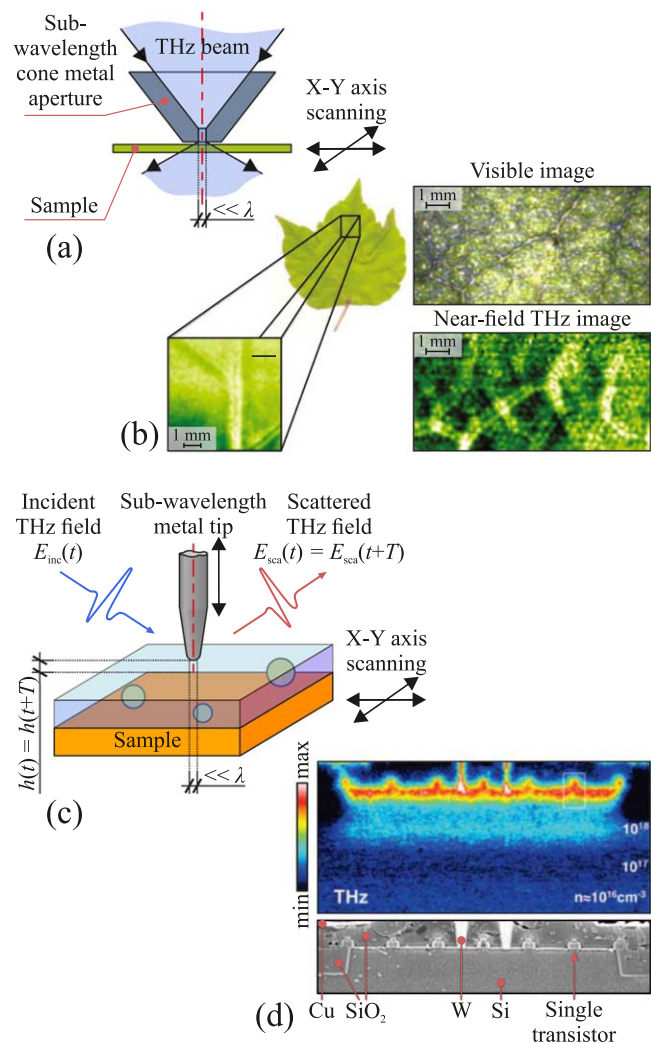
Figure 21. Representative examples of two distinct types of the THz near-field scanning-probe microscopy: (a), (b) a scheme of the 0.15 λ-resolution THz microscope based on a cone metal aperture/ diaphragm, as well as results of its application for the imaging of a leaf, respectively; (c), (d) a scheme of the 10^{-3} λ-resolution THz microscope based on a metal tip/cantilever, as well as results of its application for the imaging of a microelectronic device. (a), (b) Reprinted from [412], with the permission of AIP Publishing. (d) Reprinted with permission from [409]. Copyright 2008 American Chemical Society.

near-field microscopy was applied to the imaging of a leaf using a conical diaphragm (see figures 21(a) and (b)), while in [349], THz images of 20 μm thick histological slices of human breast tumors were obtained using a bull's-eye aperture coupled to a PE fiber. Nevertheless, scanning-probe microscopy still requires a high-power emitter and sensitive detectors in order to collect a low-intensity scattered THz field. Such emitters and detectors remain rare, expensive and cumbersome, making the THz scanning-probe near-field microscopy an instrument of laboratory research.

Some of the above-mentioned techniques have already been applied to the imaging of biological tissues, and others remain instruments of laboratory research. It would take time to adapt them to the imaging of biological tissues, as well as to transfer them to clinical practice.

4.3.3. Improving speed of the terahertz-data acquisition. The speed of THz-data acquisition in TPS and TPI is limited by the power of the emitter, as well as by the sensitivity and time response of the detector. Modern TPS requires tens of seconds (or, in certain cases, several minutes) to detect the THz waveform with the appropriate signal-to-noise ratio and dynamic range. In turn, the TPI implies a raster scan of the sample surface by a focused THz beam, while the THz waveform is detected for each point of the sample surface; this leads to a dramatic increase in the THz image acquisition time, i.e. up to tens of minutes (or even several hours) depending on the image dimensions or spatial step. Obviously, such a slow performance restricts the potential of THz pulse systems in clinical applications, which usually require close-to-real-time operation. In order to mitigate the difficulty posed by pure data acquisition, nowadays, numerous approaches are being developed for the needs of rapid or real-time TPS and TPI.

The first approach is mechanical sampling using an optical delay line with a high scanning rate. Pioneer works on this topic were dedicated to galvanometer-based delay lines, followed by rotating prisms in the optical path. Then the design of an aluminum optical delay stage was reported based on a circular involute reflector, which includes the linear operation, the high repetition rate of 300–400 Hz, the scanning range of more than 1 m, and the absence of backslash error [413]. The authors state that its characteristics can be adjusted by the proper choice of a reflector radius and DC motor. Recently, the authors of [414, 415] demonstrated the implementation of a fast rotary optical delay line, which does not require the use of a lock-in amplifier, is comprised of a rotating blade, and which was reported to provide the acquisition rate of 192 Hz.

The second approach implies optical sampling (OS) by introducing a variable time-delay between the pump and probe beams, i.e. OS by cavity tuning [416], which controls the time-delay by tuning the repetition rate of the femtosecond laser. Also, the high speed of THz-data acquisition can be achieved by an electronically controlled OS [417], which uses two femtosecond lasers, while the difference between their repetition rates is controlled using a piezoelectric transducer. A promising approach is polarization-controlled OS using a single femtosecond laser [418], as well as an asynchronous OS [419, 420].

The third approach proposes a THz quasi time-domain spectrometer (THz-QTDS), in which the femtosecond laser is replaced by a simple multimode laser diode operating at 659 nm and which is competitive to conventional TPS [421]. Recently, a fiber-coupled THz-QTDS system driven by a laser with the wavelength of 1550 nm was also demonstrated, showcasing a bandwidth greater than 1.5 THz and a dynamic range of 60 dB [422]. By merging the TPS and TPI with semiconductor laser technology, one would expect significant benefits for the real-life applications of THz technology.

Finally, novel principles of THz image formation could improve the data acquisition speed [400]. In particular, the multiplexing of THz-wave photoconductive detectors on a single chip with their further electrical or optical read-out
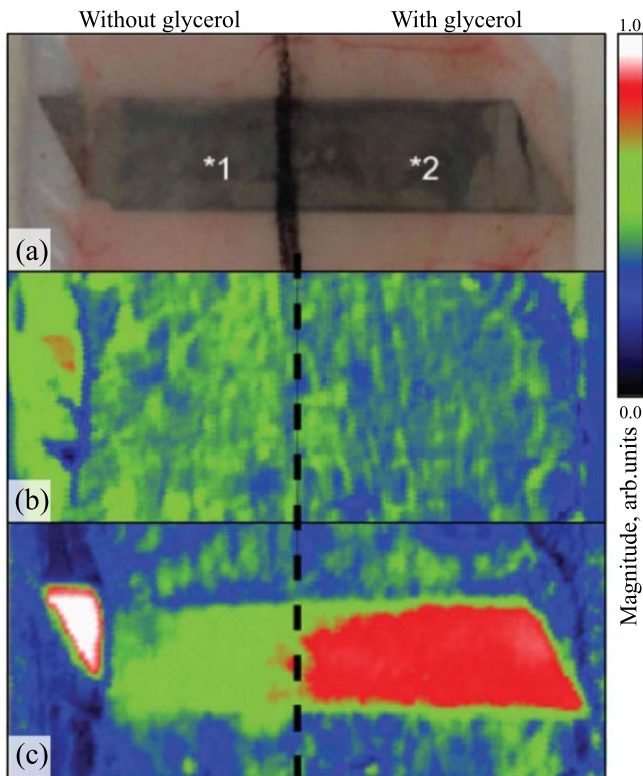
Without glycerol   With glycerol   1.0

Figure 22. A representative example of the THz-wave penetration depth enhancement using the immersion optical clearing, where glycerol is applied to a 224 μm thick abdomen skin tissue extracted surgically from a mouse: (a) a visual image of the sample; (b), (c) THz images of the knife below a tissue using peak-to-peak values of the entire THz time-domain waveform or of the THz waveform part in the delay range starting from 7.5 ps, respectively. Reproduced with permission from [436].

[423, 424], or THz holography and compressed sensing [399, 425, 426] seem to be very promising for the THz imaging of biological objects.

4.4. Improving depth of the terahertz wave penetration in tissues

The high absorption of THz radiation by water contained in tissues is a severe reason for the reduction in the penetration depth and corresponding applicability of THz techniques in biophotonics. One promising solution to this problem is immersion optical clearing [12, 427, 428]. Among other approaches to increase penetration depth, such as tissue freezing [306, 429–431], dehydration by heating [432], formalin fixing [304], paraffin embedding [274, 289] and lyophilization [305], immersion optical clearing features essential benefits, i.e. it is rather low-cost and can be applied *in vivo*.

This method is based on the application of specific biocompatible chemical agents to a tissue, which leads to water diffusion from the tissue and agent diffusion into it caused by agent–tissue interaction with the final substitution of either free or weakly bound water by an agent. This process provides the temporal and reversible reduction of water content, i.e. dehydration and reduction of dielectric contrast, that is to

say refractive index matching, in tissues. The latter generally forms the principle of immersion optical clearing in the visible and IR ranges, associated with the significant suppression of light scattering thanks to the achievement of tissue spatial homogeneity in the area of agent application. Tissue dehydration is also important because of tissue shrinkage and better ordering [12, 312]. In the THz range, where water strongly absorbs radiation, the reduction of water content is considered to be more important, leading to the increased depth of THz-wave penetration in tissues [433–435]. For example (see figure 22), glycerol, which has a lower absorption coefficient compared to water, enables the change of the THz optical properties of tissues and the higher contrast of the TPI of the metal target placed behind the skin tissue sample, when the appropriate signal processing is applied [436]. One should also keep in mind that immersion optical clearing leads to a reduction of the effective refractive index of the considered tissue layer, thus reducing the Fresnel reflectivity and corresponding losses in THz measurement systems.

For successful immersion optical clearing, penetration enhancing agents (PEAs), which temporarily change the tissue structure and content, should be biocompatible and non-toxic, possess hyperosmotic status, a high diffusion coefficient, and low THz-wave absorption. Fortunately, a significant variety of substances and chemicals meet such requirements and demonstrate immersion clearing ability. We list a few of them: glycerol, polyethylene glycol, propylene glycol, ethylene glycol, dimethyl sulfoxide, etc. Despite being commonly used in the visible and IR ranges, at present, there is a lack of data about their THz optical properties, mainly the refractive index and absorption coefficient. Therefore, the selection of an appropriate PEA is not a simple task, and several works have concentrated on the study of the THz and diffusion properties of PEAs (e.g. see [309, 310, 312, 437]). Nevertheless, to the best of our knowledge, a full-blown study of THz-PEAs and their interaction with different biological objects (both *ex vivo* and *in vivo*) has not been done yet.

Optical immersion clearing is typically described by the diffusion equation [438], which in the first-order approximation has the solution

$$C_a(t) = 1/2 \int_0^d C_a(x,t)dx \cong C_{a0}(1 - \exp(-t/\tau)), \quad (8)$$

where $C_a(t)$ is the volume-averaged concentration of an agent at a particular diffusion time t, x is the spatial coordinate along the sample depth, d is the sample thickness, and τ is the characteristic diffusion time, related to the diffusion coefficient $D_f \sim 1/\tau$. The diffusion coefficient and the characteristic diffusion time determine the rate of the clearing process and characterize the applicability of PEA to control the properties of a particular tissue. Diffusion kinetics may differ for healthy and diseased tissues [439–444], thus forming the basis for additional characterization of a pathology. Therefore, knowledge of these parameters is rather essential. Due to the absence of direct methods for their measurement, one needs indirect approaches, based on, for example, weight measurements, OCT, visible light penetration, or THz

spectroscopy, as well as an appropriate physical model, which connects the corresponding measured parameters with the diffusion parameters [445, 446]. Recent studies demonstrate the complex kinetics of tissue clearing and show that the diffusion of PEA as well as the osmotic pressure and water flow should be included in such models [447, 448].

We briefly characterize other common tissue dehydration and THz-wave penetration enhancing methods. Tissue freezing is quite a simple method for *ex vivo* THz measurements. Despite conventional freezing leading to ice crystal formation and destroying the tissue structure [50], one can apply lyophilization—the snap freezing of a tissue at low-pressure and in low-temperature conditions—which retains the tissue structure [311]. Paraffin-embedding is a common and well-known method in biology and medicine applied to microscopy and morphology. Being used to fix the tissue samples, it also provides the substitution of water, which is remarkable for THz measurements, since it leads to an increase of the penetration depth [289]. In connection with novel developments in THz microscopy (see section 4.3.2), this method of tissue preparation is able to provide more precise data about specific cells and their agglomerations. Similar to immersion optical clearing, compression optical clearing is also applicable *in vivo*. It is based on the temporal local dehydration of tissue and more close packing of its components due to mechanical squeezing or stretching [186, 449]. Unfortunately, this method is only relevant for soft tissues. According to studies from [186], the average refractive index of human skin undergoes significant changes of over 10% when mechanical pressure of 1.5 to 3.5 N cm^{-2} is applied (see also [450]). Such results should be accounted for in all contact THz measurements, since they are very sensitive to the physical force applied to a subject and to the occlusion effects.

4.5. Multiplexing different label-free imaging modalities to improve tissue characterization

Combining THz spectroscopy and imaging with other modern label-free imaging modalities can significantly improve the efficiency of benign and malignant neoplasm diagnosis. By employing electromagnetic waves of different frequency ranges, we are able to collect information about the various specific endogenous markers of a neoplasm due to the diverse mechanisms of electromagnetic-wave–tissue interaction in different spectral ranges. Furthermore, by combining rather low-resolution THz imaging with modern imaging modalities in the visible and IR ranges, which feature a much higher spatial resolution thanks to the much smaller wavelengths, one can improve the quality of the merged image [110, 250]. For example, in [251], reflection-mode TPI was combined with polarization-sensitive optical imaging and applied to study the freshly excised BCC-samples *ex vivo* (see figure 23). TPI allows the tumor margins to be delineated, while co- and cross-polarized optical images provide information about the skin tissue structure (i.e. epidermis, collagen, sebaceous glands and hair follicles). In [78], the prospect of combining THz spectroscopy and imaging with other optical techniques for studying glycated biological tissues is discussed.
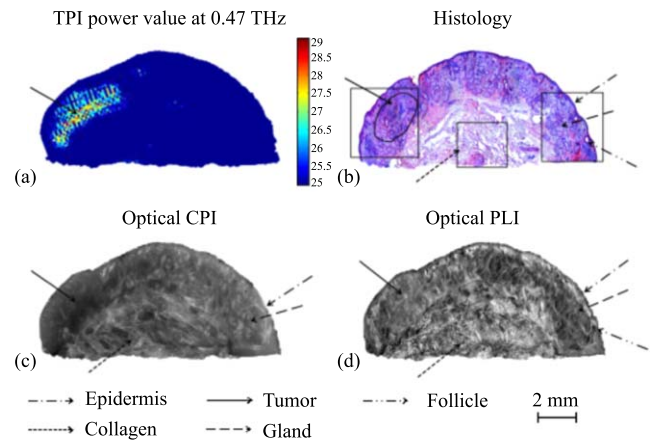

Figure 23. An example of combining tissue imaging in the visible and THz ranges for the diagnosis of BCC *ex vivo*: (a) a TPI image at a frequency of 0.47 THz; (b) an H&E-stained histological image; (c) a cross-polarized optical image (CPI); (d) a polarized light optical image (PLI). [251] John Wiley & Sons. © 2016 Wiley Periodicals, Inc.

Multimodal diagnosis principles seem to be very promising in the intraoperative neurodiagnosis of tumors. In particular, the authors of [291] compared the results of TPI, MRI, OCT and fluorescence imaging relying on green fluorescence protein (GFP) and protoporphyrin IX (PpIX), white light imaging and H&E-stained histology using a unitary whole brain sample *ex vivo* from a mouse with a glioma model. Tumors were clearly seen on the GFP and PpIX fluorescence images, though weakly developed tumors demonstrated low fluorescence intensity; OCT images provided detailed information about the brain tissue structure, but distinct tumor regions could not be visualized. In [451], an approach for intraoperative neurodiagnosis based on TPS and OCT was proposed; it was shown that TPS can be applied to differentiate gliomas and normal brain tissues, while OCT can be utilized to discriminate between high-grade and low-grade gliomas.

Although there is a limited number of papers dedicated to combining THz technology with other modalities of tissue spectroscopy and imaging, it appears advantageous to couple THz technology with thermography [452], multi-spectral imaging [26, 453], OCT [454], high frequency ultrasound imaging [455], Raman spectroscopy [456], polarization imaging [110, 251] and multi-photon microscopy methods [457].

5. Conclusion

In this review, we have tried to highlight the recent, remarkable developments and research results as well as urgent problems in the field of the THz diagnosis of malignant and benign neoplasms. We draw the attention of our readers to the origin of interest in this field, which is based on THz-wave–tissue interaction, and discuss the existing methods and models for its description. Additionally, we touch on the problem of studying the biological effects of tissue exposure to THz waves, where the strong diversity of the results has stimulated the active experimental and theoretical

investigations. The main development of THz technology in recent years, including application to neoplasm studies, is closely related to the increased technical opportunities of modern THz instruments and methods of signal processing. We review the most common of them, highlighting the relevant problems regarding biological tissue measurements, such as the low penetration depth and delivery of THz radiation to difficult-to-access organs and tissues. The summarized results of the THz measurements of healthy (intact) tissues, malignant and benign neoplasms with different nosology and localization demonstrate the differences in their THz dielectric properties, as well as the various origins of the observed contrasts, connected with the water content and structural changes in tissues. The review of existing and developing THz methods and systems for aiding histology, non-invasive, minimally invasive and intraoperative diagnosis emphasizes the continuous expansion of THz technology toward clinical practice. Nevertheless, a huge amount of problems will have to be solved in the future.

Acknowledgments

ORCID iDs

K I Zaytsev ⓘ https://orcid.org/0000-0002-1067-0978
M A Shchedrina ⓘ https://orcid.org/0000-0002-4265-012X

References

[1] Huang Z et al 2016 Breast cancer incidence and mortality: trends over 40 years among women in Shanghai Chin. Ann. Oncol. 27 1129–34

[2] Karimkhani C et al 2017 Global skin disease morbidity and mortality: an update from the global burden of disease study JAMA Dermatol. 153 406–12

[3] Ostrom Q, Gittleman H, Truitt G, Boscia A, Kruchko C and Barnholtz-Sloan J 2018 CBTRUS statistical report: primary brain and other central nervous system tumors diagnosed in the United States in 2011–2015 Neuro Oncol. 20 iv1–86

[4] Bray F, Ferlay J, Soerjomataram I, Siegel R, Torre L and Jemal A 2018 Global cancer statistics 2018: GLOBOCAN estimates of incidence and mortality worldwide for 36 cancers in 185 countries CA Cancer J. Clin. 68 394–424

[5] Siegel R, Miller K and Jemal A 2019 Cancer statistics CA Cancer J. Clin. 69 7–34

[6] Rogers H, Armbrecht E, Coldiron B, Albertini J, McDonald M, Dinehart S, Hendi A, Hruza G, Fosko S and Moody B 2014 Properly selected skin cancer treatments are very effective J. Investig. Dermatol. 134 1133–5

[7] Barnhill R, Fine J, Roush G and Berwick M 1996 Predicting five-year outcome for patients with cutaneous melanoma in a population-based study Cancer 78 427–32

[8] Arumi-Uria M, McNutt N and Finnerty B 2003 Grading of atypia in nevi: correlation with melanoma risk Modern Pathol. 16 764–71

[9] Louis D, Perry A, Reifenberger G, von Deimling A, Figarella-Branger D, Cavenee W K, Ohgaki H, Wiestler O D, Kleihues P and Ellison D W 2016 The 2016 World Health Organization classification of tumors of the central nervous system: a summary Acta Neuropathol. 131 803–20

[10] Garzon-Muvdi T, Kut C, Li X and Chaichana K 2017 Intraoperative imaging techniques for glioma surgery Future Oncol. 13 1731–45

[11] Tuchin V 2013 Handbook of Coherent-Domain Optical Methods (New York: Springer) (https://doi.org/10.1007/978-1-4614-5176-1)

[12] Tuchin V 2015 Tissue Optics: Light Scattering Methods and Instruments for Medical Diagnosis 3rd edn (Bellingham, WA: SPIE Press) (https://doi.org/10.1117/3.1003040)

[13] Tuchin V 2016 Handbook of Optical Biomedical Diagnostics 2nd edn (Bellingham, WA: SPIE Press) (https://doi.org/10.1117/3.2219603)

[14] Mehdorn H, Schwartz F, Dawirs S, Hedderich J, Dorner L and Nabavi A 2011 High-field iMRI in glioblastoma surgery: improvement of resection radicality and survival for the patient? Intraoperative Imaging ed M N Pamir, V Seifert and T Kiris (Wien: Springer) (https://doi.org/10.1007/978-3-211-99651-5_16)

[15] Schatlo B, Fandino J, Smoll N, Wetzel O, Remonda L, Marbacher S, Perrig W, Landolt H and Fathi A-R 2015 Outcomes after combined use of intraoperative MRI and 5-aminolevulinic acid in high-grade glioma surgery Neuro Oncol. 17 1560–7

[16] Rubegni P, Burroni M, Perotti R, Fimiani M, Andreassi L, Cevenini G, Dell'Eva G and Barbini P 2002 Digital dermoscopy analysis and artificial neural network for the differentiation of clinically atypical pigmented skin lesions: a retrospective study J. Investig. Dermatol. 119 471–4

[17] Esteva A, Kuprel B, Novoa R, Ko J, Swetter S, Blau H and Thrun S 2017 Dermatologist-level classification of skin cancer with deep neural networks Nature 542 115–8

[18] Lu G and Fei B 2014 Medical hyperspectral imaging: a review J. Biomed. Opt. 19 010901

[19] Patel R, Khan A, Kamionek M, Kandil D, Quinlan R and Yaroslavsky A 2013 Delineating breast ductal carcinoma using combined dye-enhanced wide-field polarization imaging and optical coherence tomography J. Biophotonics 6 679–86

[20] Patel R, Khan A, Quinlan R and Yaroslavsky A 2014 Polarization-sensitive multimodal imaging for detecting breast cancer Cancer Res. 74 4685–93

[21] Yaroslavsky A, Feng X and Neel V 2017 Optical mapping of nonmelanoma skin cancers-a pilot clinical study Lasers Surg. Med. 49 803–9

[22] Yaroslavsky A, Feng X, Muzikansky A and Hamblin M 2019 Fluorescence polarization of methylene blue as a

quantitative marker of breast cancer at the cellular level *Sci. Rep.* **9** 940

[23] Stummer W, Pichlmeier U, Meinel T, Wiestler O, Zanella F and Reulen H-J 2006 Fluorescence-guided surgery with 5-aminolevulinic acid for resection of malignant glioma: a randomised controlled multicentre phase III trial *Lancet Oncol.* **7** 392–401

[24] Pustogarov N, Panteleev D, Goryaynov S, Ryabova A, Rybalkina E, Revishchin A, Potapov A and Pavlova G 2017 Hiding in the shadows: CPOX expression and 5-ALA induced fluorescence in human glioma cells *Mol. Neurobiol.* **54** 5699–708

[25] Potapov A A *et al* 2016 Laser biospectroscopy and 5-ALA fluorescence navigation as a helpful tool in the meningioma resection *Neurosurg. Rev.* **39** 437–47

[26] Chernomyrdin N V *et al* 2019 Differentiation of basal cell carcinoma and healthy skin using multispectral modulation autofluorescence imaging: a pilot study *J. Biomed. Photon. Eng.* **5** 010302

[27] de Boer J, Leitgeb R and Wojtkowski M 2017 Twenty-five years of optical coherence tomography: the paradigm shift in sensitivity and speed provided by Fourier domain OCT *Biomed. Opt. Express* **8** 3248–80

[28] Vasefi F, MacKinnon N, Farkas D and Kateb B 2016 Review of the potential of optical technologies for cancer diagnosis in neurosurgery: a step toward intraoperative neurophotonics *Neurophotonics* **4** 011010

[29] Yi-Quan X Y, Mo Y-Q, Wen M-J, Cheng S-T, Huo X-J and Chen Q 2018 Optical coherence tomography for the diagnosis of malignant skin tumors: a meta-analysis *J. Biomed. Opt.* **23** 020902

[30] Yashin K S *et al* 2019 Cross-polarization optical coherence tomography for brain tumor imaging *Frontiers Oncol.* **9** 201

[31] Tromberg B, Shah N, Lanning R, Cerussi A, Espinoza J, Pham T, Svaasand L and Butler J 2000 Non-invasive in vivo characterization of breast tumors using photon migration spectroscopy *Neoplasia* **2** 26–40

[32] Cerussi A, Shah N, Hsiang D, Durkin A, Butler J and Tromberg B 2006 In vivo absorption, scattering, and physiologic properties of 58 malignant breast tumors determined by broadband diffuse optical spectroscopy *J. Biomed. Opt.* **11** 044005

[33] Kholodtsova M, Daul C, Loschenov V and Blondel W 2016 Spatially and spectrally resolved particle swarm optimization for precise optical property estimation using diffuse-reflectance spectroscopy *Opt. Express* **24** 12682–700

[34] Kienast Y, von Baumgarten M, Fuhrmann L, Klinkert W, Goldbrunner R, Herms J and Winkler F 2010 Real-time imaging reveals the single steps of brain metastasis formation *Nat. Med.* **16** 116–22

[35] Lahiri B, Bagavathiappan S, Jayakumar T and Philip J 2012 Medical applications of infrared thermography: a review *Infrared Phys. Technol.* **55** 221–35

[36] Cao Q, Zhegalova N, Wang S, Akers W and Berezin M 2013 Multispectral imaging in the extended near-infrared window based on endogenous chromophores *J. Biomed. Opt.* **18** 101318

[37] Wilson R, Nadeau K, Jaworski F, Rowland R, Nguyen J, Crouzet C, Saager R, Choi B, Tromberg B and Durkin A 2014 Quantitative short-wave infrared multispectral imaging of in vivo tissue optical properties *J. Biomed. Opt.* **19** 086011

[38] Jermyn M, Mok K, Mercier J, Desroches J, Pichette J, Saint-Arnaud K, Bernstein L, Guiot M-C, Petrecca K and Leblond F 2015 Intraoperative brain cancer detection with Raman spectroscopy in humans *Sci. Transl. Med.* **7** 274ra19

[39] Jermyn M, Desroches J, Mercier J, St-Arnaud K, Guiot M-C, Leblond F and Petrecca K 2016 Raman spectroscopy detects

distant invasive brain cancer cells centimeters beyond MRI capability in humans *Biomed. Opt. Express* **7** 5129–37

[40] Orringer D *et al* 2017 Rapid intraoperative histology of unprocessed surgical specimens via fibre-laser-based stimulated Raman scattering microscopy *Nat. Biomed. Eng.* **1** 0027

[41] Itoh A, Ueno E, Tohno E, Kamma H, Takahashi H, Shiina T, Yamakawa M and Matsumura T 2006 Breast disease: clinical application of US elastography for diagnosis *Radiology* **239** 341–50

[42] Galanzha E, Shashkov E, Kelly T, Kim J-W, Yang L and Zharov V 2009 In vivo magnetic enrichment and multiplex photoacoustic detection of circulating tumour cells *Nat. Nanotechnol.* **4** 855–60

[43] Kircher M *et al* 2012 A brain tumor molecular imaging strategy using a new triple-modality MRI-photoacoustic-Raman nanoparticle *Nat. Med.* **18** 829–34

[44] Galanzha E and Zharov V 2012 Photoacoustic flow cytometry *Methods* **57** 280–96

[45] Margueritat J, Virgone-Carlotta A, Monnier S, Delanoe-Ayari H, Mertani H, Berthelot A, Martinet Q, Dagany X, Riviere C, Rieu J-P and Dehoux T 2019 High-frequency mechanical properties of tumors measured by Brillouin light scattering *Phys. Rev. Lett.* **122** 018101

[46] Lee Y-S 2009 *Principles of Terahertz Science and Technology* (New York: Springer) (https://doi.org/10.1007/978-0-387-09540-0)

[47] Rubens H and Nichols E 1897 Heat rays of great wave length *Phys. Rev.* **4** 314–23

[48] Auston D 1975 Picosecond optoelectronic switching and gating in silicon *Appl. Phys. Lett.* **26** 101–3

[49] Yang X, Zhao X, Yang K, Liu Y, Liu Y, Fu W and Luo Y 2016 Biomedical applications of terahertz spectroscopy and imaging *Trends Biotechnol.* **34** 810–24

[50] Smolyanskaya O *et al* 2018 Terahertz biophotonics as a tool for studies of dielectric and spectral properties of biological tissues and liquids *Prog. Quantum Electron.* **62** 1–77

[51] Tuchin V 2015 Tissue optics and photonics: biological tissue structures *J. Biomed. Photon. Eng.* **1** 3–21

[52] Møller U, Cooke D G, Tanaka K and Jepsen P U 2009 Terahertz reflection spectroscopy of Debye relaxation in polar liquids *J. Opt. Soc. Am.* B **26** A113–25

[53] DiGirolamo M and Owens J L 1976 Water content of rat adipose tissue and isolated adipocytes in relation to cell size *Am. J. Physiol.* **231** 1568–72

[54] Ashworth P, Pickwell-MacPherson E, Provenzano E, Pinder S, Purushotham A, Pepper M and Wallace V 2009 Terahertz pulsed spectroscopy of freshly excised human breast cancer *Opt. Express* **17** 12444–54

[55] Oh S *et al* 2014 Study of freshly excised brain tissues using terahertz imaging *Biomed. Opt. Express* **5** 2837–42

[56] Parrott E, Sy S, Blu T, Wallace V and Pickwell-MacPherson E 2011 Terahertz pulsed imaging in vivo: measurements and processing methods *J. Biomed. Opt.* **16** 106010

[57] Zaytsev K, Gavdush A, Chernomyrdin N and Yurchenko S 2015 Highly accurate in vivo terahertz spectroscopy of healthy skin: variation of refractive index and absorption coefficient along the human body *IEEE Trans. Terahertz Sci. Technol.* **5** 817–27

[58] Pickwell E, Cole B, Fitzgerald A, Wallace V and Pepper M 2004 Simulation of terahertz pulse propagation in biological systems *Appl. Phys. Lett.* **84** 2190–2

[59] Pickwell E, Fitzgerald A, Cole B, Taday P, Pye R, Ha T, Pepper M and Wallace V 2005 Simulating the response of terahertz radiation to basal cell carcinoma using ex vivo spectroscopy measurements *J. Biomed. Opt.* **10** 064021

[60] Walker G, Berry E, Smye S, Zinov'ev N, Fitzgerald A, Miles R, Chamberlain M and Smith M 2004 Modelling the

propagation of terahertz radiation through a tissue simulating phantom *Phys. Med. Biol.* **49** 1853–64

[61] Pickwell E, Cole B, Fitzgerald A, Pepper M and Wallace V 2004 *In vivo* study of human skin using pulsed terahertz radiation *Phys. Med. Biol.* **49** 1595–607

[62] Ney M and Abdulhalim I 2011 Modeling of reflectometric and ellipsometric spectra from the skin in the terahertz and submillimeter waves region *J. Biomed. Opt.* **16** 067006

[63] Fitzgerald A, Pickwell-MacPherson E and Wallace V 2014 Use of finite difference time domain simulations and Debye theory for modelling the terahertz reflection response of normal and tumour breast tissue *PLoS One* **9** 1–9

[64] Truong B, Tuan H, Wallace V, Fitzgerald A and Nguyen H 2015 The potential of the double Debye parameters to discriminate between basal cell carcinoma and normal skin *IEEE Trans. Terahertz Sci. Technol.* **5** 990–8

[65] Truong B, Tuan H, Fitzgerald A, Wallace V and Nguyen H 2015 A dielectric model of human breast tissue in terahertz regime *IEEE Trans. Biomed. Eng.* **62** 699–707

[66] Ronne C, Thrane L, Astrand P-O, Wallqvist A, Mikkelsen K and Keiding S 1997 Investigation of the temperature dependence of dielectric relaxation in liquid water by THz reflection spectroscopy and molecular dynamics simulation *J. Chem. Phys.* **107** 5319–31

[67] Kindt J and Schmuttenmaer C 1996 Far-infrared dielectric properties of polar liquids probed by femtosecond terahertz pulse spectroscopy *J. Phys. Chem.* **100** 10373–9

[68] Asaki M, Redondo A, Zawodzinski T and Taylor A 2002 Dielectric relaxation of electrolyte solutions using terahertz transmission spectroscopy *J. Chem. Phys.* **116** 8469–82

[69] Yurchenko S and Zaytsev K 2014 Spectroscopy of Nafion in terahertz frequency range *J. Appl. Phys.* **116** 113508

[70] Truong B, Tuan H, Kha H and Nguyen H 2013 Debye parameter extraction for characterizing interaction of terahertz radiation with human skin tissue *IEEE Trans. Biomed. Eng.* **60** 1528–37

[71] Tielrooij K J, Paparo D, Piatkowski L, Bakker H J and Bonn M 2009 Dielectric relaxation dynamics of water in model membranes probed by terahertz spectroscopy *Biophys. J.* **97** 2484–92

[72] Torii T, Chiba H, Tanabe T and Oyama Y 2017 Measurements of glucose concentration in aqueous solutions using reflected THz radiation for applications to a novel sub-THz radiation non-invasive blood sugar measurement method *Digital Health* **3** 2055207617729534

[73] Duponchel L, Laurette S, Hatirnaz B, Treizebre A, Affouard F and Bocquet B 2013 Terahertz microfluidic sensor for in situ exploration of hydration shell of molecules *Chemometr. Intell. Lab. Syst.* **123** 28–35

[74] Morozov N A 1907 *Periodic Systems of the Structure of Matter: The Theory of the Formation of Chemical Elements* (Moscow: Izdatelskii Dom Sytina)

[75] Nagai M, Yada H, Arikawa T and Tanaka K 2006 Terahertz time-domain attenuated total reflection spectroscopy in water and biological solution *Int. J. Infrared Millim. Waves* **27** 505–15

[76] Shiraga K, Ogawa Y, Kondo N, Irisawa A and Imamura M 2013 Evaluation of the hydration state of saccharides using terahertz time-domain attenuated total reflection spectroscopy *Food Chem.* **140** 315–20

[77] Arikawa T, Nagai M and Tanaka K 2008 Characterizing hydration state in solution using terahertz time-domain attenuated total reflection spectroscopy *Chem. Phys. Lett.* **457** 12–7

[78] Smolyanskaya O *et al* 2019 Multimodal optical diagnostics of glycated biological tissues *Biochemistry (Moscow)* **84** S124–43

[79] Shiraga K, Suzuki T, Kondo N, Baerdemaeker J D and Ogawa Y 2015 Quantitative characterization of hydration state and destructuring effect of monosaccharides and disaccharides on water hydrogen bond network *Carbohydr. Res.* **406** 46–54

[80] Cherkasova O P, Nazarov M M and Shkurinov A P 2016 Investigation of bovine serum albumin glycation by THz spectroscopy *Proc. SPIE* **9917** 991706

[81] Fanali G, di Masi A, Trezza V, Marino M, Fasano M and Ascenzi P 2012 Human serum albumin: from bench to bedside *Mol. Aspects Med.* **33** 209–90

[82] Cole K S and Cole R H 1941 Dispersion and absorption in dielectrics I. Alternating current characteristics *J. Chem. Phys.* **9** 341–51

[83] Cole K S and Cole R H 1942 Dispersion and absorption in dielectrics II. Direct current characteristics *J. Chem. Phys.* **10** 98–105

[84] Davidson D 1961 Dielectric relaxation in liquids: I. The representation of relaxation behavior *Can. J. Chem.* **39** 571–94

[85] Havriliak S and Negami S 1966 A complex plane analysis of α-dispersions in some polymer systems *J. Polymer Sci.* **14** 99–117

[86] Bykhovskaia M, Gelmont B, Globus T, Woolard D, Samuels A, Duong T and Zakrzewska K 2001 Prediction of DNA far-IR absorption spectra based on normal mode analysis *Theor. Chem. Acc.* **106** 22–7

[87] Globus T, Woolard D, Samuels A, Gelmont B, Hesler J, Crowe T and Bykhovskaia M 2002 Submillimeter-wave Fourier transform spectroscopy of biological macromolecules *J. Appl. Phys.* **91** 6105–13

[88] Woolard D *et al* 2002 Submillimeter-wave phonon modes in DNA macromolecules *Phys. Rev.* E **65** 051903

[89] Markelz A, Whitmire S, Hillebrecht J and Birge R 2002 THz time domain spectroscopy of biomolecular conformational modes *Phys. Med. Biol.* **47** 3797–805

[90] Globus T, Woolard D, Khromova T, Crowe T, Bykhovskaia M, Gelmont B, Hesler J and Samuels A 2003 THz-spectroscopy of biological molecules *J. Biol. Phys.* **29** 89–100

[91] Globus T, Bykhovskaia M, Woolard D and Gelmont B 2003 Sub-millimetre wave absorption spectra of artificial RNA molecules *J. Phys. D: Appl. Phys.* **36** 1314–22

[92] Globus T, Woolard D, Crowe T, Khromova T, Gelmont B and Hesler J 2006 Terahertz Fourier transform characterization of biological materials in a liquid phase *J. Phys. D: Appl. Phys.* **39** 3405–13

[93] Li X, Globus T, Gelmont B, Salay L and Bykhovski B 2008 Terahertz absorption of DNA decamer duplex *J. Phys. Chem.* A **112** 12090–6

[94] He Y, Ku P, Knab J, Chen J and Markelz A 2008 Protein dynamical transition does not require protein structure *Phys. Rev. Lett.* **101** 178103

[95] Xie Z, Bykhovski A, Gelmont B, Globus T and Jensen J 2010 Computational modeling of the molecular complex formed by DIPAIN II and T-2 toxin *IEEE Sensors J.* **10** 541–6

[96] Alijabbari N, Chen Y, Sizov I, Globus T and Gelmont B 2012 Molecular dynamics modeling of the sub-THz vibrational absorption of thioredoxin from E. coli *J. Mol. Model.* **18** 2209–18

[97] Singh R, George D, Benedict J, Korter T and Markelz A 2012 Improved mode assignment for molecular crystals through anisotropic terahertz spectroscopy *J. Phys. Chem.* A **116** 10359–64

[98] Lipps F, Levy S and Markelz A 2012 Hydration and temperature interdependence of protein picosecond dynamics *Phys. Chem. Chem. Phys.* **14** 6375–81

[99] Sizov I, Rahman M, Gelmont B, Norton M and Globus T 2013 Sub-THz spectroscopic characterization of vibrational modes in artificially designed DNA monocrystal *Chem. Phys.* **425** 121–5

[100] Globus T, Sizov I and Gelmont B 2014 Sub-THz specific relaxation times of hydrogen bond oscillations in E. coli thioredoxin. Molecular dynamics and statistical analysis *Faraday Discuss.* **171** 179–93

[101] Acbas G, Niessen K, Snell E and Markelz A 2014 Optical measurements of long-range protein vibrations *Nat. Commun.* **5** 3076

[102] Vaks V, Semenova A, Guseva Y and Panin A 2017 Phenomenological model and experimental study of DNA absorption spectra in THz range *Opt. Quantum Electron.* **49** 193

[103] Niessen K, Xu M, George D, Chen M, Ferre-D'Amare A, Snell E, Cody V, Pace J, Schmidt M and Markelz A 2019 Protein and RNA dynamical fingerprinting *Nat. Commun.* **10** 1026

[104] Globus T, Gelmont B and Sizov I 2014 Overview of terahertz spectral characterization for biological identification *Biological Identification. DNA Amplification and Sequencing, Optical Sensing, Lab-On-Chip and Portable Systems* ed R P Schaudies (Cambridge: Woodhead Publishing) (https://doi.org/10.1533/9780857099167.3.281)

[105] Cheon H, Yang H-J, Lee S-H, Kim Y and Son J-H 2016 Terahertz molecular resonance of cancer DNA *Sci. Rep.* **6** 37103

[106] Globus T, Moskaluk C, Pramoonjago P, Gelmonta B, Moyer A, Bykhovski A and Ferranc J 2019 Sub-terahertz vibrational spectroscopy of ovarian cancer and normal control tissue for molecular diagnostic technology *Cancer Biomarkers* **24** 1–15

[107] Globus T, Sizov I, Ferrance J, Jazaeri A, Bryant J, Moyer A, Gelmont B, Kester M and Bykhovski A 2016 Sub-terahertz vibrational spectroscopy for microRNA based diagnostic of ovarian cancer *Converg. Sci. Phys. Oncol.* **2** 045001

[108] Bykhovski A and Gelmont B 2010 The influence of environment on terahertz spectra of biological molecules *J. Phys. Chem.* B **114** 12349–57

[109] Chernomyrdin N V *et al* 2018 Reflection-mode continuous-wave 0.15λ-resolution terahertz solid immersion microscopy of soft biological tissues *Appl. Phys. Lett.* **113** 111102

[110] Joseph C, Patel R, Neel V, Giles R and Yaroslavsky A 2014 Imaging of ex vivo nonmelanoma skin cancers in the optical and terahertz spectral regions. Optical and terahertz skin cancers imaging *J. Biophotonics* **7** 295–303

[111] Fan B, Neel V and Yaroslavsky A 2017 Multimodal imaging for nonmelanoma skin cancer margin delineation *Lasers Surg. Med.* **49** 319–26

[112] Yaroslavsky A, Joseph C, Patel R, Muzikansky A, Neel V and Giles R 2017 Delineating nonmelanoma skin cancer margins using terahertz and optical imaging *J. Biomed. Photon. Eng.* **3** 010301

[113] International Commission on Non-Ionizing Radiation Protection (ICNIRP) 1998 Guidelines for limiting exposure to time-varying electric, magnetic and electromagnetic fields (up to 300 GHz) *Health Physics* **74** 494–522

[114] Scientific Committee on Emerging and Newly Identified Health Risks (SCENIHR) 2015 Opinion on potential health effects of exposure to electromagnetic fields (EMF), health effects of EMF *Bioelectromagnetics* **36** 480–4

[115] Wilmink G and Grundt J 2011 Invited review article: current state of research on biological effects of terahertz radiation *J. Infrared Millim. Terahertz Waves* **32** 1074–122

[116] Ramundo Orlando A and Gallerano G 2009 Terahertz radiation effects and biological applications *J. Infrared Millim. Terahertz Waves* **30** 1308–18

[117] Berry E, Walker G, Fitzgerald A, Zinovâev N, Chamberlain M, Smye S, Miles R and Smith M 2003 Do in vivo terahertz imaging systems comply with safety guidelines? *J. Laser Appl.* **15** 192–8

[118] Kristensen T, Withayachumnankul W, Uhd Jepsen P and Abbott D 2010 Modeling terahertz heating effects on water *Opt. Express* **18** 4727–39

[119] Fröhlich H 1980 Advances in electronics and electron physics *The Biological Effects of Microwaves and Related Questions* vol 53 ed L Marton and C Marton (New York: Elsevier) pp 85–152

[120] Preto J 2016 Classical investigation of long-range coherence in biological systems *Chaos* **26** 123116

[121] Alexandrov B, Gelev V, Bishop A, Usheva A and Rasmussen K 2010 DNA breathing dynamics in the presence of a terahertz field *Phys. Lett.* A **374** 1214–7

[122] Chitanvis S 2006 Can low-power electromagnetic radiation disrupt hydrogen bonds in dsDNA? *J. Polym. Sci.* B **44** 2740–7

[123] Alexandrov L, Rasmussen K, Bishop A and Alexandrov B 2017 Evaluating the role of coherent delocalized phonon-like modes in DNA cyclization *Sci. Rep.* **7** 9731

[124] Kulipanov G *et al* 2015 Novosibirsk free electron laser—facility description and recent experiments *IEEE Trans. Terahertz Sci. Technol.* **5** 798–809

[125] Demidova E, Goryachkovskaya T, Mescheryakova I, Malup T, Semenov A, Vinokurov N, Kolchanov N, Popik V and Peltek S 2016 Impact of terahertz radiation on stress-sensitive genes of E. coli cell *IEEE Trans. Terahertz Sci Technol.* **6** 435–41

[126] Bogomazova A, Vassina E, Goryachkovskaya T, Popik V, Sokolov A, Kolchanov N, Lagarkova M, Kiselev S and Peltek S 2015 No DNA damage response and negligible genome-wide transcriptional changes in human embryonic stem cells exposed to terahertz radiation *Sci. Rep.* **5** 7749

[127] Son J-H 2014 *Terahertz Biomedical Science and Technology* 1st edn (Boca Raton, FL: CRC Press) (https://doi.org/10.1201/b17060)

[128] Weightman P 2012 Prospects for the study of biological systems with high power sources of terahertz radiation *Phys. Biol.* **9** 053001

[129] Feldman Y, Puzenko A, Ben Ishai P, Caduff A and Agranat A 2008 Human skin as arrays of helical antennas in the millimeter and submillimeter wave range *Phys. Rev. Lett.* **100** 128102

[130] Feldman Y, Puzenko A, Ben Ishai P, Caduff A, Davidovich I, Sakran F and Agranat A 2009 The electromagnetic response of human skin in the millimetre and submillimetre wave range *Phys. Med. Biol.* **54** 3341–63

[131] Tripathi S, Miyata E, Ishai P and Kawase K 2015 Morphology of human sweat ducts observed by optical coherence tomography and their frequency of resonance in the terahertz frequency region *Sci. Rep.* **5** 9071

[132] Tripathi S, Ishai P and Kawase K 2018 Frequency of the resonance of the human sweat duct in a normal mode of operation *Biomed. Opt. Express* **9** 1301–8

[133] Betzalel N, Ishai P and Feldman Y 2018 The human skin as a sub-THz receiver—does 5G pose a danger to it or not? *Environ. Res.* **163** 208–16

[134] Romanenko S, Begley R, Harvey A, Hool L and Wallace V 2017 The interaction between electromagnetic fields at megahertz, gigahertz and terahertz frequencies with cells, tissues and organisms: risks and potential *J. Royal Soc. Interface* **14** 20170585

[135] Yamazaki S, Harata M, Idehara T, Konagaya K, Yokoyama G, Hoshina H and Ogawa Y 2018 Actin polymerization is activated by terahertz irradiation *Sci. Rep.* **8** 9990

[136] Fedorov V, Serdyukov D, Cherkasova O, Popova S and Nemova E 2017 The influence of terahertz radiation on the cell's genetic apparatus *J. Opt. Technol.* **84** 509–14

[137] Il'ina I, Sitnikov D and Agranat M 2018 State-of-the-art of studies of the effect of terahertz radiation on living biological systems *High Temp.* **56** 789–810

[138] Bondar N, Kovalenko I, Avgustinovich D, Khamoyan A and Kudryavtseva N 2008 Behavioral effect of terahertz waves in male mice *Bull. Exp. Biol. Med.* **145** 401–5

[139] Fedorov V and Weisman N 2017 The development of F1 progeny from mature egg cells after terahertz radiation of parental drosophila *Biophysics* **62** 460–5

[140] Fedorov V 2017 The biological effects of terahertz laser radiation as a fundamental premise for designing diagnostic and treatment methods *Biophysics* **62** 324–30

[141] Kiseliov V, Makolinets V, Mitryaeva N and Radionov V 2012 Application of terahertz lasers setup for the investigation of the influence of HHF-radiation on the tumor processes *37th Int. Conf. Infrared, Millimeter, and Terahertz Waves* pp 1–2

[142] Hintzsche H and Stopper H 2012 Effects of terahertz radiation on biological systems *Crit. Rev. Environ. Sci. Technol.* **42** 2408–34

[143] Mattsson M-O, Zeni O and Simko M 2018 Is there a biological basis for therapeutic applications of millimetre waves and THz waves? *J. Infrared Millim. Terahertz Waves* **39** 863–78

[144] Park G-S, Kim Y, Han H, Han J, Ahn J, Son J-H, Park W-Y and Jeong Y 2012 *Convergence of Terahertz Sciences in Biomedical Systems* (Berlin: Springer) (https://doi.org/10.1007/978-94-007-3965-9)

[145] Angeluts A, Gapeyev A, Esaulkov M, Kosareva O, Matyunin S, Nazarov M, Pashovkin T, Solyankin P, Cherkasova O and Shkurinov A 2014 Study of terahertz-radiation-induced DNA damage in human blood leukocytes *Quantum Electron.* **44** 247–51

[146] Zeni O *et al* 2004 Cytogenetic observations in human peripherial blood leukocytes following in vitro exposure to THz radiation: a pilot study *Health Phys.* **92** 349–57

[147] Doria A *et al* 2004 THz radiation studies on biological systems at the ENEA FEL facility *Infrared Phys. Technol.* **45** 339–47

[148] Borovkova M, Serebriakova M, Fedorov V, Sedykh E, Vaks V, Lichutin A, Salnikova A and Khodzitsky M 2017 Investigation of terahertz radiation influence on rat glial cells *Biomed. Opt. Express* **8** 273–80

[149] Echchgadda I, Grundt J, Cerna C, Roth C, Ibey B and Wilmink G 2014 Terahertz stimulate specific signaling pathways in human cells *39th Int. Conf. Infrared, Millimeter, and Terahertz Waves (IRMMW-THz)* pp 1–2

[150] Wilmink G, Rivest B, Ibey B, Roth C, Bernhard J and Roach W 2010 Quantitative investigation of the bioeffects associated with terahertz radiation *Proc. SPIE* **7562** 75620L

[151] Korenstein-Ilan A, Barbul A, Hasin P, Eliran A, Gover A and Korenstein R 2008 Terahertz radiation increases genomic instability in human lymphocytes *Radiat. Res.* **170** 224–34

[152] Hintzsche H, Jastrow C, Kleine-Ostmann T, Krst U, Schrader T and Stopper H 2012 Terahertz electromagnetic fields (0.106 THz) do not induce manifest genomic damage in vitro *PLoS One* **7** 1–8

[153] Yaekashiwa N, Otsuki S, Hayashi S and Kawase K 2017 Investigation of the non-thermal effects of exposing cells to 70-300 GHz irradiation using a widely tunable source *J. Radiat. Res.* **59** 116–21

[154] Wilmink G, Grundt J, Cerna C, Roth C, Kuipers M, Lipscomb D, Echchgadda I and Ibey B 2011 Terahertz radiation preferentially activates the expression of genes responsible for the regulation of plasma membrane properties *Int. Conf. Infrared, Millimeter, and Terahertz Waves* pp 1–3

[155] Titova L, Ayesheshim A, Golubov A, Rodriguez-Juarez R, Woycicki R, Hegmann F and Kovalchuk O 2013 Intense THz pulses down-regulate genes associated with skin cancer and psoriasis: a new therapeutic avenue? *Sci. Rep.* **3** 2363

[156] Titova L, Ayesheshim A, Golubov A, Fogen D, Rodriguez-Juarez R, Hegmann F and Kovalchuk O 2013 Intense THz pulses cause H2AX phosphorylation and activate DNA damage response in human skin tissue *Biomed. Opt. Express* **4** 559–68

[157] Kim K-T, Park J, Jo S, Jung S, Kwon O, Gallerano G, Park W-Y and Park G-S 2013 High-power femtosecond-terahertz pulse induces a wound response in mouse skin *Sci. Rep.* **3** 2296

[158] Echchgadda I, Cerna C, Sloan M, Elam D and Ibey B 2015 Effects of different terahertz frequencies on gene expression in human keratinocytes *Proc. SPIE* **9321** 93210Q

[159] Franchini V *et al* 2018 Study of the effects of 0.15 terahertz radiation on genome integrity of adult fibroblasts *Environ. Mol. Mutagen.* **59** 476–87

[160] Fukasawa T, Sato T, Watanabe J, Hama Y, Kunz W and Buchner R 2005 Relation between dielectric and low-frequency Raman spectra of hydrogen-bond liquids *Phys. Rev. Lett.* **95** 197802

[161] Bernier M, Garet F, Coutaz J, Minamide H and Sato A 2016 Accurate characterization of resonant samples in the terahertz regime through a technique combining time-domain spectroscopy and Kramers-Kronig analysis *IEEE Trans. Terahertz Sci. Technol.* **6** 442–50

[162] Sizov F and Rogalski A 2010 THz detectors *Prog. Quantum Electron.* **34** 278–347

[163] Shurakov A, Lobanov Y and Goltsman G 2016 Superconducting hot-electron bolometer: from the discovery of hot-electron phenomena to practical applications *Supercond. Sci. Technol.* **29** 023001

[164] Han Q, Gao T, Zhang R, Chen Y, Chen J, Liu G, Zhang Y, Liu Z, Wu X and Yu D 2013 Highly sensitive hot electron bolometer based on disordered graphene *Sci. Rep.* **3** 3533

[165] Skoromets V, Němec H, Goian V, Kamba S and Kužel P 2018 Performance comparison of time-domain terahertz, multi-terahertz, and Fourier transform infrared spectroscopies *J. Infrared Millim. Terahertz Waves* **39** 1249–63

[166] Mankova A A *et al* 2013 Terahertz time-domain and FTIR spectroscopic study of interaction of α-chymotrypsin and protonated tris with 18-crown-6 *Chem. Phys. Lett.* **560** 55–9

[167] Zhang Y, Peng X-H, Chen Y, Chen J, Curioni A, Andreoni W, Nayak S and Zhang X-C 2008 A first principle study of terahertz (THz) spectra of acephate *Chem. Phys. Lett.* **452** 59–66

[168] Ding T, Li R, Zeitler J A, Huber T L, Gladden L F, Middelberg A P J and Falconer R J 2010 Terahertz and far infrared spectroscopy of alanine-rich peptides having variable ellipticity *Opt. Express* **18** 27431–44

[169] Lavrukhin D *et al* 2019 Shaping the spectrum of terahertz photoconductive antenna by frequency-dependent impedance matching *Semicond. Sci. Technol.* **34** 034005

[170] Yardimci N T, Turan D, Cakmakyapan S and Jarrahi M 2018 A high-responsivity and broadband photoconductive terahertz detector based on a plasmonic nanocavity *Appl. Phys. Lett.* **113** 251102

[171] Ponomarev D S, Gorodetsky A, Yachmenev A E, Pushkarev S S, Khabibullin R A, Grekhov M M, Zaytsev K I, Khusyainov D I, Buryakov A M and Mishina E D 2019 Enhanced terahertz emission from strain-induced InGaAs/InAlAs superlattices *J. Appl. Phys.* **125** 151605

[172] Nahata A, Weling A and Heinz T 1996 A wideband coherent terahertz spectroscopy system using optical rectification and electro-optic sampling *Appl. Phys. Lett.* **69** 2321–3

[173] Gavdush A *et al* 2019 Terahertz spectroscopy of gelatin-embedded human brain gliomas of different grades: a road

toward intraoperative THz diagnosis *J. Biomed. Opt.* **24** 027001

[174] Lucarini V, Saarinen J, Peiponen K-E and Vartiainen E 2005 *Kramers–Kronig Relations in Optical Materials Research (Springer Series in Optical Sciences)* vol 110 (Berlin: Springer) (https://doi.org/10.1007/b138913)

[175] Peiponen K-E, Vartiainen E M, Unuma T, Axel Zeitler J, Silfsten P, Venäläinen T and Kishida H 2013 Dispersion relations for evaluating the complex refractive index of medium without the information of its thickness *Appl. Phys. Lett.* **102** 181110

[176] Tuononen H, Gornov E, Zeitler J A, Aaltonen J and Peiponen K-E 2010 Using modified Kramers–Kronig relations to test transmission spectra of porous media in THz-TDS *Opt. Lett.* **35** 631–3

[177] Silfsten P, Kontturi V, Ervasti T, Ketolainen J and Peiponen K-E 2011 Kramers–Kronig analysis on the real refractive index of porous media in the terahertz spectral range *Opt. Lett.* **36** 778–80

[178] Wilmink G *et al* 2011 Development of a compact terahertz time-domain spectrometer for the measurement of the optical properties of biological tissues *J. Biomed. Opt.* **16** 047006

[179] Grootendorst M *et al* 2017 Use of a handheld terahertz pulsed imaging device to differentiate benign and malignant breast tissue *Biomed. Opt. Express* **8** 2932–45

[180] Reid C, Pickwell-MacPherson E, Laufer J, Gibson A, Hebden J and Wallace V 2010 Accuracy and resolution of THz reflection spectroscopy for medical imaging *Phys. Med. Biol.* **55** 4825–38

[181] Huang S, Ashworth P, Kan K, Chen Y, Wallace V, Zhang Y-T and Pickwell-MacPherson E 2009 Improved sample characterization in terahertz reflection imaging and spectroscopy *Opt. Express* **17** 3848–54

[182] Fan S, Parrott E, Ung B and Pickwell-MacPherson E 2016 Calibration method to improve the accuracy of THz imaging and spectroscopy in reflection geometry *Photon. Res.* **4** A29–35

[183] Chen X, Parrott E, Ung B-Y and Pickwell-MacPherson E 2017 A robust baseline and reference modification and acquisition algorithm for accurate THz imaging *IEEE Trans. Terahertz Sci. Technology* **7** 493–501

[184] Zhang R, He Y, Liu K, Zhang L, Zhang S, Pickwell-MacPherson E, Zhao Y and Zhang C 2017 Composite multiscale entropy analysis of reflective terahertz signals for biological tissues *Opt. Express* **25** 23669–76

[185] Sun Q, Parrott E, He Y and Pickwell-MacPherson E 2018 *In vivo* thz imaging of human skin: accounting for occlusion effects *J. Biophoton.* **11** e201700111

[186] Wang J, Stantchev R, Sun Q, Chiu T-W, Ahuja A and Pickwell MacPherson E 2018 THz in vivo measurements: the effects of pressure on skin reflectivity *Biomed. Opt. Express* **9** 6467–76

[187] Sun Q, Stantchev R, Wang J, Parrott E, Cottenden A, Chiu T-W, Ahuja A and Pickwell-MacPherson E 2019 In vivo estimation of water diffusivity in occluded human skin using terahertz reflection spectroscopy *J. Biophoton.* **12** e201800145

[188] Volkov A 1987 Submillimeter BWO spectroscopy of solids *Int. J. Infrared Millim. Waves* **8** 55–61

[189] Komandin G, Chuchupal S, Lebedev S, Goncharov Y, Korolev A, Porodinkov O, Spektor I and Volkov A 2013 BWO generators for terahertz dielectric measurements *IEEE Trans. Terahertz Sci. Technol.* **3** 440–4

[190] Vaks V L, Domracheva E G, Pripolzin S I, Sobakinskaya E A, Chernyaeva M B, Anfert'ev V A, Semenova A V and Shatrova Y S 2014 Methods and instruments of high-resolution transient THz spectroscopy

for diagnostics of socially important diseases *Phys. Wave Phenom.* **22** 177–84

[191] Yablokov A A, Anfertev V A, Revin L S, Balakirev V Y, Chernyaeva M B, Domracheva E G, Illyuk A V, Pripolzin S I and Vaks V L 2015 Two-frequency THz spectroscopy for analytical and dynamical research *IEEE Trans. Terahertz Sci. Technol.* **5** 845–51

[192] Gompf B, Gerull M, Müller T and Dressel M 2006 THz-micro-spectroscopy with backward-wave oscillators *Infrared Phys. Technol.* **49** 128–32

[193] Eisele H, Rydberg A and Haddad G I 2000 Recent advances in the performance of InP Gunn devices and GaAs tunnett diodes for the 100–300 GHz frequency range and above *IEEE Trans. Microwave Theory Tech.* **48** 626–31

[194] Ahi K 2017 Review of GaN-based devices for terahertz operation *Opt. Eng.* **56** 090901

[195] Iomdina E N, Goltsman G N, Seliverstov S V, Sianosyan A A, Teplyakova K O and Rusova A A 2016 Study of transmittance and reflectance spectra of the cornea and the sclera in the THz frequency range *J. Biomed. Opt.* **21** 097002

[196] Taylor Z D *et al* 2015 THz and mm-wave sensing of corneal tissue water content: in vivo sensing and imaging results *IEEE Trans. Terahertz Sci. Technol.* **5** 184–96

[197] Sung S *et al* 2018 THz imaging system for in vivo human cornea *IEEE Trans. Terahertz Sci. Technol.* **8** 27–37

[198] Preu S, Döhler G H, Malzer S, Wang L J and Gossard A C 2011 Tunable, continuous-wave terahertz photomixer sources and applications *J. Appl. Phys.* **109** 061301

[199] Roggenbuck A, Schmitz H, Deninger A, Mayorga I C, Hemberger J, Gsten R and Grninger M 2010 Coherent broadband continuous-wave terahertz spectroscopy on solid-state samples *New J. Phys.* **12** 043017

[200] Shikata J, Kawase K, Karino K, Taniuchi T and Ito H 2000 Tunable terahertz-wave parametric oscillators using LiNbO₃ and MgO:LiNbO₃ crystals *IEEE Trans. Microwave Theory Tech.* **48** 653–61

[201] Köhler R, Tredicucci A, Beltram F, Beere H E, Linfield E H, Davies A G, Ritchie D A, Iotti R C and Rossi F 2002 Terahertz semiconductor-heterostructure laser *Nature* **417** 156–9

[202] Williams B S 2007 Terahertz quantum-cascade lasers *Nat. Photonics* **1** 517–25

[203] Nakanishi A, Fujita K, Horita K and Takahashi H 2019 Terahertz imaging with room-temperature terahertz difference-frequency quantum-cascade laser sources *Opt. Express* **27** 1884–93

[204] Locatelli M, Ravaro M, Bartalini S, Beere H E, Consolino L, Vitiello M S, Cicchi R, Pavone F and Natale P De 2015 Real-time terahertz digital holography with a quantum cascade laser *Sci. Rep.* **5** 13566

[205] Naftaly M 2013 Metrology issues and solutions in THz time-domain spectroscopy: noise, errors, calibration *IEEE Sensors J.* **13** 8–17

[206] Skorobogatiy M, Sadasivan J and Guerboukha H 2018 Statistical models for averaging of the pump-probe traces: example of denoising in terahertz time-domain spectroscopy *IEEE Trans. Terahertz Sci. Technol.* **8** 287–98

[207] Harris F J 1978 On the use of windows for harmonic analysis with the discrete Fourier transform *Proc. IEEE* **66** 51–83

[208] Vázquez-Cabo J, Chamorro-Posada P, Fraile-Peláez F J, Rubiños-López Ó, López-Santos J M and Martín-Ramos P 2016 Windowing of THz time-domain spectroscopy signals: a study based on lactose *Opt. Commun.* **366** 386–96

[209] Galvão R K H, Hadjiloucas S, Zafiropoulos A, Walker G C, Bowen J W and Dudley R A 2007 Optimization of apodization functions in terahertz transient spectrometry *Opt. Lett.* **32** 3008–10

[210] Bafluelos-Saucedo M A 2015 Compensation of THz spectrum spurious oscillations by local apodization *IEEE Sensors* pp 1–4

[211] Naylor D A and Tahic M K 2007 Apodizing functions for Fourier transform spectroscopy *J. Opt. Soc. Am.* A **24** 3644

[212] Giuliano B M *et al* 2019 Broadband spectroscopy of astrophysical ice analogs: I. Direct measurement of complex refractive index of CO ice using terahertz pulsed spectroscopy *Astron. Astrophys.* **629** A112

[213] Pei J, Ye P and Xie W 2009 Optimal wavelet analysis for THz-TDS pulse signals *Proc. SPIE* **7277** 727708

[214] Chen Y, Huang S and Pickwell-MacPherson E 2010 Frequency-wavelet domain deconvolution for terahertz reflection imaging and spectroscopy *Opt. Express* **18** 1177

[215] Zaytsev K I, Chernomyrdin N V, Gorevoy A V, Trofimov N E, Fokina I N, Alekhnovich V I, Karasik V E and Yurchenko S O 2014 An approach for automatic construction of the wavelet-domain de-noising procedure for THz pulsed spectroscopy signal processing *J. Phys. Conf. Ser.* **486** 012034

[216] Chernomyrdin N V, Nosov P A, Reshetov I V, Gavdush A A, Kudrin K, Zaytsev K I, Fokina I N, Karasik V E and Yurchenko S O 2014 Wavelet-domain de-noising technique for THz pulsed spectroscopy *Proc. SPIE* **9216** 921611

[217] Dolganova I, Chernomyrdin N, Aleksandrova P, Beshplav S-I, Potapov A, Reshetov I, Kurlov V, Tuchin V and Zaytsev K 2018 Nanoparticle-enabled experimentally trained wavelet-domain denoising method for optical coherence tomography *J. Biomed. Opt.* **23** 091406

[218] Dong J, Citrin D S, Walker G C, Bianca Jackson J, Melis M, Bowen J W, Giovanacci D and Locquet A 2016 Terahertz frequency-wavelet domain deconvolution for stratigraphic and subsurface investigation of art painting *Opt. Express* **24** 26972–85

[219] Huang N E and Wu Z 2008 A review on Hilbert–Huang transform: method and its applications *Rev. Geophys.* **46** 1–23

[220] Qiao X L, Zhang X M, Ren J J, Zhang D D, Cao G H and Li L J 2017 Mean estimation empirical mode decomposition method for terahertz time-domain spectroscopy de-noising *Appl. Opt.* **56** 7138–45

[221] Wilbert D S, Balci S, Baughman W E, Yokus H, Kim S M and Kung P 2013 Observation of hydrofluoric acid burns on osseous tissues by means of terahertz spectroscopic imaging *IEEE Trans. Terahertz Sci. Technol.* **3** 387–94

[222] Wallace V, Fitzgerald A, Shankar S, Flanagan N, Pye R, Cluff J and Arnone D 2004 Terahertz pulsed imaging of basal cell carcinoma ex vivo and in vivo *Br. J. Dermatol.* **151** 424–32

[223] Walker G C, Bowen J W, Labaune J, Jackson J-B, Hadjiloucas S, Roberts J, Mourou G and Menu M 2012 Terahertz deconvolution *Opt. Express* **20** 27230–41

[224] Zaytsev K, Karasik V, Dolganova I and Alekhnovich V I 2013 Invariant embedding technique for medium permittivity profile reconstruction using terahertz time-domain spectroscopy *Opt. Eng.* **52** 068203

[225] Mittleman D M 2018 Twenty years of terahertz imaging [invited] *Opt. Express* **26** 9417–31

[226] Jinno H *et al* 2009 High-resolution time-of-flight terahertz tomography using a femtosecond fiber laser *Opt. Express* **17** 7533–9

[227] Guillet J P, Recur B, Frederique L, Bousquet B, Canioni L, Manek-Hönninger I, Desbarats P and Mounaix P 2014 Review of terahertz tomography techniques *J. Infrared Millim. Terahertz Waves* **35** 382–411

[228] Woodward R, Wallace V, Pye R, Cole B, Arnone D, Linfield E and Pepper M 2003 Terahertz pulse imaging of ex vivo basal cell carcinoma *J. Investig. Dermatol.* **120** 72–8

[229] Lai W, Pelaz B, Cao H, Yin Z, del Pino P, Zhang Q, Deng G and Yang J 2018 Antireflection self-reference method based on ultrathin metallic nanofilms for improving terahertz reflection spectroscopy *Opt. Express* **26** 19470–8

[230] Nagai M, Yada H, Arikawa T and Tanaka K 2006 Terahertz time-domain attenuated total reflection spectroscopy in water and biological solution *Int. J. Infrared Millim. Waves* **27** 505–15

[231] Pupeza I, Wilk R and Koch M 2007 Highly accurate optical material parameter determination with THz time-domain spectroscopy *Opt. Express* **15** 4335–50

[232] Zaytsev K, Gavdush A, Karasik V, Alekhnovich V, Nosov P, Lazarev V, Reshetov I and Yurchenko S 2014 Accuracy of sample material parameters reconstruction using terahertz pulsed spectroscopy *J. Appl. Phys.* **115** 193105

[233] Zaytsev K, Kudrin K, Karasik V, Reshetov I and Yurchenko S 2015 In vivo terahertz spectroscopy of pigmentary skin nevi: pilot study of non-invasive early diagnosis of dysplasia *Appl. Phys. Lett.* **106** 053702

[234] Grognot M and Gallot G 2015 Quantitative measurement of permeabilization of living cells by terahertz attenuated total reflection *Appl. Phys. Lett.* **107** 103702

[235] Zou Y, Liu Q, Yang X, Huang H-C, Li J, Du L-H, Li Z-R, Zhao J-H and Zhu L-G 2018 Label-free monitoring of cell death induced by oxidative stress in living human cells using terahertz atr spectroscopy *Biomed. Opt. Express* **9** 14–24

[236] Shiraga K, Ogawa Y, Suzuki T, Kondo N, Irisawa A and Imamura M 2013 Determination of the complex dielectric constant of an epithelial cell monolayer in the terahertz region *Appl. Phys. Lett.* **102** 053702

[237] Han Y, Zhang Z, Liu H, Zhang C, Yang Y, Zhang X, Wang F, Liu X and Zhang Z 2018 Dimensionality reduction for identification of hepatic tumor samples based on terahertz time-domain spectroscopy *IEEE Trans. Terahertz Sci. Technol.* **8** 271–7

[238] Kistenev Y, Tuchin V, Borisov A, Lazareva E, Nikolaev V, Tuchina D, Vrazhnov D and Yanina I 2019 Medical diagnosis using NIR and THz tissue imaging and machine learning methods *Proc. SPIE* **10877** 108770J

[239] Sun Q, He Y, Liu K, Fan S, Parrott E and Pickwell-MacPherson E 2017 Recent advances in terahertz technology for biomedical applications *Quant. Imaging Med. Surg.* **7** 345–55

[240] Yu L, Hao L, Meiqiong T, Jiaoqi H, Wei L, Jinying D, Xueping C, Weiling F and Yang Z 2019 The medical application of terahertz technology in non-invasive detection of cells and tissues: opportunities and challenges *RSC Adv.* **9** 9354–63

[241] Chen H *et al* 2011 High-sensitivity in vivo THz transmission imaging of early human breast cancer in a subcutaneous xenograft mouse model *Opt. Express* **19** 21552–62

[242] Yamaguchi S, Fukushi Y, Kubota O, Itsuji T, Ouchi T and Yamamoto S 2016 Origin and quantification of differences between normal and tumor tissues observed by terahertz spectroscopy *Phys. Med. Biol.* **68** 6808–20

[243] Masson J-B, Sauviat M-P, Martin J-L and Gallot G 2006 Ionic contrast terahertz near-field imaging of axonal water fluxes *Proc. Natl Acad. Sci.* **103** 4808–12

[244] Joseph C S *et al* 2009 Terahertz spectroscopy of intrinsic biomarkers for non-melanoma skin cancer *Proc. SPIE* **7215** 72150I

[245] Son J-H 2009 Terahertz electromagnetic interactions with biological matter and their applications *J. Appl. Phys.* **105** 102033

[246] Sy S, Huang S, Wang Y-X, Yu J, Ahuja A, Zhang Y-T and Pickwell-MacPherson E 2010 Terahertz spectroscopy of liver cirrhosis: investigating the origin of contrast *Phys. Med. Biol.* **55** 7587–96

[247] Park J, Choi H, Cho K-S, Kim K-R and Son J-H 2011 Terahertz spectroscopic imaging of a rabbit VX2 hepatoma model *J. Appl. Phys.* **109** 064704

[248] Ney M and Abdulhalim I 2016 Comprehensive Monte-Carlo simulator for optimization of imaging parameters for high sensitivity detection of skin cancer at the THz *Proc. SPIE* **9721** 97210W

[249] Doradla P, Alavi K, Joseph C and Giles R 2013 Detection of colon cancer by continuous-wave terahertz polarization imaging technique *J. Biomed. Opt.* **18** 090504

[250] Yaroslavsky A, Joseph C, Patel R, Muzikansky A, Neel V and Giles R 2017 Delineating nonmelanoma skin cancer margins using terahertz and optical imaging *J. Biomed. Photon. Eng.* **3** 010301

[251] Fan B, Neel V A and Yaroslavsky A N 2017 Multimodal imaging for nonmelanoma skin cancer margin delineation *Lasers Surg. Med.* **49** 319–26

[252] Woodward R, Wallace V, Cole B, Pye R, Arnone D, Linfield E and Pepper M 2002 Terahertz pulse imaging in reflection geometry of skin tissue using time-domain analysis techniques *Proc. SPIE* **4625** 160–9

[253] Pickwell E and Wallace V 2006 Biomedical applications of terahertz technology *J. Phys. D: Appl. Phys.* **39** R301–10

[254] Chen Y, Huang S and Pickwell-MacPherson E 2010 Frequency-wavelet domain deconvolution for terahertz reflection imaging and spectroscopy *Opt. Express* **18** 1177–90

[255] Echchgadda I, Grundt A, Tarango J M, Ibey B, Tongue T, Liang M, Xin G and Wilmink H 2013 Using a portable terahertz spectrometer to measure the optical properties of in vivo human skin *J. Biomed. Opt.* **18** 120503

[256] Lipscomb D, Echchgadda I, Peralta X and Wilmink G 2013 Determination of the optical properties of melanin-pigmented human skin equivalents using terahertz time-domain spectroscopy *Proc. SPIE* **8585** 85850F

[257] Vilagosh Z, Lajevardipour A and Wood A 2018 Modelling terahertz radiation absorption and reflection with computational phantoms of skin and associated appendages *Proc. SPIE* **10456** 104560M

[258] Vilagosh Z, Lajevardipour A and Wood A W 2019 Computational phantom study of frozen melanoma imaging at 0.45 terahertz *Bioelectromagnetics* **40** 118–27

[259] Lajevardipour A, Wood A, McIntosh R and Iskra S 2016 Estimation of dielectric values for tissue water in the terahertz range *Bioelectromagnetics* **37** 563–7

[260] Woodward R, Cole B, Wallace V, Pye R, Arnone D, Linfield E and Pepper M 2002 Terahertz pulse imaging in reflection geometry of human skin cancer and skin tissue *Phys. Med. Biol.* **47** 3853–63

[261] Woodward R, Wallace V, Pye R, Cole B, Arnone D, Linfield E and Pepper M 2003 Terahertz pulse imaging of ex vivo basal cell carcinoma *J. Investig. Dermatol.* **120** 72–8

[262] Wallace V, Fitzgerald A, Pickwell E, Pye R, Taday P, Flanagan N and Ha T 2006 Terahertz pulsed spectroscopy of human basal cell carcinoma *Appl. Spectrosc.* **60** 1127–33

[263] Zaytsev K, Kudrin K, Koroleva S, Fokina I, Volodarskaya S, Novitskaya A, Perov A, Karasik V and Yurchenko S 2014 Medical diagnostics using terahertz pulsed spectroscopy *J. Phys. Conf. Ser.* **486** 012014

[264] Kong K, Rowlands C, Varma S, Perkins W, Leach I, Koloydenko A, Williams H and Notingher I 2013 Diagnosis of tumors during tissue-conserving surgery with integrated autofluorescence and Raman scattering microscopy *Proc. Natl Acad. Sci.* **110** 15189–94

[265] Takamori S, Kong K, Varma S, Leach I, Williams H and Notingher I 2015 Optimization of multimodal spectral imaging for assessment of resection margins during mohs micrographic surgery for basal cell carcinoma *Biomed. Opt. Express* **6** 98–111

[266] Zaitsev K, Chernomyrdin N, Kudrin K, Reshetov I and Yurchenko S 2015 Terahertz spectroscopy of pigmentary skin nevi in vivo *Opt. Spectrosc.* **119** 404–10

[267] Arumi-Uria M, McNutt N and Finnerty B 2003 Grading of atypia in nevi: correlation with melanoma risk *Mod. Pathol.* **16** 764–71

[268] Leachman S *et al* 2016 *Methods of Melanoma Detection* ed H L Kaufman and J M Mehnert (Cham: Springer) pp 51–105

[269] Rosendahl C, Tschandl P, Cameron A and Kittler H 2011 Diagnostic accuracy of dermatoscopy for melanocytic and nonmelanocytic pigmented lesions *J. Am. Acad. Dermatol.* **64** 1068–73

[270] Barata C, Celebi M and Marques J 2017 Development of a clinically oriented system for melanoma diagnosis *Pattern Recognit.* **69** 270–85

[271] Sim Y, Park J, Ahn K-M, Park C and Son J-H 2013 Terahertz imaging of excised oral cancer at frozen temperature *Biomed. Opt. Express* **4** 1413–21

[272] Wickham J 1987 The new surgery *Br. Med. J.* **295** 1581–2

[273] Reid C, Fitzgerald A, Reese G, Goldin R, Tekkis P, O'Kelly P, Pickwell-MacPherson E, Gibson A and Wallace V 2011 Terahertz pulsed imaging of freshly excised human colonic tissues *Phys. Med. Biol.* **56** 4333–53

[274] Wahaia F, Kasalynas I, Venckevicius R, Seliuta D, Valusis G, Urbanowicz A, Molis G, Carneiro F, Carvalho Silva C and Granja P 2016 Terahertz absorption and reflection imaging of carcinoma-affected colon tissues embedded in paraffin *J. Mol. Struct.* **1107** 214–9

[275] Doradla C, Joseph P and Giles R 2017 Terahertz endoscopic imaging for colorectal cancer detection: current status and future perspectives *World J. Gastrointest. Endosc.* **9** 346–58

[276] Hou D, Li X, Cai J, Ma Y, Kang X, Huang P and Zhang G 2014 Terahertz spectroscopic investigation of human gastric normal and tumor tissues *Phys. Med. Biol.* **59** 5423–40

[277] Ji Y *et al* 2015 Feasibility of terahertz reflectometry for discrimination of human early gastric cancers *Biomed. Opt. Express* **6** 1398–406

[278] Formanek F, Brun M-A and Yasuda A 2011 Contrast improvement of terahertz images of thin histopathologic sections *Biomed. Opt. Express* **2** 58–64

[279] Chen H, Ma S-H, Yan W-X, Wu X-M and Wang X-Z 2013 The diagnosis of human liver cancer by using THz fiber-scanning near-field imaging *Chin. Phys. Lett.* **30** 030702

[280] Duan F, Wang Y-Y, Xu D-G, Shi J, Chen L-Y, Cui L, Bai Y-H, Xu Y, Yuan J and Chang C 2019 Feasibility of terahertz imaging for discrimination of human hepatocellular carcinoma *World J. Gastrointest. Oncol.* **11** 153–60

[281] Doradla P, Alavi K, Joseph C and Giles R 2014 Single-channel prototype terahertz endoscopic system *J. Biomed. Opt.* **19** 080501

[282] Ito K, Katagiri T and Matsuura Y 2017 Analysis of transmission properties of terahertz hollow-core optical fiber by using time-domain spectroscopy and application for remote spectroscopy *J. Opt. Soc. Am. B* **34** 60–5

[283] Fitzgerald A, Wallace V, Jimenez-Linan M, Bobrow L, Pye R, Purushotham A and Arnone D 2006 Terahertz pulsed imaging of human breast tumors *Radiology* **239** 533–40

[284] Fitzgerald A, Wallace V, Pinder S, Purushotham A, O'Kelly P and Ashworth P 2012 Classification of terahertz-pulsed imaging data from excised breast tissue *J. Biomed. Opt.* **17** 016005

[285] Grootendorst M *et al* 2017 Use of a handheld terahertz pulsed imaging device to differentiate benign and malignant breast tissue *Biomed. Opt. Express* **8** 2932–45

[286] Truong B, Fitzgerald A, Fan S and Wallace V 2018 Concentration analysis of breast tissue phantoms with terahertz spectroscopy *Biomed. Opt. Express* **9** 1334–49

[287] Cassar Q, Al-Ibadi A, Mavarani L, Hillger P, Grzyb J, MacGrogan G, Zimmer T, Pfeiffer U, Guillet J-P and

Mounaix P 2018 Pilot study of freshly excised breast tissue response in the 300–600 GHz range *Biomed. Opt. Express* **9** 2930–42

[288] Png G, Flook R, Ng B-H and Abbott D 2009 Terahertz spectroscopy of snap-frozen human brain tissue: an initial study *Electron. Lett.* **45** 343–5

[289] Meng K *et al* 2014 Terahertz pulsed spectroscopy of paraffin-embedded brain glioma *J. Biomed. Opt.* **19** 077001

[290] Yamaguchi S, Fukushi Y, Kubota O, Itsuji T, Ouchi T and Yamamoto S 2016 Brain tumor imaging of rat fresh tissue using terahertz spectroscopy *Sci. Rep.* **6** 30124

[291] Ji Y B *et al* 2016 Terahertz reflectometry imaging for low and high grade gliomas *Sci. Rep.* **6** 36040

[292] Chernomyrdin N V *et al* 2018 In vitro terahertz spectroscopy of gelatin-embedded human brain tumors: a pilot study *Proc. SPIE* **10716** 107160S

[293] McIntyre G 2006 Cell hydration as the primary factor in carcinogenesis: a unifying concept *Med. Hypotheses* **66** 518–26

[294] Fan S, Ung B, Parrott E and Pickwell-MacPherson E 2015 Gelatin embedding: a novel way to preserve biological samples for terahertz imaging and spectroscopy *Phys. Med. Biol.* **60** 2703–13

[295] Zhao H, Wang Y, Chen L, Shi J, Ma K, Tang L, Xu D, Yao J, Feng H and Chen T 2018 High-sensitivity terahertz imaging of traumatic brain injury in a rat model *J. Biomed. Opt.* **23** 036015

[296] Shi J *et al* 2018 Automatic evaluation of traumatic brain injury based on terahertz imaging with machine learning *Opt. Express* **26** 6371–81

[297] Hefti M, Mehdorn H, Albert I and Dorner L 2010 Fluorescence-guided surgery for malignant glioma: a review on aminolevulinic acid induced protoporphyrin IX photodynamic diagnostic in brain tumors *Curr. Med. Imaging Rev.* **6** 254–8

[298] Chang E F *et al* 2009 Multiinstitutional validation of the University of California at San Francisco low-grade glioma prognostic scoring system *J. Florida Med. Assoc.* **111** 203–10

[299] Chen B, Wang H, Ge P, Zhao J, Li W, Gu H, Wang G, Luo Y and Chen D 2012 Gross total resection of glioma with the intraoperative fluorescence-guidance of fluorescein sodium *Int. J. Med. Sci.* **9** 708–14

[300] Dolganova I N *et al* 2018 Wavelet-domain de-noising of OCT images of human brain malignant glioma *Proc. SPIE* **10717** 107171X

[301] Katyba G, Zaytsev K, Dolganova I, Shikunova I, Chernomyrdin N, Yurchenko S, Komandin G, Reshetov I, Nesvizhevsky V and Kurlov V 2018 Sapphire shaped crystals for waveguiding, sensing and exposure applications *Prog. Cryst. Growth Charact. Mater.* **64** 133–51

[302] Shikunova I, Stryukov D, Rossolenko S, Kiselev A and Kurlov V 2017 Neurosurgery contact handheld probe based on sapphire shaped crystal *J. Cryst. Growth* **457** 265–9

[303] Knobloch P *et al* 2002 Medical THz imaging: an investigation of histo-pathological samples *Phys. Med. Biol.* **47** 3875–84

[304] Sun Y, Fischer B and Pickwell-MacPherson E 2009 Effects of formalin fixing on the terahertz properties of biological tissues *J. Biomed. Opt.* **14** 064017

[305] Png G, Choi J, Ng B-H, Mickan S, Abbott D and Zhang X-C 2008 The impact of hydration changes in fresh bio-tissue on THz spectroscopic measurements *Phys. Med. Biol.* **53** 3501–17

[306] Oh S, Kim S-H, Jeong K, Park Y, Huh Y-M, Son J-H and Suh J-S 2013 Measurement depth enhancement in terahertz imaging of biological tissues *Opt. Express* **21** 21299–305

[307] Kolesnikov A, Kolesnikova E, Popov A, Nazarov M, Shkurinov A and Tuchin V 2014 In vitro terahertz monitoring of muscle tissue dehydration under the action of hyperosmotic agents *Quantum Electron.* **44** 633–40

[308] Kolesnikov A, Kolesnikova E, Kolesnikova K, Tuchina D, Popov A, Skaptsov A, Nazarov M, Shkurinov A, Terentyuk A and Tuchin V 2014 THz monitoring of the dehydration of biological tissues affected by hyperosmotic agents *Phys. Wave Phenom.* **22** 169–76

[309] Smolyanskaya O, Schelkanova I, Kulya M, Odlyanitskiy E, Goryachev I, Tcypkin A, Grachev Y, Toropova Y and Tuchin V 2018 Glycerol dehydration of native and diabetic animal tissues studied by THz-TDS and NMR methods *Biomed. Opt. Express* **9** 1198–215

[310] Musina G R *et al* 2018 Terahertz spectroscopy of immersion optical clearing agents: DMSO, PG, EG, PEG *Proc. SPIE* **10800** 108000F

[311] He Y, Ung B-Y, Parrott E, Ahuja A and Pickwell-MacPherson E 2016 Freeze-thaw hysteresis effects in terahertz imaging of biomedical tissues *Biomed. Opt. Express* **7** 4711–7

[312] Bashkatov A *et al* 2018 Measurement of tissue optical properties in the context of tissue optical clearing *J. Biomed. Opt.* **23** 091416

[313] Rogalin V, Kaplunov I and Kropotov G 2018 Optical materials for the THz range *Opt. Spectrosc.* **125** 1053–64

[314] Grischkowsky D, Keiding S, van Exter M and Fattinger C 1990 Far-infrared time-domain spectroscopy with terahertz beams of dielectrics and semiconductors *J. Opt. Soc. Am.* B **7** 2006–15

[315] Ryou A and Simon J 2017 Active cancellation of acoustical resonances with an FPGA FIR filter *Rev. Sci. Instrum.* **88** 013101

[316] Katyba G M *et al* 2018 Sapphire photonic crystal waveguides for terahertz sensing in aggressive environments *Adv. Opt. Mater.* **6** 1800573

[317] Vignes J-L, Frappart C, Di Costanzo T, Rouchaud J-C, Mazerolles L and Michel D 2008 Ultraporous monoliths of alumina prepared at room temperature by aluminium oxidation *J. Mater. Sci.* **43** 1234–40

[318] Khodan A, Nguyen T, Esaulkov M, Kiselev M, Amamra M, Vignes J-L and Kanaev A 2018 Porous monoliths consisting of aluminum oxyhydroxide nanofibrils: 3D structure, chemical composition, and phase transformations in the temperature range 25-1700oc *J. Nanopart. Res.* **20** 194

[319] Khodan A, Kopitsa G, Yorov K, Baranchikov A, Ivanov V, Feoktystov A and Pipich V 2018 Structural analysis of aluminum oxyhydroxide aerogel by small angle x-ray scattering *J. Surf. Invest.* **12** 296–305

[320] Beauvy M, Vignes J-L, Michel D, Mazerolles L, Frappart C and Di Costanzo T 2004 Proede d prparation d'alumins hydrats monolithiques, d'alumins amorphhes ou rlstallises, d'aluminats et de materiaux omposlts par oxidation d'alumlnium metallique ou d'alliag d'aluminum *Patent* FR2847569 2004-05-28 (BOPI 2004-22)

[321] Bouslama M, Amamra M, Brinza O, Tieng S, Chhor K, Abderrabba M, Vignes J-L and Kanaev A 2011 Isolation of titania nanoparticles in monolithic ultraporous alumina: effect of nanoparticle aggregation on anatase phase stability and photocatalytic activity *Appl. Catal.* A **402** 156–61

[322] Bouslama M, Amamra M, Jia Z, Ben Amar M, Chhor K, Brinza O, Abderrabba M, Vignes J-L and Kanaev A 2012 Nanoparticulate TiO_2-Al_2O_3 photocatalytic media: effect of particle size and polymorphism on photocatalytic activity *ACS Catalysis* **2** 1884–92

[323] Huang Z-R, Jiang D, Michel D, Mazerolles L, Ferrand A, Costanzo T D and Vignes J-L 2002 Nickel-alumina nanocomposite powders prepared by novel in situchemical reduction *J. Mater. Res.* **17** 3177–81

[324] Guerboukha H, Yan G, Skorobogata O and Skorobogatiy M 2014 Silk foam terahertz waveguides *Adv. Opt. Mater.* **2** 1181–92

[325] Ma T, Guerboukha H, Girard M, Squires A, Lewis R and Skorobogatiy M 2016 3D printed hollow-core terahertz optical waveguides with hyperuniform disordered dielectric reflectors *Adv. Opt. Mater.* **4** 2085–94

[326] Nazarov M, Shilov A, Margushev Z, Bzheumikhov K, Ozheredov I, Angeluts A, Sotsky A and Shkurinov A 2018 A flexible terahertz waveguide for delivery and filtering of quantum-cascade laser radiation *Appl. Phys. Lett.* **113** 131107

[327] Anthony J, Leonhardt R, Leon-Saval S and Argyros A 2011 THz propagation in kagome hollow-core microstructured fibers *Opt. Express* **19** 18470–8

[328] Li J, Ma T, Nallapan K, Guerboukha H and Skorobogatiy M 2017 3D printed hollow core terahertz Bragg waveguides with defect layers for surface sensing applications *Opt. Express* **25** 4126–44

[329] Gallot G, Jamison S, Mcgowan R and Grischkowsky D 2000 Terahertz waveguides *J. Opt. Soc. Am.* B **17** 851–63

[330] Bao H, Nielsen K, Bang O and Jepsen P 2015 Dielectric tube waveguides with absorptive cladding for broadband, low-dispersion and low loss THz guiding *Sci. Rep.* **5** 7620

[331] Bowden B, Harrington J and Mitrofanov O 2008 Fabrication of terahertz hollow-glass metallic waveguides with inner dielectric coatings *J. Appl. Phys.* **104** 093110

[332] Chen L-J, Chen H-W, Kao T-F, Lu J-Y and Sun C-K 2006 Low-loss subwavelength plastic fiber for terahertz waveguiding *Opt. Lett.* **31** 308–10

[333] Mcgowan R, Gallot G and Grischkowsky D 1999 Propagation of ultrawideband short pulses of terahertz radiation through submillimeter-diameter circular waveguides *Opt. Lett.* **24** 1431–3

[334] Navarro-Cia M, Vitiello M, Bledt C, Melzer J, Harrington J and Mitrofanov O 2013 Terahertz wave transmission in flexible polystyrene-lined hollow metallic waveguides for the 2.5–5 THz band *Opt. Express* **21** 23748–55

[335] Hidaka T, Minamide H, Ito H, Nishizawa J, Tamura K and Ichikawa S 2005 Ferroelectric PVDF cladding terahertz waveguide *J. Lightwave Technol.* **23** 2469–73

[336] Lai C-H, You B, Lu J-Y, Liu T-A, Peng J-L, Sun C-K and Chang H-C 2010 Modal characteristics of antiresonant reflecting pipe waveguides for terahertz waveguiding *Opt. Express* **18** 309–22

[337] Wang K and Mittleman D 2004 Metal wires for terahertz wave guiding *Nature* **432** 376–9

[338] Wang K and Mittleman D M 2005 Guided propagation of terahertz pulses on metal wires *J. Opt. Soc. Am.* B **22** 2001–8

[339] Mbonye M, Mendis R and Mittleman D 2009 A terahertz two-wire waveguide with low bending loss *Appl. Phys. Lett.* **95** 233506

[340] Naman O, New-Tolley M, Lwin R, Tuniz A, Al-Janabi A, Karatchevtseva I, Fleming S, Kuhlmey B and Argyros A 2013 Indefinite media based on wire array metamaterials for the THz and mid-IR *Adv. Opt. Mater.* **1** 971–7

[341] Cao H and Nahata A 2005 Coupling of terahertz pulses onto a single metal wire waveguide using milled grooves *Opt. Express* **13** 7028–34

[342] Pahlevaninezhad H and Darcie T 2010 Coupling of terahertz waves to a two-wire waveguide *Opt. Express* **18** 22614–24

[343] Markov A, Guerboukha H and Skorobogatiy M 2014 Hybrid metal wire- dielectric terahertz waveguides: challenges and opportunities *J. Opt. Soc. Am.* B **31** 2587–600

[344] You B and Lu J-Y 2017 Terahertz fiber sensing *Terahertz Spectroscopy: A Cutting Edge Technology* ed J Uddin (Rijeka: InTech) (https://doi.org/10.5772/66345)

[345] Hassani A, Dupuis A and Skorobogatiy M 2008 Porous polymer fibers for low-loss terahertz guiding *Opt. Express* **16** 6340–51

[346] Ma T, Markov A, Wang L and Skorobogatiy M 2015 Graded index porous optical fibers-dispersion management in terahertz range *Opt. Express* **23** 7856–69

[347] Jamison S, McGowan R and Grischkowsky D 2000 Single-mode waveguide propagation and reshaping of sub-ps terahertz pulses in sapphire fibers *Appl. Phys. Lett.* **76** 1987–9

[348] Minin I, Minin O, Katyba G, Chernomyrdin N, Kurlov V, Zaytsev K, Yue L, Wang Z and Christodoulides D 2019 Experimental observation of a photonic hook *Appl. Phys. Lett.* **114** 031105

[349] Chiu C-M, Chen H-W, Huang Y-R, Hwang Y-J, Lee W-J, Huang H-Y and Sun C-K 2009 All-terahertz fiber-scanning near-field microscopy *Opt. Lett.* **34** 1084–6

[350] Nazarov M, Shilov A, Bzheumikhov K, Margushev Z, Sokolov V, Sotsky A and Shkurinov A 2018 Eight-capillary cladding THz waveguide with low propagation losses and dispersion *IEEE Trans. Terahertz Sci. Technol.* **8** 183–91

[351] Setti V, Vincetti L and Argyros A 2013 Flexible tube lattice fibers for terahertz applications *Opt. Express* **21** 3388–99

[352] Duguay M, Kokubun Y, Koch T and Pfeiffer L 1986 Antiresonant reflecting optical waveguides in SiO$_2$-Si multilayer structures *Appl. Phys. Lett.* **49** 13–5

[353] Skorobogatiy M and Dupuis A 2007 Ferroelectric all-polymer hollow Bragg fibers for terahertz guidance *Appl. Phys. Lett.* **90** 2005–8

[354] Dupuis A, Stoeffler K, Ung B, Dubois C and Skorobogatiy M 2011 Transmission measurements of hollow-core THz Bragg fibers *J. Opt. Soc. Am.* B **28** 896–907

[355] Sakoda K 2010 *Optical Properties of Photonic Crystals* (Berlin: Springer) (https://doi.org/10.1007/B138376)

[356] Vincetti L 2009 Hollow core photonic band gap fibers for THz applications *Microwave Opt. Technol. Lett.* **51** 1711–4

[357] Geng Y, Tan X, Wang P and Yao J 2008 Transmission loss and dispersion in plastic terahertz photonic band-gap fibers *Appl. Phys.* B **91** 333–6

[358] Ren G, Gong Y, Shum P, Yu X and Hu J 2009 Polarization maintaining air-core bandgap fibers for terahertz wave guiding *IEEE J. Quantum Electron.* **45** 506–13

[359] Nielsen K, Rasmussen H, Jepsen P and Bang O 2011 Porous-core honeycomb bandgap THz fiber *Opt. Lett.* **36** 666–8

[360] Zaytsev K, Katyba G, Kurlov V, Shikunova I, Karasik V and Yurchenko S 2016 Terahertz photonic crystal waveguides based on sapphire shaped crystals *IEEE Trans. Terahertz Sci. Technol.* **6** 576–82

[361] Katyba G, Zaytsev K, Rossolenko S, Shikunova I, Shikunov S, Stryukov D, Yurchenko S and Kurlov V 2017 Technological aspects of manufacturing terahertz photonic crystal waveguides based on sapphire shaped crystals *Proc. SPIE* **10333** 103331C

[362] Kawase K, Shikata J-I and Ito H 2002 Terahertz wave parametric source *J. Phys. D: Appl. Phys.* **35** R1–14

[363] Bhowmick S, Huang G, Guo W, Lee C S, Bhattacharya P, Ariyawansa G and Perera A G U 2010 High-performance quantum ring detector for the 1–3 terahertz range *Appl. Phys. Lett.* **96** 231103

[364] Jiang L, Li S S, Yeh N-T, Chyi J-I, Ross C E and Jones K S 2003 In$_{0.6}$Ga$_{0.4}$As/GaAs quantum-dot infrared photodetector with operating temperature up to 260 K *Appl. Phys. Lett.* **82** 1986–8

[365] Bauer M, Venckevicius R, Kasalynas I, Boppel S, Mundt M, Minkevicius L, Lisauskas A, Valusis G, Krozer V and Roskos H 2014 Antenna-coupled field-effect transistors for multi-spectral terahertz imaging up to 4.25 THz *Opt. Express* **22** 19235–41

[366] Vainshtein S, Kostamovaara J, Yuferev V, Knap W, Fatimy A and Diakonova N 2007 Terahertz emission from collapsing field domains during switching of a gallium arsenide bipolar transistor *Phys. Rev. Lett.* **99** 176601

[367] Vainshtein S N, Duan G, Mikhnev V A, Zemlyakov V E, Egorkin V I, Kalyuzhnyy N A, Maleev N A, Näpänkangas J, Sequeiros R B and Kostamovaara J T 2018 Interferometrically enhanced sub-terahertz picosecond imaging utilizing a miniature collapsing-field-domain source *Appl. Phys. Lett.* **112** 191104

[368] Vainshtein S, Javadyan V, Duan G, Tsendin K, Hovhannisyan R and Kostamovaara J 2012 Chalcogenide glass surface passivation of a GaAs bipolar transistor for unique avalanche terahertz emitters and picosecond switches *Appl. Phys. Lett.* **100** 073505

[369] Lepeshov S, Gorodetsky A, Krasnok A, Rafailov E and Belov P 2016 Enhancement of terahertz photoconductive antenna operation by optical nanoantennas *Laser Photon. Rev.* **11** 1600199

[370] Oh Y-J and Jeong K-H 2012 Glass nanopillar arrays with nanogap-rich silver nanoislands for highly intense surface enhanced Raman scattering *Adv. Mater.* **24** 2234–7

[371] Miyamaru F, Saito Y, Takeda M W, Liu L, Hou B, Wen W and Sheng P 2009 Emission of terahertz radiations from fractal antennas *Appl. Phys. Lett.* **95** 221111

[372] Lavrukhin D V *et al* 2019 Terahertz photoconductive emitter with dielectric-embedded high-aspect-ratio plasmonic grating for operation with low-power optical pumps *AIP Adv.* **9** 015112

[373] Yang S, Hashemi M R, Berry C W and Jarrahi M 2014 7.5% optical-to-terahertz conversion efficiency offered by photoconductive emitters with three-dimensional plasmonic contact electrodes *IEEE Trans. Terahertz Sci. Technol.* **4** 575–81

[374] Mitrofanov O, Brener I, Luk T S and Reno J L 2015 Photoconductive terahertz near-field detector with a hybrid nanoantenna array cavity *ACS Photon.* **2** 1763–8

[375] Lepeshov S, Gorodetsky A, Krasnok A, Toropov N, Vartanyan A, Belov T P, Alu A and Rafailov E 2018 Boosting terahertz photoconductive antenna performance with optimised plasmonic nanostructures *Sci. Rep.* **8** 6624

[376] Mitrofanov O, Siday T, Thompson R, Luk T, Brener I and Reno J 2018 Efficient photoconductive terahertz detector with all-dielectric optical metasurface *APL Photon.* **3** 051703

[377] McBryde D, Barnes M E, Berry S A, Gow P, Beere H E, Ritchie D A and Apostolopoulos V 2014 Fluence and polarisation dependence of gaas based lateral photo-dember terahertz emitters *Opt. Express* **22** 3234–43

[378] Gow P, Berry S, McBryde D, Barnes M, Beere H, Ritchie D and Apostolopoulos V 2013 Multiple lateral photo-dember terahertz emitters illuminated by a cylindrical micro-lens array *Appl. Phys. Lett.* **103** 252101

[379] Ryzhii V *et al* 2016 Two-dimensional plasmons in lateral carbon nanotube network structures and their effect on the terahertz radiation detection *J. Appl. Phys.* **120** 044501

[380] Ryzhii V, Otsuji T, Ryzhii M, Ponomarev D S, Karasik V E, Leiman V G, Mitin V and Shur M S 2018 Electrical modulation of terahertz radiation using graphene-phosphorene heterostructures *Semicond. Sci. Technol.* **33** 124010

[381] Ryzhii V, Ryzhii M, Ponomarev D S, Leiman V G, Mitin V, Shur M S and Otsuji T 2019 Negative photoconductivity and hot-carrier bolometric detection of terahertz radiation in graphene-phosphorene hybrid structures *J. Appl. Phys.* **125** 151608

[382] Ponomarev D S, Lavrukhin D V, Yachmenev A E, Khabibullin R A, Semenikhin I E, Vyurkov V V, Ryzhii M, Otsuji T and Ryzhii V 2018 Lateral terahertz hot-electron

bolometer based on an array of Sn nanothreads in GaAs *J. Phys. D: Appl. Phys.* **51** 135101

[383] Ponomarev D, Lavrukhin D, Yachmenev A, Khabibullin R, Semenikhin I, Vyurkov V, Ryzhii M, Otsuji T and Ryzhii V 2018 Sn-nanothreads in GaAs matrix and their sub- and terahertz applications *J. Phys. Conf. Ser.* **1092** 012166

[384] Chernomyrdin N V *et al* 2017 Wide-aperture aspherical lens for high-resolution terahertz imaging *Rev. Sci. Instrum.* **88** 014703

[385] Abbe E 1873 Beiträge zur theorie des mikroskops und der mikroskopischen wahrnehmung *Arch. Mikrosk. Anat.* **9** 413–68

[386] Born M and Wolf E 1999 *Principles of Optics* 7th edn (Cambridge: Cambridge University Press) (https://doi.org/10.1017/CBO9781139644181)

[387] Lo Y H and Leonhardt R 2008 Aspheric lenses for terahertz imaging *Opt. Express* **16** 15991–8

[388] Luk'yanchuk B, Paniagua-Dominguez R, Minin I, Minin O and Wang Z 2017 Refractive index less than two: photonic nanojets yesterday, today and tomorrow *Opt. Mater. Express* **7** 1820–47

[389] Minin I, Minin O, Ponomarev D and Glinskiy I 2018 Photonic hook plasmons: a new curved surface wave *Ann. Phys.* **530** 1800359

[390] Chen Z, Taflove A and Backman V 2004 Photonic nanojet enhancement of backscattering of light by nanoparticles: a potential novel visible-light ultramicroscopy technique *Opt. Express* **12** 1214–20

[391] Nguyen Pham H, Hisatake S, Minin O, Nagatsuma T and Minin I 2017 Enhancement of spatial resolution of terahertz imaging systems based on terajet generation by dielectric cube *APL Photon.* **2** 056106

[392] Yue L, Minin O, Wang Z, Monks J, Shalin A and Minin I 2018 Photonic hook: a new curved light beam *Opt. Lett.* **43** 771–4

[393] Chernomyrdin N, Schadko A, Lebedev S, Tolstoguzov V, Kurlov V, Reshetov I, Spektor I, Skorobogatiy M, Yurchenko S and Zaytsev K 2017 Solid immersion terahertz imaging with sub-wavelength resolution *Appl. Phys. Lett.* **110** 221109

[394] Chernomyrdin N V *et al* 2019 Terahertz microscope based on solid immersion effect for imaging of biological tissues *Opt. Spectrosc.* **126** 644–51

[395] Zhang Y, Zhou W, Wang X, Cui Y and Sun W 2008 Terahertz digital holography *Strain* **44** 380–5

[396] McClatchey K, Reiten M and Cheville R 2001 Time resolved synthetic aperture terahertz impulse imaging *Appl. Phys. Lett.* **79** 4485–7

[397] Bandyopadhyay A, Stepanov A, Schulkin B, Federici M, Sengupta A, Gary D, Federici J, Barat R, Michalopoulou Z-H and Zimdars D 2006 Terahertz interferometric and synthetic aperture imaging *J. Opt. Soc. Am.* A **23** 1168–78

[398] Bulbul A, Vijayakumar A and Rosen J 2018 Superresolution far-field imaging by coded phase reflectors distributed only along the boundary of synthetic apertures *Optica* **5** 1607

[399] Guerboukha H, Nallappan K and Skorobogatiy M 2018 Exploiting k-space/frequency duality toward real-time terahertz imaging *Optica* **5** 109–16

[400] Guerboukha H, Nallappan K and Skorobogatiy M 2018 Toward real-time terahertz imaging *Adv. Opt. Photon.* **10** 843–938

[401] Huang H, Rong L, Wang D, Li W, Deng Q, Li B, Wang Y, Zhan Z, Wang X and Wu W 2016 Synthetic aperture in terahertz in-line digital holography for resolution enhancement *Appl. Opt.* **55** A43–8

[402] Deng Q, Li W, Wang X, Li Z, Huang H, Shen C, Zhan Z and Zou R 2017 High-resolution terahertz inline digital

holography based on quantum cascade laser *Opt. Eng.* **56** 113102

[403] Rong L, Latychevskaia T, Wang D, Zhou X, Huang H, Li Z and Wang Y 2014 Terahertz in-line digital holography of dragonfly hindwing: amplitude and phase reconstruction at enhanced resolution by extrapolation *Opt. Express* **22** 17236–45

[404] Balbekin N S, Cassar Q, Smolyanskaya O A, Kulya M S, Petrov N V, MacGrogan G, Guillet J-P, Mounaix P and Tuchin V V 2019 Terahertz pulse time-domain holography method for phase imaging of breast tissue *Proc. SPIE* **10887** 108870G

[405] Rong L, Latychevskaia T, Chen C, Wang D, Yu Z, Zhou X, Li Z, Huang H, Wang Y and Zhou Z 2015 Terahertz in-line digital holography of human hepatocellular carcinoma tissue *Sci. Rep.* **5** 8445

[406] Guo L, Wang X, Han P, Sun W, Feng S, Ye J and Zhang Y 2017 Observation of dehydration dynamics in biological tissues with terahertz digital holography [invited] *Appl. Opt.* **56** F173–8

[407] Chen H-T, Kersting R and Cho G 2003 Terahertz imaging with nanometer resolution *Appl. Phys. Lett.* **83** 3009–11

[408] Adam A 2011 Review of near-field terahertz measurement methods and their applications *J. Infrared Millim. Terahertz Waves* **32** 976–1019

[409] Huber A, Keilmann F, Wittborn J, Aizpurua J and Hillenbrand R 2008 Terahertz near-field nanoscopy of mobile carriers in single semiconductor nanodevices *Nano Lett.* **8** 3766–70

[410] Ishihara K, Ikari T, Minamide H, Shikata J-I, Ohashi K, Yokoyama H and Ito H 2005 Terahertz near-field imaging using enhanced transmission through a single subwavelength aperture *Japan. J. Appl. Phys.* **44** L929–31

[411] Ishihara K, Ohashi K, Ikari T, Minamide H, Yokoyama H, Shikata J-I and Ito H 2006 Terahertz-wave near-field imaging with subwavelength resolution using surface-wave-assisted bow-tie aperture *Appl. Phys. Lett.* **89** 201120

[412] Schade U, Holldack K, Kuske P, Wüstefeld G and Hübers H-W 2004 THz near-field imaging employing synchrotron radiation *Appl. Phys. Lett.* **84** 1422–4

[413] Xu J and Zhang X-C 2004 Circular involute stage *Opt. Lett.* **29** 2082–4

[414] Guerboukha H, Markov A, Qu H and Skorobogatiy M 2015 Time resolved dynamic measurements at THz frequencies using a rotary optical delay line *IEEE Trans. Terahertz Sci. Technol.* **5** 564–72

[415] Skorobogatiy M 2014 Linear rotary optical delay lines *Opt. Express* **22** 11812–33

[416] Wilk R, Hochrein T, Koch M, Mei M and Holzwarth R 2011 Terahertz spectrometer operation by laser repetition frequency tuning *J. Opt. Soc. Am.* B **28** 592–5

[417] Kim Y and Yee D-S 2010 High-speed terahertz time-domain spectroscopy based on electronically controlled optical sampling *Opt. Lett.* **35** 3715–7

[418] Kolano M, Gräf B, Weber S, Molter D and von Freymann G 2018 Single-laser polarization-controlled optical sampling system for THz-TDS *Opt. Lett.* **43** 1351–4

[419] Elzinga P A, Lytle F E, Jian Y, King G B and Laurendeau N M 1987 Pump/probe spectroscopy by asynchronous optical sampling *Appl. Spectrosc.* **41** 2–4

[420] Dawson Baker R, Tolga Yardimci N, Ou Y-H, Kieu K and Jarrahi M 2018 Self-triggered asynchronous optical sampling terahertz spectroscopy using a bidirectional mode-locked fiber laser *Sci. Rep.* **8** 14802

[421] Rehn A, Mikerov M, Preu S, Koch M and Balzer J C 2018 Enhancing the performance of THz quasi time-domain spectroscopy systems by low duty cycle laser operation *Opt. Express* **26** 32758–64

[422] Kohlhaas R B, Rehn A, Nellen S, Koch M, Schell M, Dietz R J B and Balzer J C 2017 Terahertz quasi time-domain spectroscopy based on telecom technology for 1550 nm *Opt. Express* **25** 12851–9

[423] Nallappan K, Li J, Guerboukha H, Markov A, Petrov B, Morris D and Skorobogatiy M 2017 A dynamically reconfigurable terahertz array antenna for 2D-imaging applications *Photonics North (PN)* (https://doi.org/10.1109/PN.2017.8090603)

[424] Nallappan K, Li J, Guerboukha H, Markov A, Petrov B, Morris D and Skorobogatiy M 2019 A dynamically reconfigurable terahertz array antenna for near-field imaging applications arXiv:1705.10624

[425] Stantchev R, Sun B, Hornett S, Hobson P, Gibson G, Padgett M and Hendry E 2016 Noninvasive, near-field terahertz imaging of hidden objects using a single-pixel detector *Sci. Adv.* **2** e1600190

[426] Stantchev R, Phillips D, Hobson P, Hornett S, Padgett M and Hendry E 2017 Compressed sensing with near-field THz radiation *Optica* **4** 989–92

[427] Genina E A, Bashkatov A N and Tuchin V V 2010 Tissue optical immersion clearing *Expert Rev. Med. Devices* **7** 825–42

[428] Zhu D, Larin K V, Luo Q and Tuchin V V 2013 Recent progress in tissue optical clearing *Laser Photonics Rev.* **7** 732–57

[429] Sim Y C, Ahn K-M, Park J Y, Park C-S and Son J-H 2013 Temperature-dependent terahertz imaging of excised oral malignant melanoma *IEEE Trans. Terahertz Sci. Technol.* **3** 368–73

[430] Hoshina H, Hayashi A, Miyoshi N, Miyamaru F and Otani C 2009 Terahertz pulsed imaging of frozen biological tissues *Appl. Phys. Lett.* **94** 123901

[431] Vilagosh A L Z and Wood A W 2019 Imaging and lesion ablation modeling in skin using freezing to enhance penetration depth of terahertz radiation *Proc. SPIE* **10851** 108510E

[432] Yu T, Wen X, Tuchin V V, Luo Q and Zhu D 2011 Quantitative analysis of dehydration in porcine skin for assessing mechanism of optical clearing *J. Biomed. Opt.* **16** 095002

[433] Nazarov M M, Shkurinov A P, Kuleshov E A and Tuchin V V 2008 Terahertz time-domain spectroscopy of biological tissues *Quantum Electron.* **38** 647–54

[434] Nazarov M, Shkurinov A, Tuchin V V and Zhang X-C 2010 *Terahertz Tissue Spectroscopy and Imaging* (London: CRC Press) pp 591–613

[435] Kolesnikov A, Kolesnikova E, Kolesnikova K, Tuchina D, Popov A P, Skaptsov A A, Nazarov M, Shkurinov A, Terentyuk A and Tuchin V 2014 THz tissues affected by hyperosmotic agents *Phys. Wave Phenom.* **22** 169–76

[436] Oh S J, Kim S-H, Jeong K, Park Y, Huh Y-M, Son J-H and Suh J-S 2013 Measurement depth enhancement in terahertz imaging of biological tissues *Opt. Express* **21** 21299–305

[437] Kim K W, Kim H, Park J, Han J K and Son J 2012 Terahertz tomographic imaging of transdermal drug delivery *IEEE Trans. Terahertz Sci. Technol.* **2** 99–106

[438] Tuchin V V 2005 *Optical Clearing of Tissues and Blood* (Bellingham, WA: SPIE Press)

[439] Tuchina D K, Shi R, Bashkatov A N, Genina E A, Zhu D, Luo Q and Tuchin V V 2015 Ex vivo optical measurements of glucose diffusion kinetics in native and diabetic mouse skin *J. Biophoton.* **8** 332–46

[440] Carvalho S, Gueiral N, Nogueira E, Henrique R, Oliveira L and Tuchin V V 2017 Glucose diffusion in colorectal mucosa-a comparative study between normal and cancer tissues *J. Biomed. Opt.* **22** 091506

[441] Carneiro I, Carvalho S, Henrique R, Oliveira L and Tuchin V V 2017 Simple multimodal optical technique for

evaluation of free/bound water and dispersion of human liver tissue *J. Biomed. Opt.* **22** 125002

[442] Tuchina D K, Timoshina P A, Tuchin V V, Bashkatov A N and Genina E A 2019 Kinetics of rat skin optical clearing at topical application of 40% glucose: ex vivo and in vivo studies *IEEE J. Sel. Top. Quantum Electron.* **25** 1–8

[443] Carneiro I, Carvalho S, Silva V, Henrique R, Oliveira L and Tuchin V V 2018 Kinetics of optical properties of human colorectal tissues during optical clearing: a comparative study between normal and pathological tissues *J. Biomed. Opt.* **23** 121620

[444] Carneiro I, Carvalho S, Henrique R, Oliveira L and Tuchin V V 2019 Kinetics of optical properties of colorectal muscle during optical clearing *IEEE J. Sel. Top. Quantum Electron.* **25** 1–8

[445] Larin K V, Ghosn M G, Bashkatov A N, Genina E A, Trunina N A and Tuchin V V 2012 Optical clearing for OCT image enhancement and in-depth monitoring of molecular diffusion *IEEE J. Sel. Top. Quantum Electron.* **18** 1244–59

[446] Bashkatov A, Genina E and Tuchin V 2011 Optical properties of skin, subcutaneous, and muscle tissues: a review *J. Innov. Opt. Heal. Sci.* **4** 9–38

[447] Oliveira L M, Carvalho M I, Nogueira E M and Tuchin V V 2014 Diffusion characteristics of ethylene glycol in skeletal muscle *J. Biomed. Opt.* **20** 051019

[448] Oliveira L M, Carvalho M I, Nogueira E M, Nogueira M E and Tuchin V V 2018 Skeletal muscle dispersion (400–1000 nm) and kinetics at optical clearing *J. Biophoton.* **11** e201700094

[449] Genina E, Bashkatov A, Sinichkin Y, Yanina I and Tuchin V 2015 Optical clearing of biological tissues: prospects of application in medical diagnostics and phototherapy *J. Biomed. Photon. Eng.* **1** 22–58

[450] Gurjarpadhye A A, Vogt W C, Liu Y and Rylander C G 2011 Effect of localized mechanical indentation on skin water content evaluated using OCT *Int. J. Biomed. Imaging* **2011** 817250

[451] Chernomyrdin N V *et al* 2019 Differentiation of healthy and malignant brain tissues using terahertz pulsed spectroscopy and optical coherence tomography *Proc. SPIE* **10864** 1086406

[452] Jones B 1998 A reappraisal of the use of infrared thermal image analysis in medicine *IEEE Trans. Med. Imaging* **17** 1019–27

[453] Stenquist B, Ericson M, Strandeberg C, Molne L, Rosen A, Larko O and Wennberg A 2006 Bispectral fluorescence imaging of aggressive basal cell carcinoma combined with histopathological mapping: a preliminary study indicating a possible adjunct to Mohs micrographic surgery *Br. J. Dermatol.* **154** 305–9

[454] Huang D *et al* 1991 Optical coherence tomography *Science* **254** 1178–81

[455] Kleinerman R, Whang T, Bard R and Marmur E 2012 Ultrasound in dermatology: principles and applications *J. Am. Acad. Dermatol.* **67** 478–87

[456] Lui H, Zhao J, McLean D and Zeng H 2012 Real-time Raman spectroscopy for in vivo skin cancer diagnosis *Cancer Res.* **72** 2491–500

[457] Paoli J, Smedh M, Wennberg A-M and Ericson M B 2008 Multiphoton laser scanning microscopy on non-melanoma skin cancer: morphologic features for future non-invasive diagnostics *J. Investig. Dermatol.* **128** 1248–55